Remarkable anticancer activity of ferrocenyl-terpyridine platinum(II) complexes in visible light with low dark toxicity

Koushambi Mitra,[a] Uttara Basu,[a] Imran Khan,[b] Basudev Maity,[a] Paturu Kondaiah[*b] and Akhil R Chakravarty[*a]

[a] *Department of Inorganic and Physical Chemistry, Indian Institute of Science and* [b] *Department of Molecular Reproduction, Development and Genetics, Indian Institute of Science, Bangalore 560012, India. E-mail: arc@ipc.iisc.ernet.in*

Electronic Supplementary Information (ESI)

Electronic Supplementary Material (ESI) for Dalton Transactions

Table of contents

Experimental

Schemes and figures

Fig. S57. UV-Visible spectra of complexes **1**, **2**, **3** and **4** treated with an excess phen and kept in dark.

Fig. S58. UV-Visible spectra of complex **4** upon irradiation

Fig. S59. Geometrically optimized structure of complex **2**

Fig. S60. HOMO-LUMO orbital pictures of **2**, **3** and **4**

Table S1. Coordinates of optimized geometry of complex **2**

Table S2. TDDFT transitions of complexes in the visible region

Analytical data for complex 4

Anal. Calcd for $C_{21}H_{15}Cl_2N_3Pt$ (**4**): C, 43.84; H, 2.63; N, 7.30. Found: C, 43.78; H, 2.65; N, 7.28. ESI-MS in MeCN: *m/z* 540 $[M - Cl]^+$ (100%). ^{1}H NMR (400 MHz, DMSO-d_6) : δ (ppm) = 9.00 (s, 2H), 8.92 (d, 2H, J = 5.2 Hz), 8.86 (d, 2H, J = 8.0 Hz), 8.54 (t, 2H, $J_1 = J_2 = 7.6$ Hz), 8.20 (m, 2H), 7.95 (t, 2H, $J_1 = 6.8$, $J_2 = 6.4$ Hz), 7.69 (m, 3H), (d, doublet; t, triplet; m, multiplet). UV-vis in DMF [λ_{max}, nm (ε, dm^3 mol^{-1} cm^{-1})]: 405 (8900), 385 (7550), 335 (25500), 280 (38500). IR data in solid phase (cm^{-1}): 3370 w, 3002 w, 2920 m, 1742 vs , 1608 vs, 1497 w, 1479 w, 1414 w, 1365w, 1033 vs, 776 vs, 497 s, 480 s, 440 s. Λ_M, S m^2 M^{-1} in DMF at 25 ^oC : 73.

DNA binding methods

The calf thymus ct-DNA was first tested for purity. The ratio of absorbance at 260 and 280 nm was approximately 1.9:1 confirming that the DNA was apparently free from protein. The concentration of DNA was determined by from the ratio of its absorption intensity at 260 nm and its known molar absorption coefficient value of 6600 dm^3 mol^{-1} cm^{-1}.[S1,S2] Absorption titration experiments were performed in Tris-HCl buffer (5 mM, pH 7.2) by varying the concentration of the ct-DNA while keeping the complex concentration as constant (2 μM in DMF). The spectra were recorded with increasing concentration of ct-DNA and after equilibration for 5 min with due correction made for the absorbance of only DNA. The regression analysis equation used is (1)

$$(\varepsilon_a-\varepsilon_f)/(\varepsilon_b-\varepsilon_f) = (b-(b^2-2K_b^2C_t[DNA]_t/s)^{1/2})/2K_bC_t, \text{-------(1)}$$

$$b = 1 + K_bC_t + K_b[DNA]_t/2s,$$

where C_t is the total metal complex concentration, ε_a is the extinction coefficient observed for the charge transfer absorption band at a given DNA concentration, ε_f is the extinction coefficient of the DNA unbound complex, ε_b is the extinction coefficient of the complex when fully bound to DNA, $[DNA]_t$ is the DNA concentration, K_b is the equilibrium binding constant, and s is the

binding site size in base pairs. The graphs were plotted and non-linear least-squares analysis was done using Origin Lab, version 6.1.

The derivative of the melting plots gave the melting temperatures (T_m) of the DNA. Ethidium bromide, a standard intercalator was used for comparison. The experiments were performed using a Cary 300 bio UV-vis spectrometer with a Cary temperature controller with increasing the temperature of the solution by 1.0 °C per min.

The viscometric experiments were performed by addition of 50 µL of the complexes in DMF (200 μM) in Tris-HCl buffer. The solution was then homogenized and the average flow times were determined at a constant temperature of 37 °C using Schott Gerate AVS 310 Automated Viscometer. The average flow time (t_0) of the only buffer solution was also measured. The viscosity values were calculated from the observed flow time of ct-DNA-containing solutions (t) duly corrected for that of the buffer alone (t_0), $\eta=(t - t_0)/t_0$. [S3]

DNA cleavage methods

Before light exposure, each sample was incubated for 1.0 h at 37 °C and analyzed for the photo-cleaved products by gel electrophoresis method as described earlier by us.[S4] The samples after incubation in a dark chamber were added to the loading buffer containing 0.25% bromophenol blue, 0.25% xylene cyanol, 30% glycerol (3 μL) and the solution was finally loaded on 1% agarose gel containing 1.0 µg/mL ethidium bromide (EB). The mechanistic investigations were done by adding different additives (NaN_3, 4mM; DMSO, 8 µL; KI, 4.0 mM; catalase, 4 units; SOD, 4 units). The gel-electrophoresis completed in about 2 h at 60 V in TAE (Tris-acetate EDTA) buffer. Bands were visualized by UV light and photographed. The extent of DNA cleavage was measured from the intensities of the bands using UVITEC Gel Documentation System. Due corrections were made for the low level of nicked circular (NC) form present in the original supercoiled (SC) DNA sample and for the low affinity of EB binding to SC compared to NC and linear forms of DNA.[S4] The concentrations of the complexes and additives corresponded to that in the 20 μL final volume of the sample using Tris buffer.

Computational details

The TDDFT calculations were done using the Gaussian 03 and 09 suites of program.[S5] The B3LYP/LanL2DZ basis set was used for computations. [S6-S9]

References

S1. S. P. Foxon, C. Metcalfe, H. Adams, M. Webb and J. A. Thomas, *Inorg. Chem.*, 2007, **46**, 409-416.

S2. M. E. Reichmann, S. A. Rice, C. A. Thomas and P. Doty, J. Am. Chem. Soc., 1954, **76**, 3047-3053.

S3. G. Cohen and H. Eisenberg, *Biopolymers*, 1969, **8**, 45-55.

S4. S. Saha, R. Majumdar, M. Roy, R. R. Dighe and A. R. Chakravarty, *Inorg. Chem.*, 2009, **48**, 2652-2663.

S5. M. J. Frisch, G. W. Trucks, H. B. Schlegel, G. E. Scuseria, M. A. Robb, J. R. Cheeseman, G. Scalmani, V. Barone, B. Mennucci, G. A. Petersson, H. Nakatsuji, M. Caricato, X. Li, H. P. Hratchian, A. F. Izmaylov, J. Bloino, G. Zheng, J. L. Sonnenberg, M. Hada, M. Ehara, K. Toyota, R. Fukuda, J. Hasegawa, M. Ishida, T. Nakajima, Y. Honda, O. Kitao, H. Nakai, T. Vreven, J. A. Montgomery Jr., J. E. Peralta, F. Ogliaro, M. Bearpark, J. J. Heyd, E. Brothers, K. N. Kudin, V. N. Staroverov, R. Kobayashi, J. Normand, K. Raghavachari, A. Rendell, J. C. Burant, S. S. Iyengar, J. Tomasi, M. Cossi, N. Rega, J. M. Millam, M. Klene, J. E. Knox, J. B. Cross, V. Bakken, C. Adamo, J. Jaramillo, R. Gomperts, R. E. Stratmann, O. Yazyev, A. J. Austin, R. Cammi, C. Pomelli, J. W. Ochterski, R. L. Martin, K. Morokuma, V. G. Zakrzewski, G. A. Voth, P. Salvador, J. J. Dannenberg, S. Dapprich, A. D. Daniels, Ö. Farkas, J. B. Foresman, J. V. Ortiz, J. Cioslowski and D. J. Fox, GAUSSIAN 09 (Revision A.1), Gaussian, Inc., Wallingford, CT, 2009.

S6. (a) A. D. Becke, Phys. Rev. A, 1988, 38, 3098–3100; (b) A. D. Becke, J. Chem. Phys., 1993, 98, 5648–5652; (c) C. Lee, W. Yang and R. G. Parr, Phys. Rev. B: Condens. Matter, 1988, 37, 785–789.

S7. W. J. Hehre, L. Radom, P. v. R. Schleyer and J. A. Pople, Ab Initio Molecular Orbital Theory, Wiley, New York, 1986, p. 65–68.

S8. J. Tomasi and M. Persico, Chem. Rev., 1994, 94, 2027–2094.

S9. (a) M. E. Casida, C. Jamorski, K. C. Casida and D. R. Salahub, J. Chem. Phys., 1998, 108, 4439–4449; (b) R. E. Stratmann, G. E. Scuseria and M. J. Frisch,
J. Chem. Phys., 1998, 109, 8218–8224.

Preparation of complexes

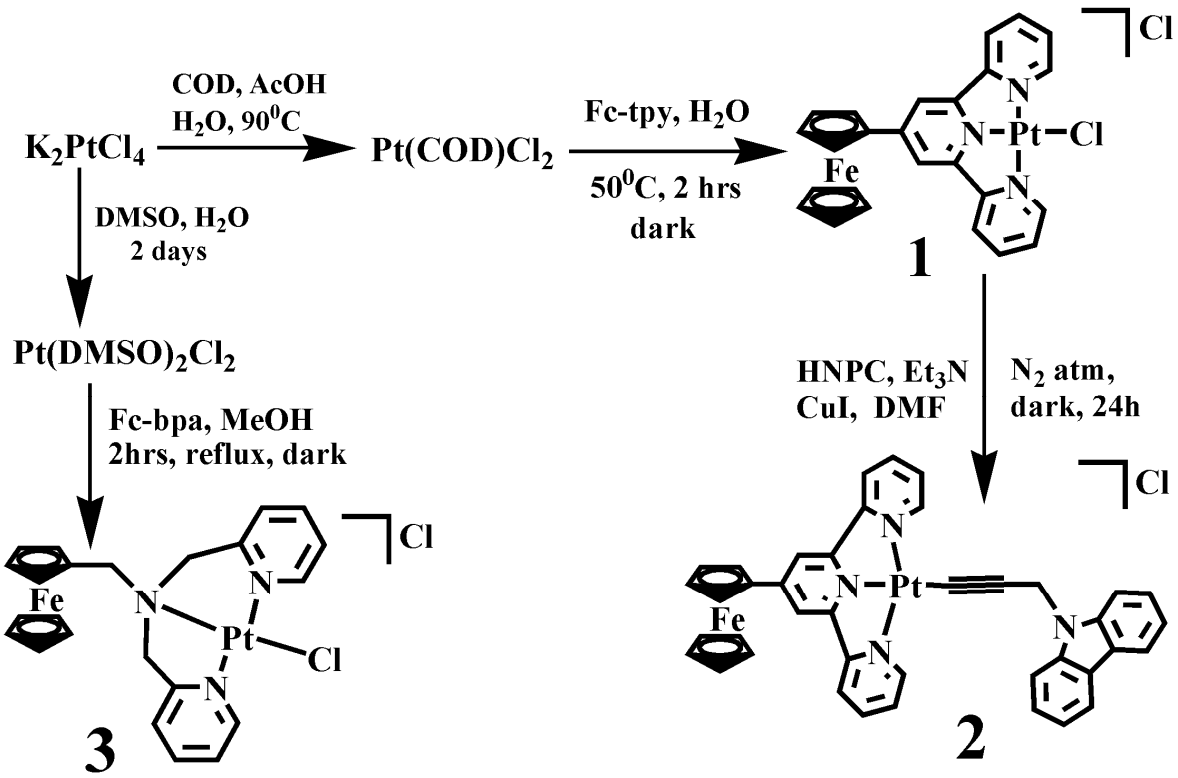

Scheme S1. Preparation of complexes **1**-**3**. COD = 1,5-cyclooctadiene; DMSO = dimethyl sulfoxide; Fc-tpy = 4′-ferrocenyl-2,2′:6",2"-terpyridine, Fc-bpa = ferrocenylmethyl bis(2-pyridylmethyl)amine; HNPC = N-propargyl-carbazole.

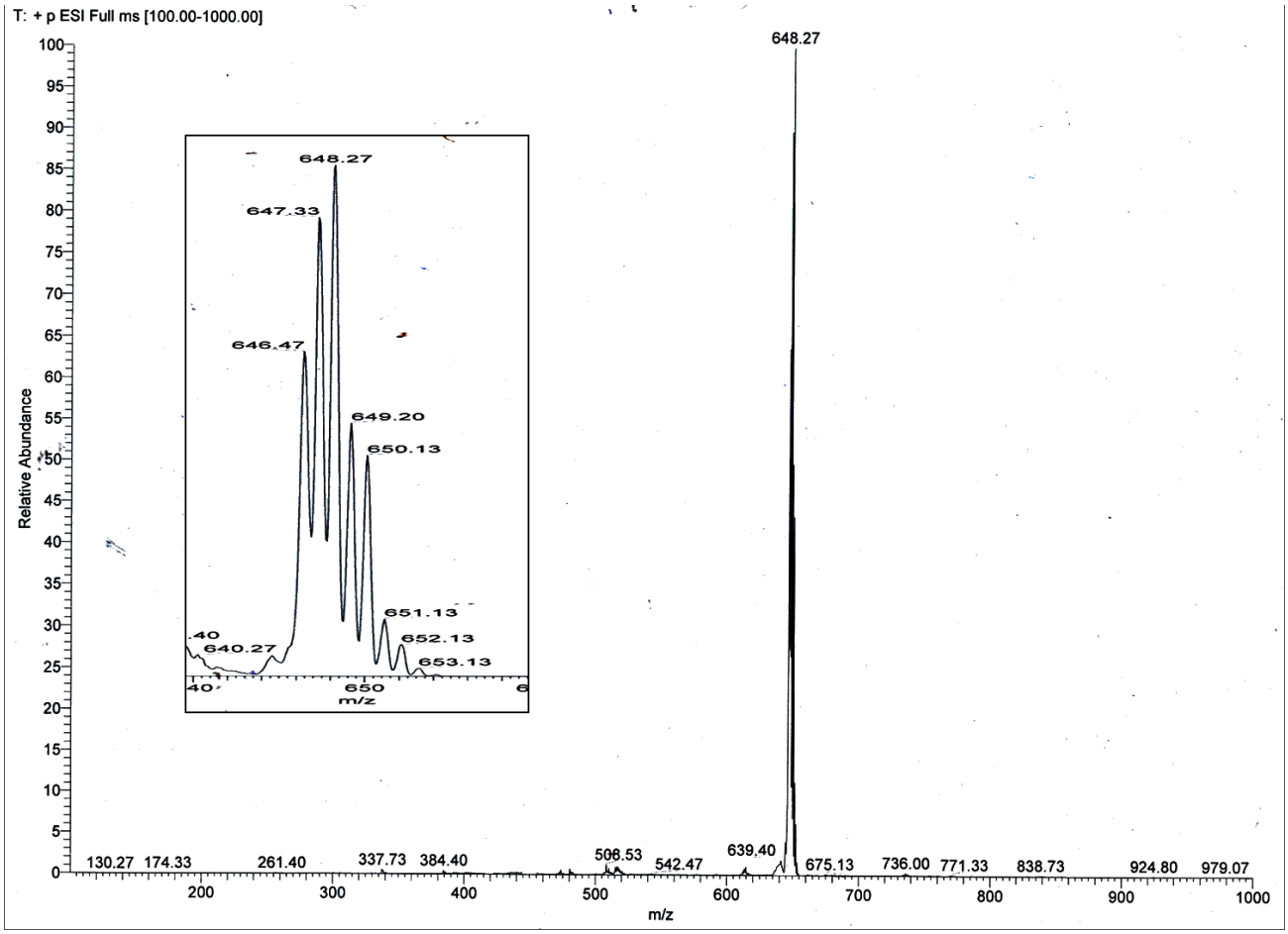

Fig. S1: The ESI-MS spectrum of [Pt(Fc-tpy)Cl]Cl (**1**) in MeCN showing prominent parent ion peak at 648 (m/z) which corresponds to $[Pt(Fc\text{-}tpy)Cl]^{+}$. Inset shows the isotopic distribution pattern for Pt(II) of the molecular ion peak.

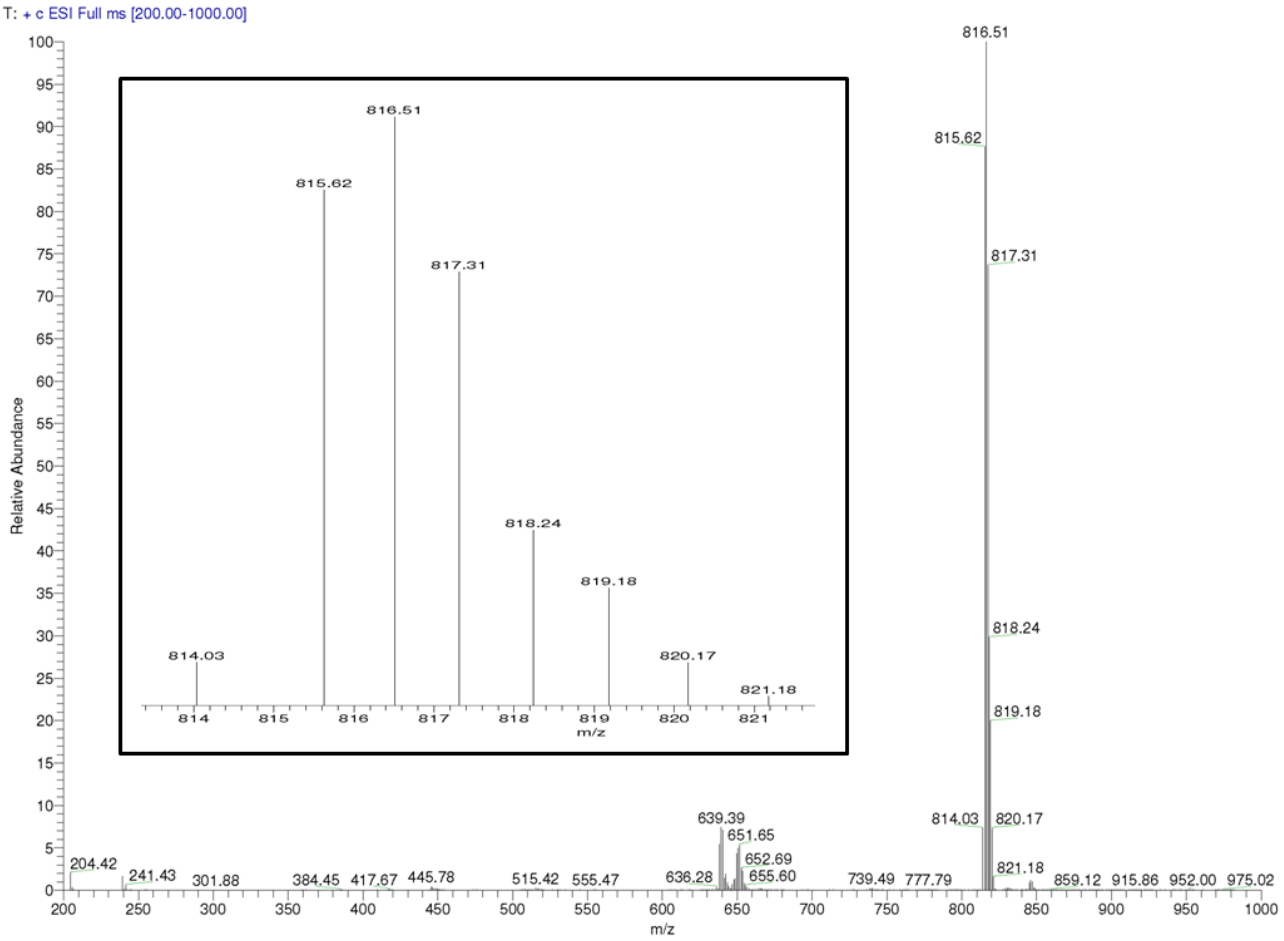

Fig. S2: The ESI-MS spectrum of [Pt(Fc-tpy)(NPC)]Cl (**2**) in MeCN showing prominent parent ion peak at 816 (m/z) which corresponds to $[Pt(Fc\text{-}tpy)(NPC)]^{+}$. Inset shows the isotopic distribution pattern for Pt(II) of the molecular ion peak.

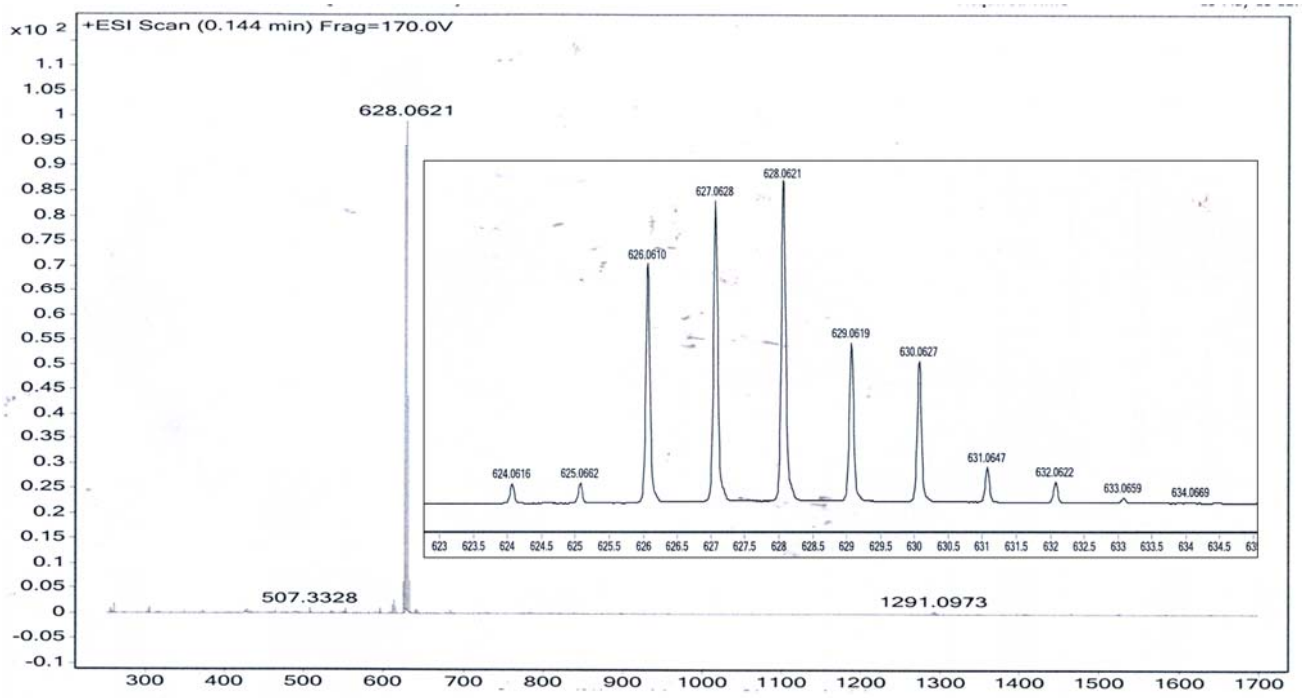

Fig. S3: The ESI-MS spectrum of [Pt(Fc-bpa)Cl]Cl (**3**) in MeCN showing prominent parent ion peak at 628 (m/z) which corresponds to $[Pt(Fc\text{-}bpa)Cl]^{+}$. Inset shows the isotopic distribution pattern for Pt(II) of the molecular ion peak.

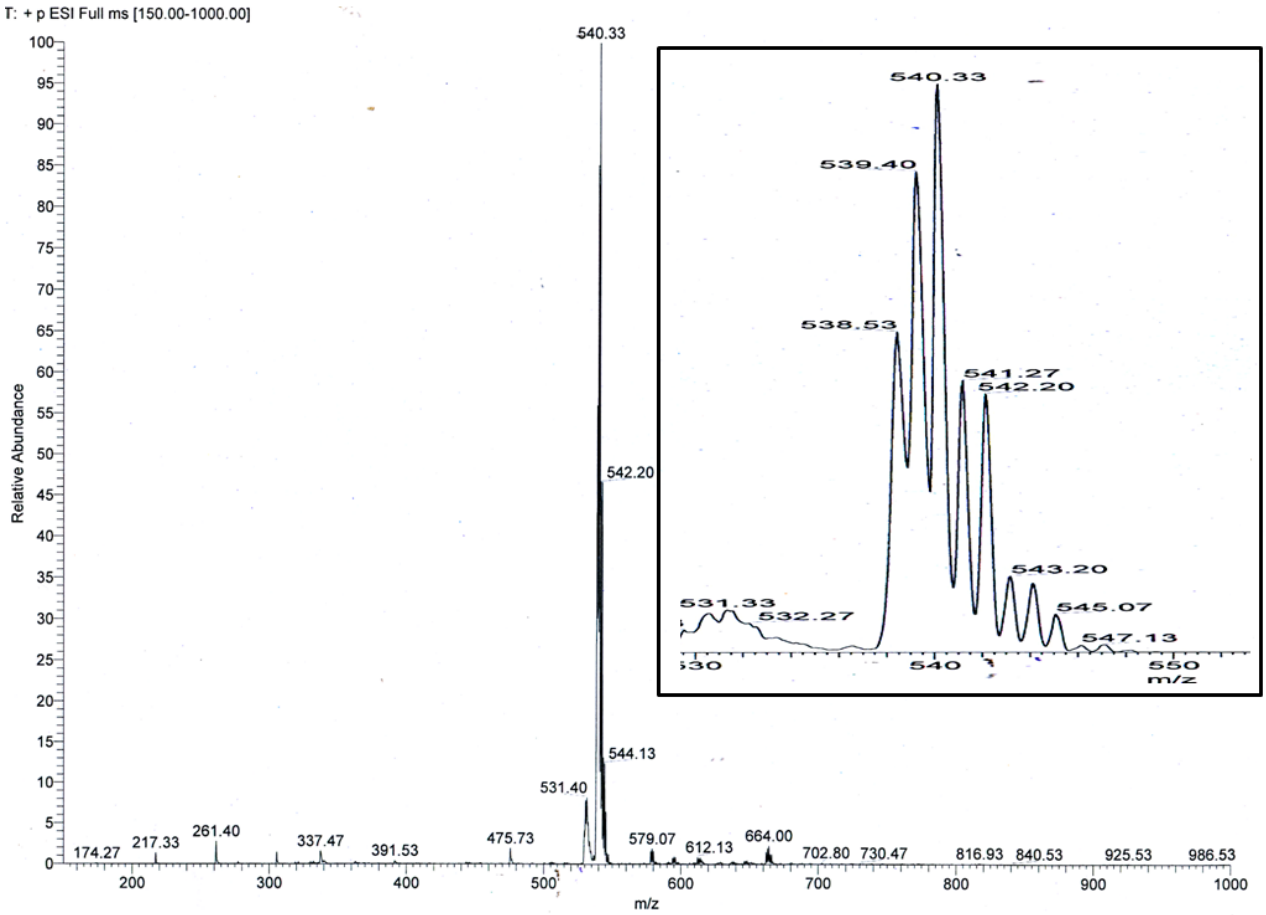

Fig. S4: The ESI-MS spectrum of [Pt(Ph-tpy)Cl]Cl (**4**) in MeCN showing prominent parent ion peak at 540 (m/z) which corresponds to $[Pt(Ph\text{-}tpy)Cl]^{+}$. Inset shows the isotopic distribution pattern for Pt(II) of the molecular ion peak.

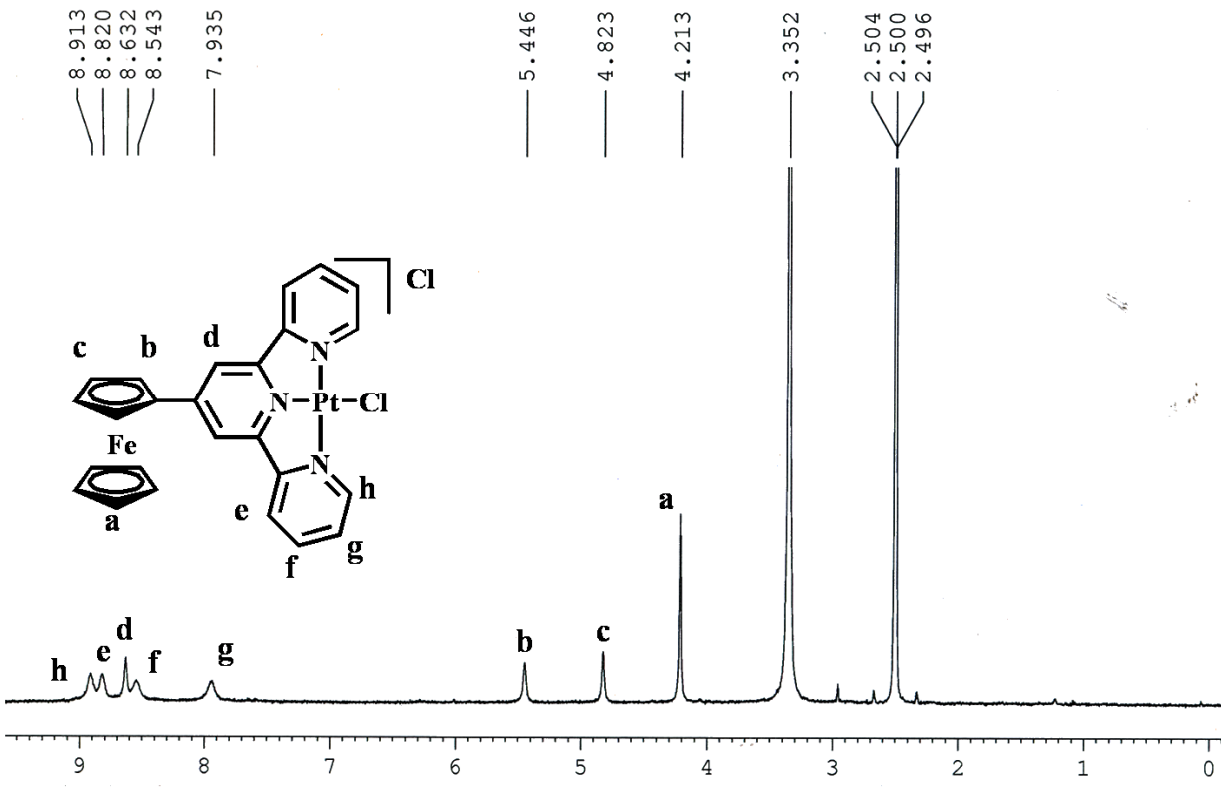

Fig. S5: ^{1}H NMR spectrum of [Pt(Fc-tpy)Cl]Cl (**1**) in DMSO-d_6.

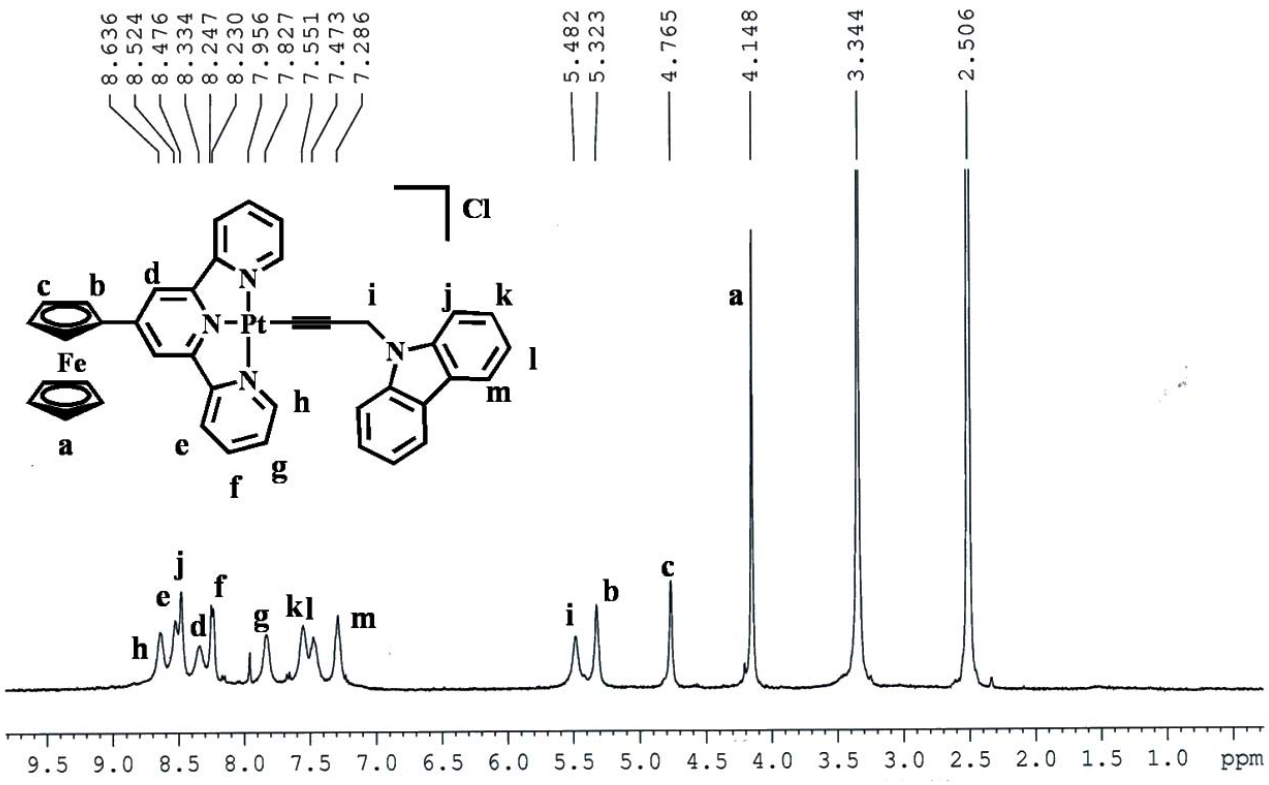

Fig. S6: ^{1}H NMR spectrum of [Pt(Fc-tpy)(NPC)]Cl (**2**) in DMSO-d_6.

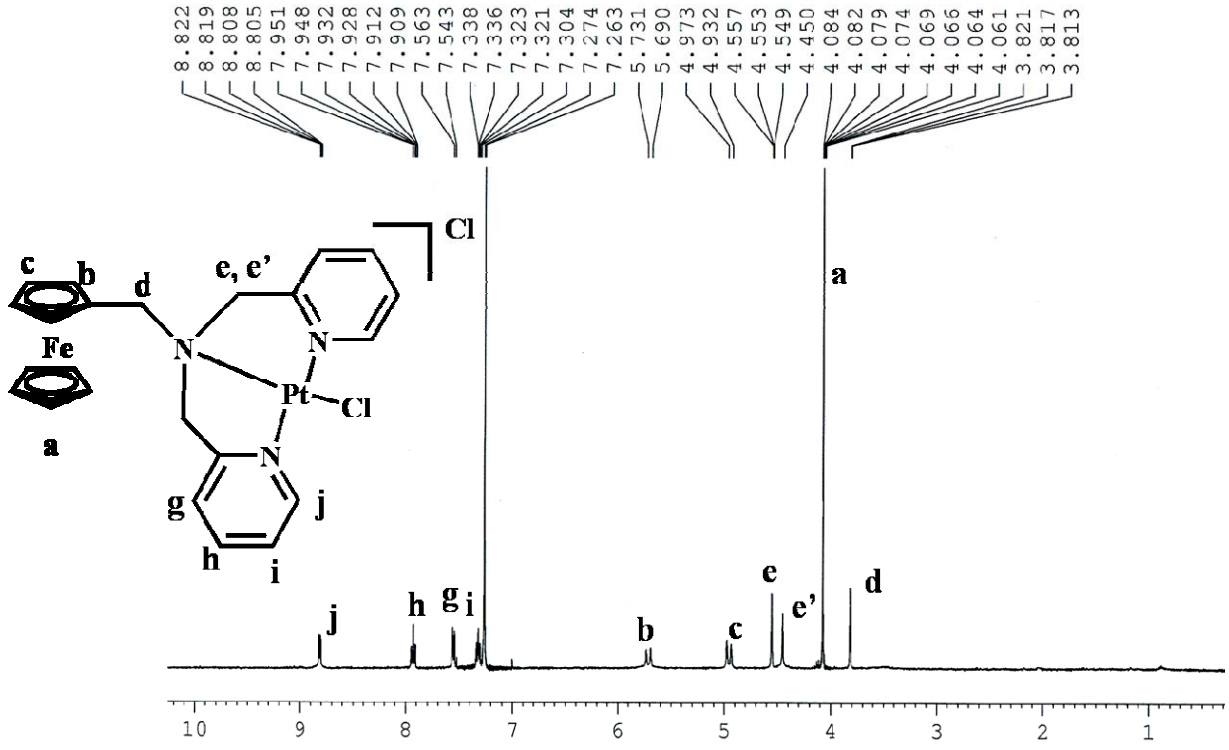

Fig. S7: ^{1}H NMR spectrum of [Pt(Fc-bpa)Cl]Cl (**3**) in $CDCl_3$.

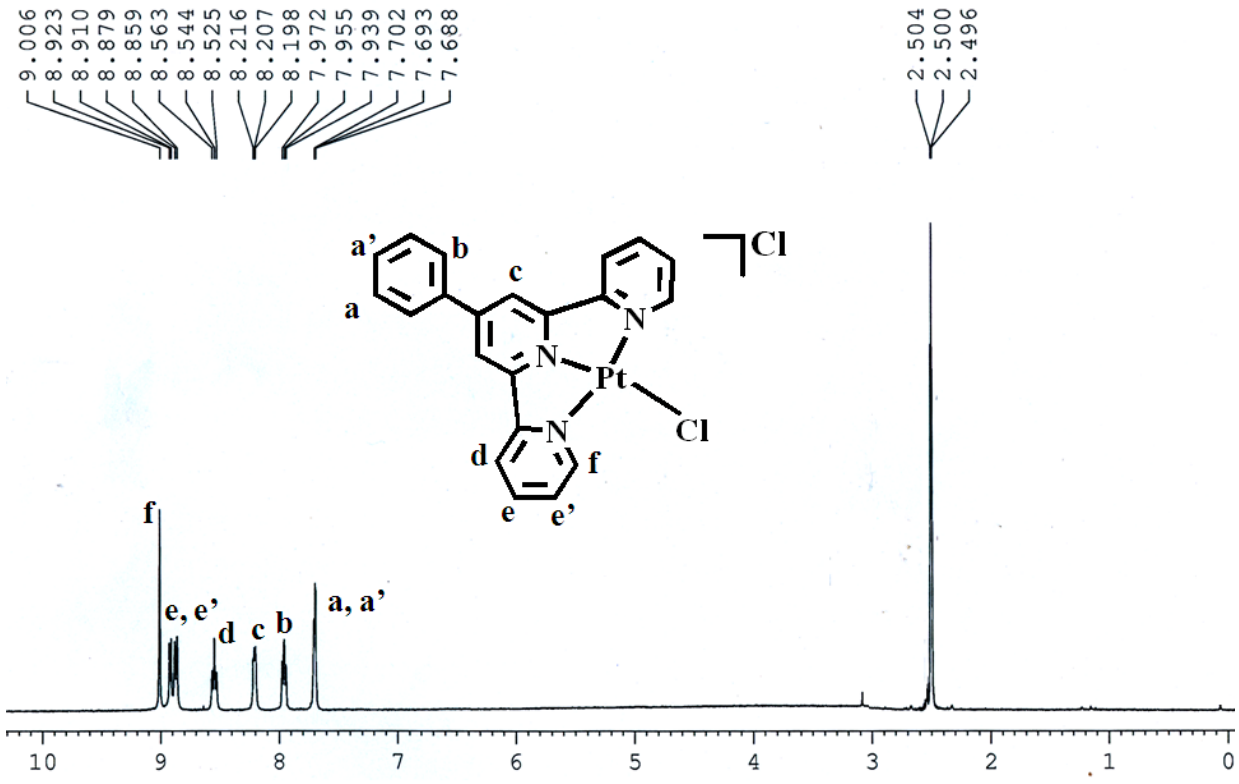

Fig. S8: ^{1}H NMR spectrum of [Pt(Ph-tpy)Cl]Cl (**4**) in DMSO-d_6.

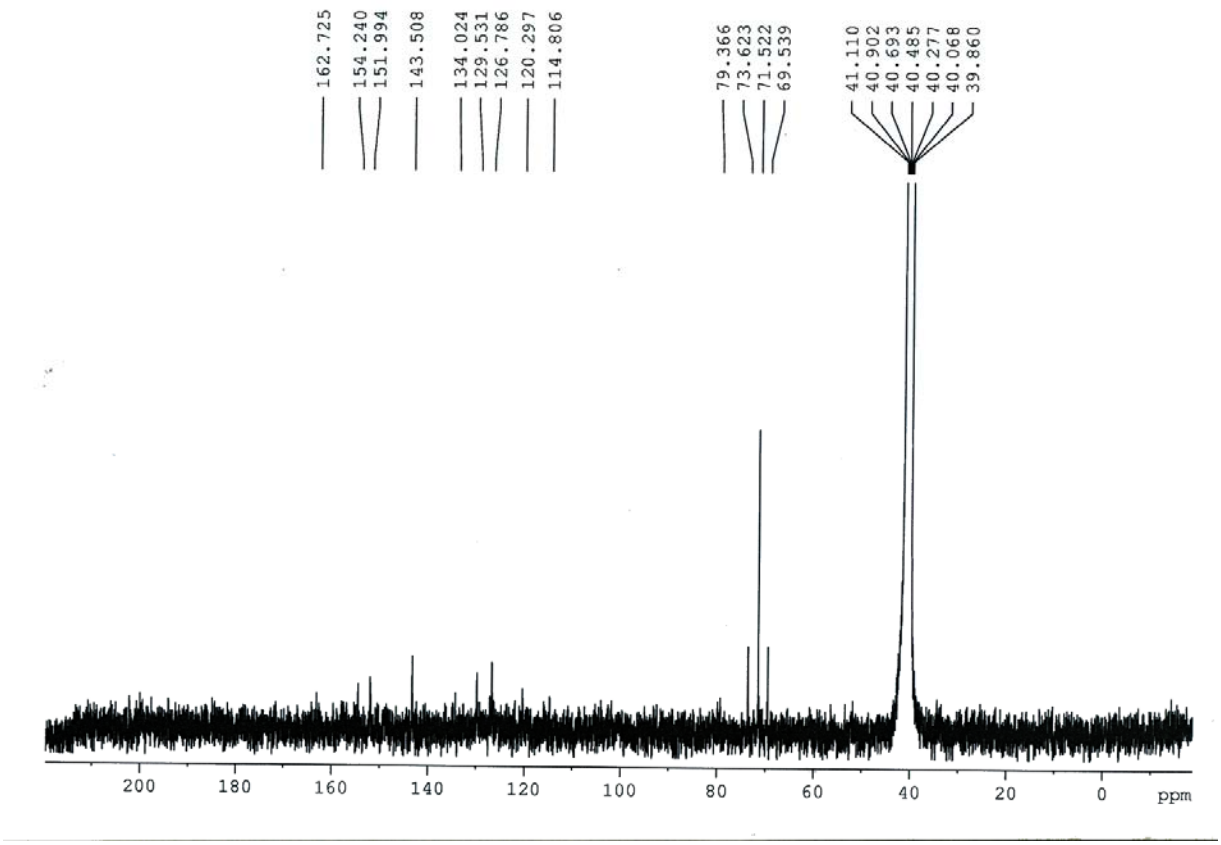

Fig. S9: ^{13}C NMR spectrum of [Pt(Fc-tpy)Cl]Cl (**1**) in DMSO-d_6.

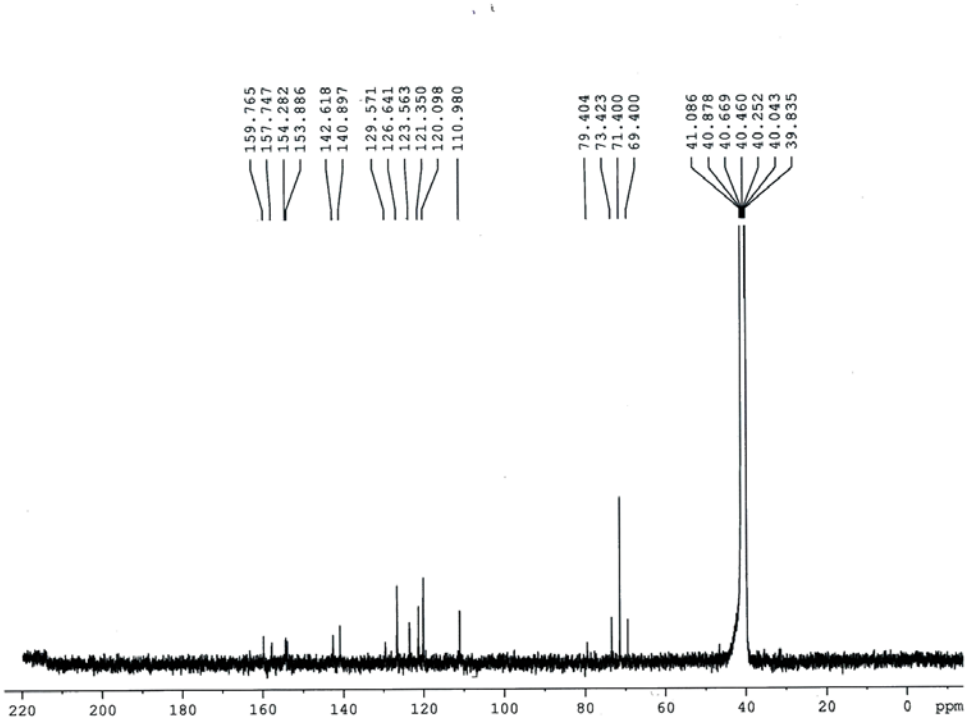

Fig. S10: ^{13}C NMR spectrum of [Pt(Fc-tpy)(NPC)]Cl (**2**) in DMSO-d_6.

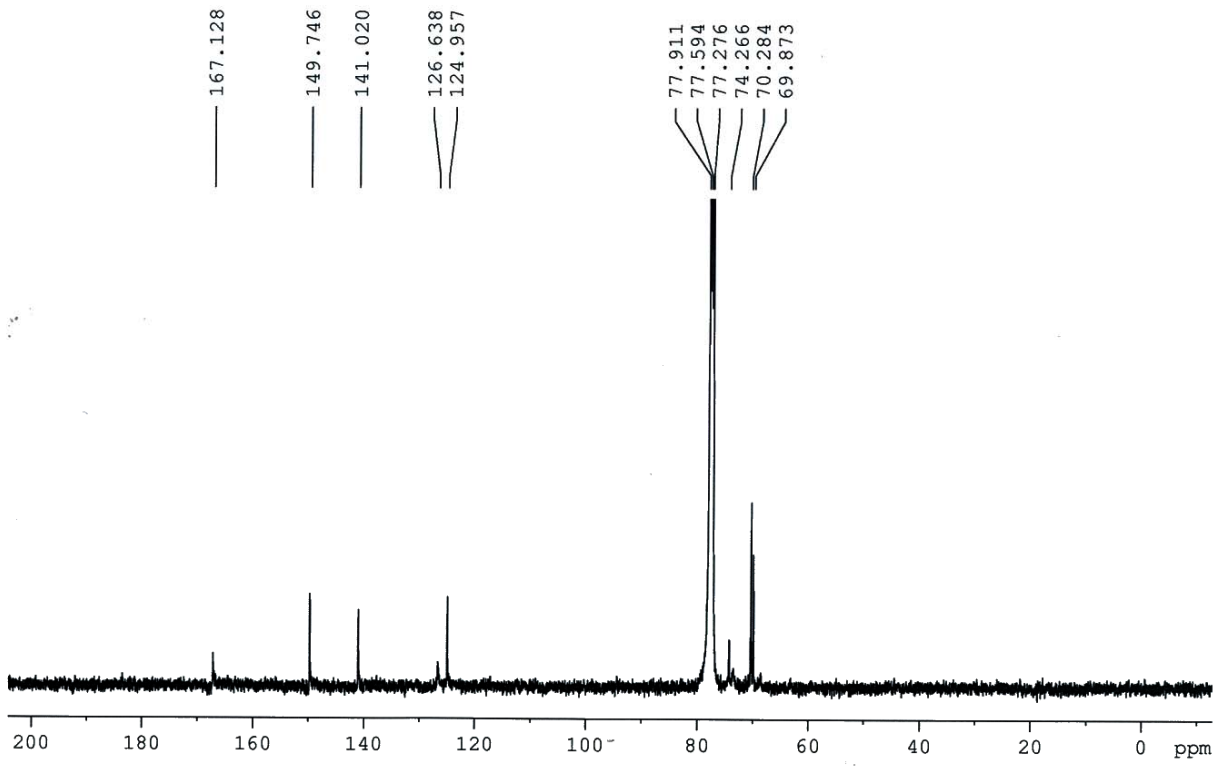

Fig. S11: ^{13}C NMR spectrum of [Pt(Fc-bpa)Cl]Cl (**3**) in $CDCl_3$.

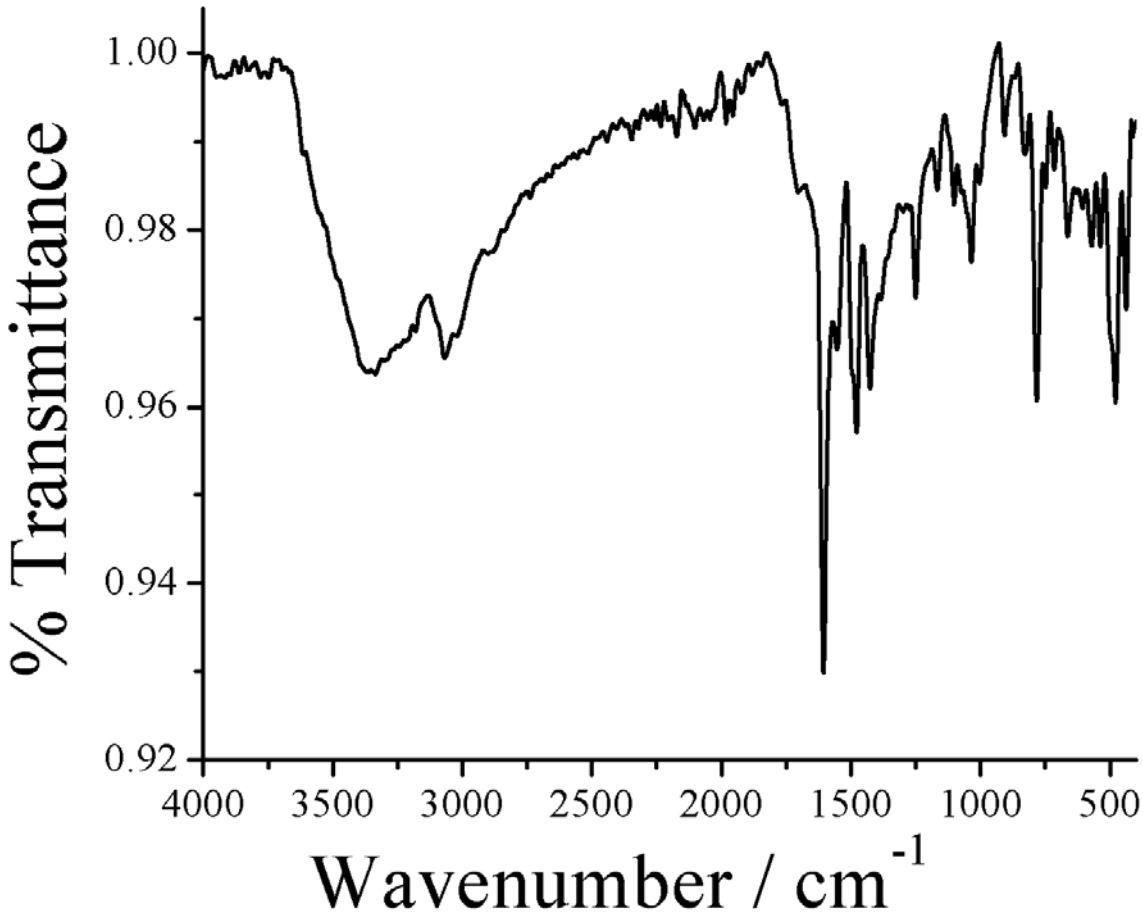

Fig. S12: The IR spectrum of [Pt(Fc-tpy)Cl]Cl (**1**) in solid phase.

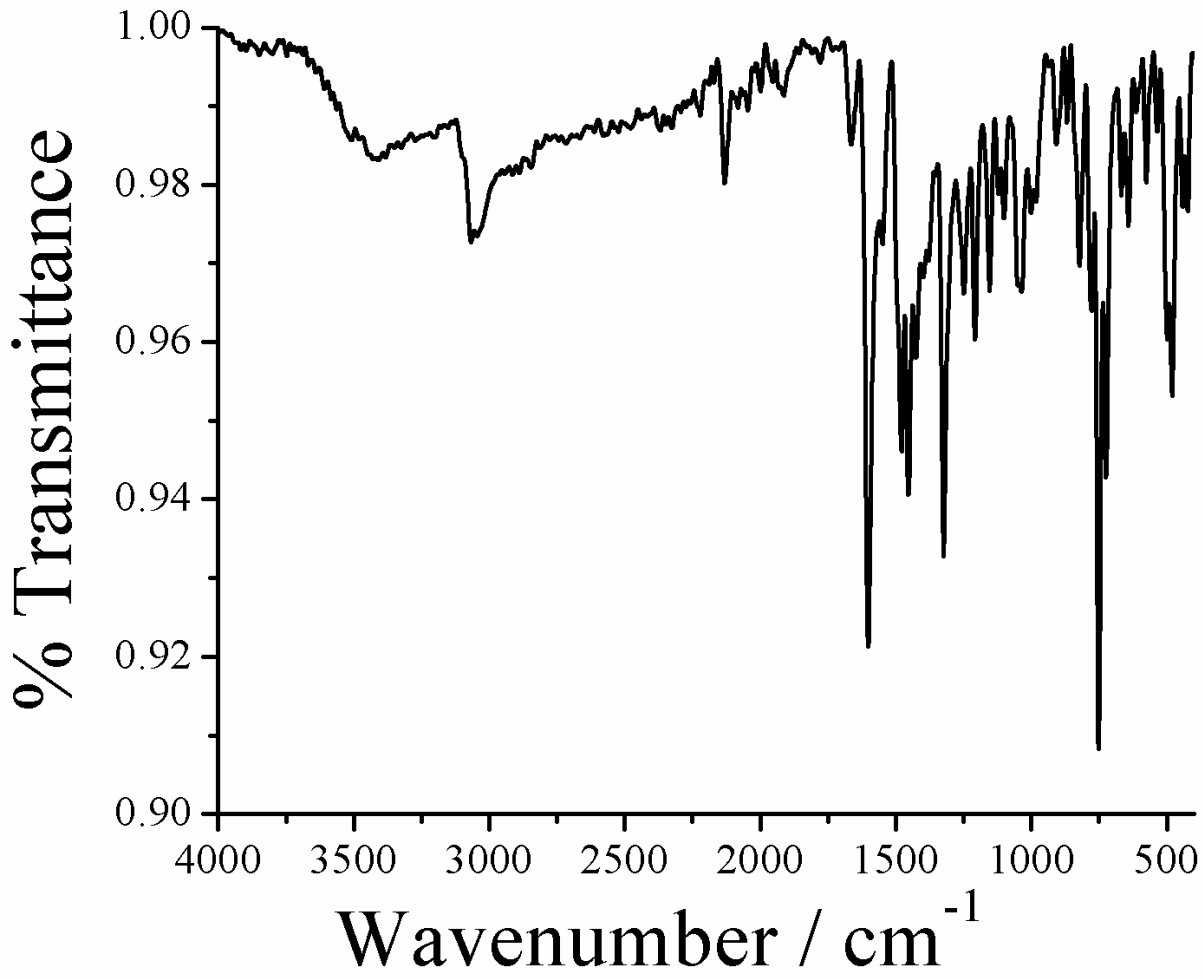

Fig. S13: The IR spectrum of [Pt(Fc-tpy)(NPC)]Cl (**2**) in solid phase.

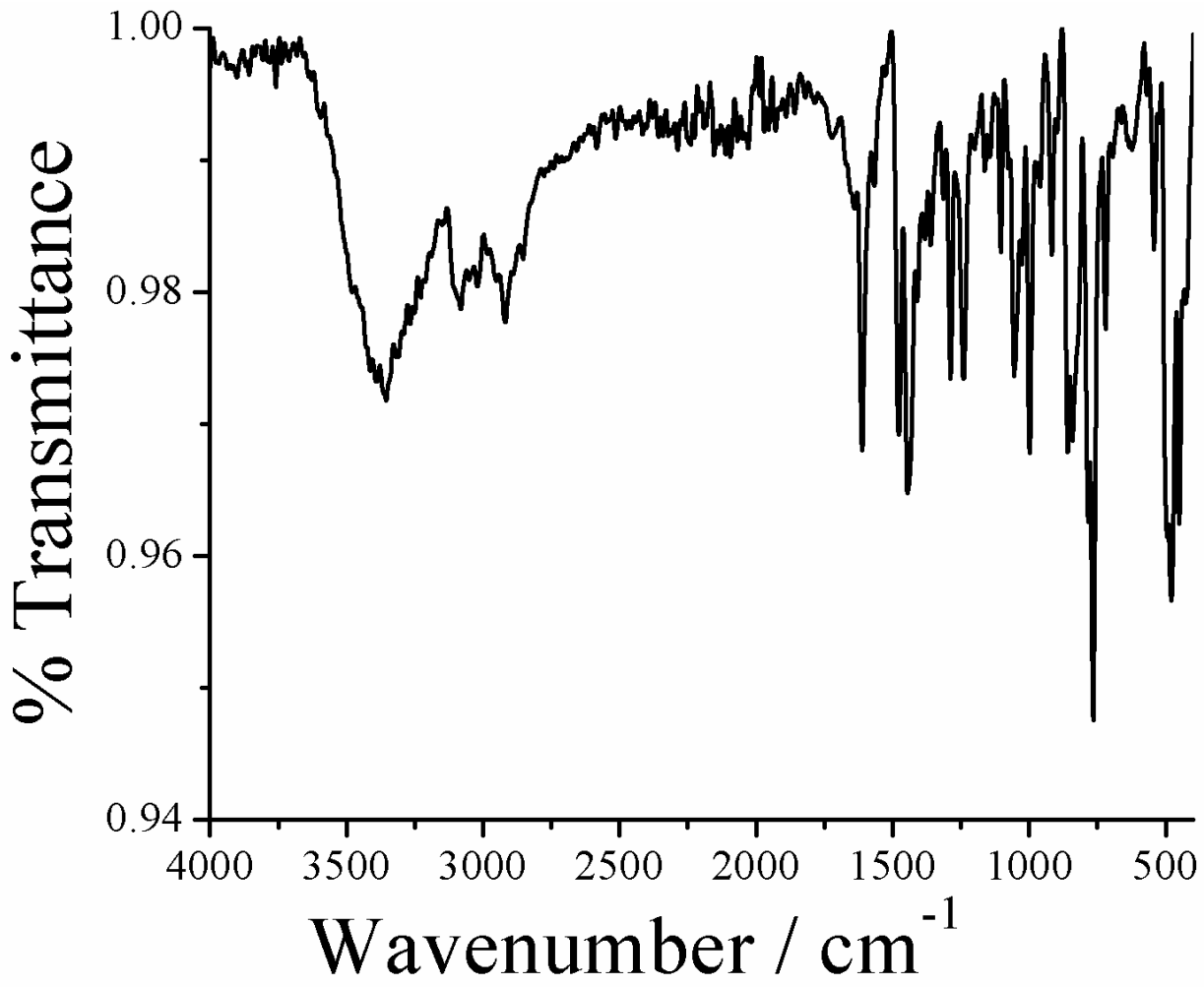

Fig. S14: The IR spectrum of [Pt(Fc-bpa)Cl]Cl (**3**) in solid phase.

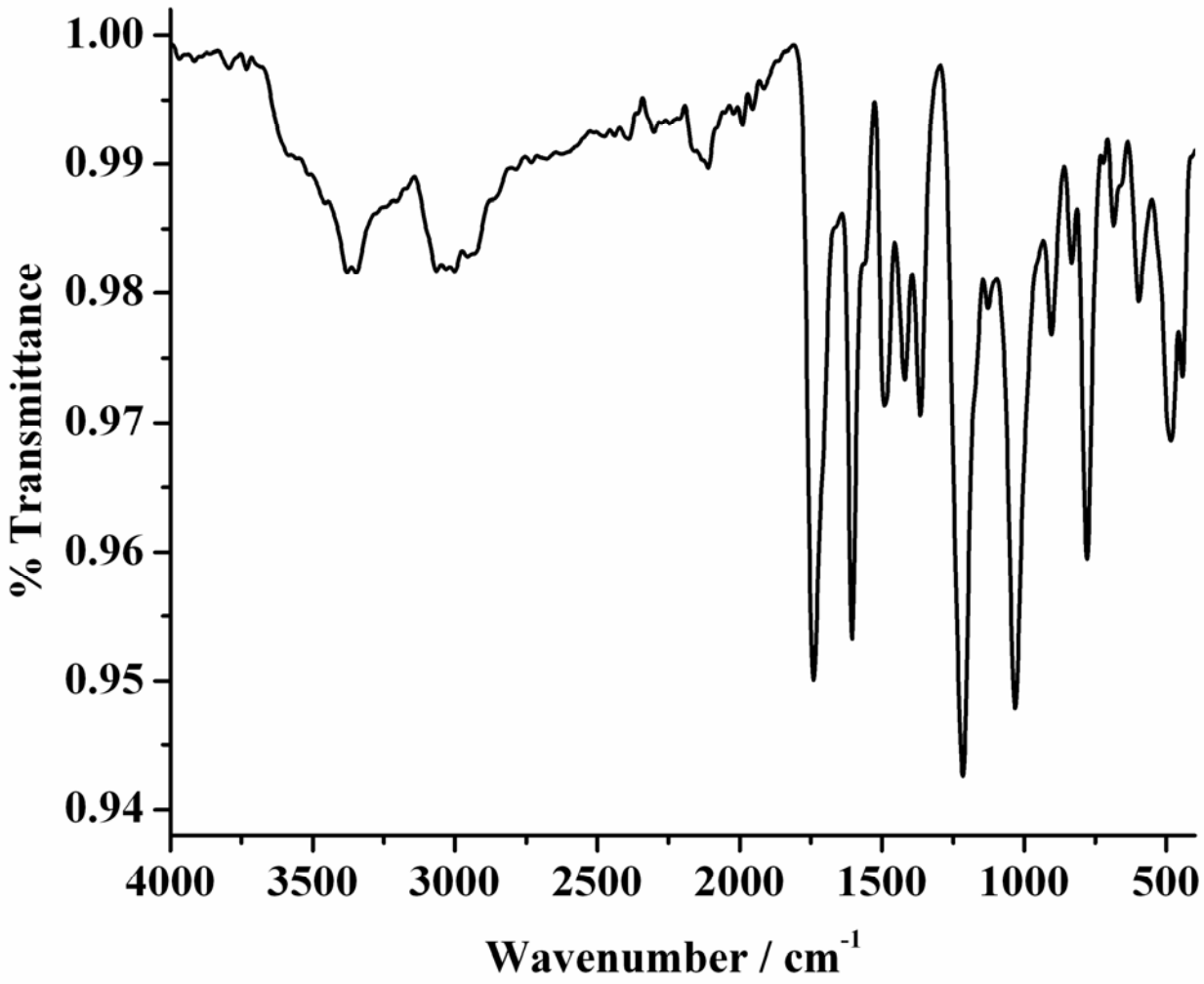

Fig. S15: The IR spectrum of [Pt(Ph-tpy)Cl]Cl (**4**) in solid phase

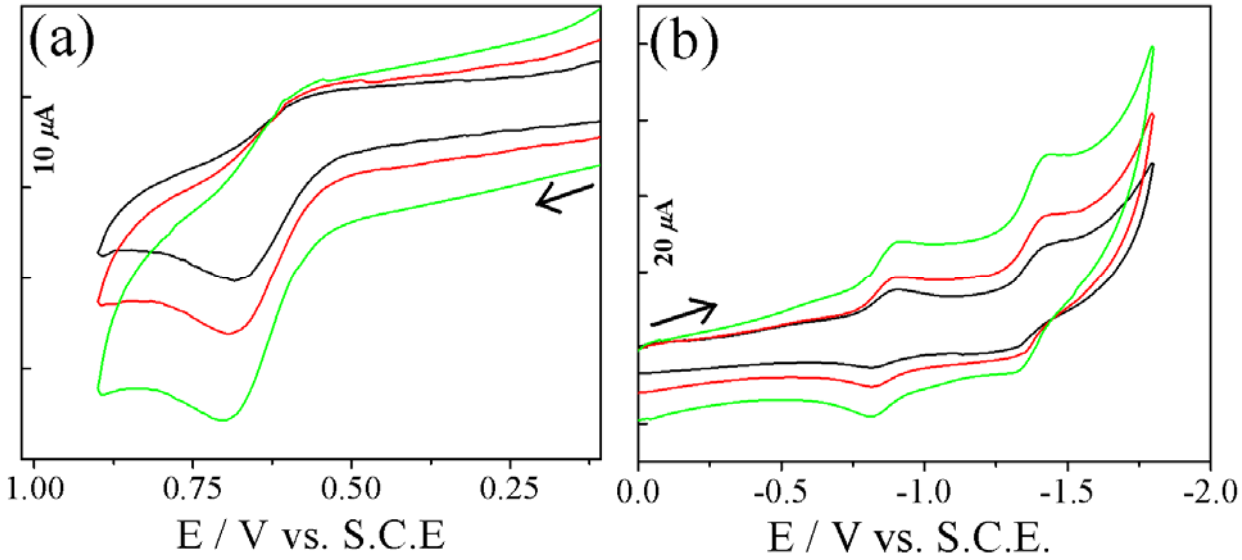

Fig. S16. Cyclic voltammograms of [Pt(Fc-tpy)Cl]Cl (**1**) showing ferrocene oxidation in anodic scan (a) and ligand reductions in cathodic scan (b) in DMF - 0.1 M TBAP with various scan rates (black, red and green for 50, 100 and 200 mV s^{-1} respectively).

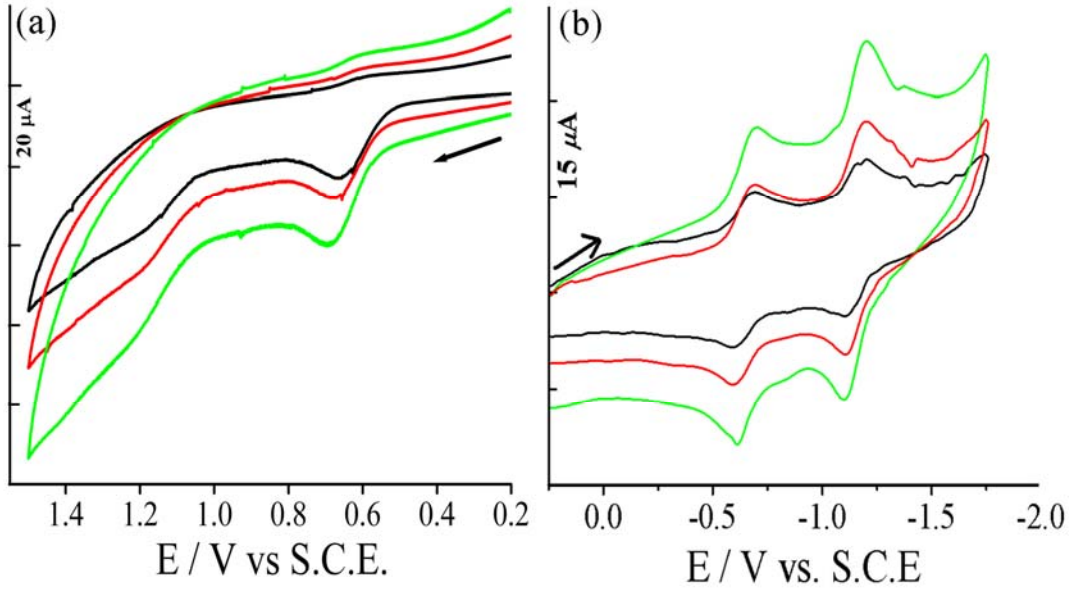

Fig.17. Cyclic voltammogram of [Pt(Fc-tpy)(NPC)]Cl (**2**) showing Fc/Fc^{+} oxidation in anodic scan (a) and ligand reductions in cathodic scan (b) in DMF - 0.1 M TBAP with various scan rates (black, red and green for 50, 100 and 200 mV s^{-1} respectively).

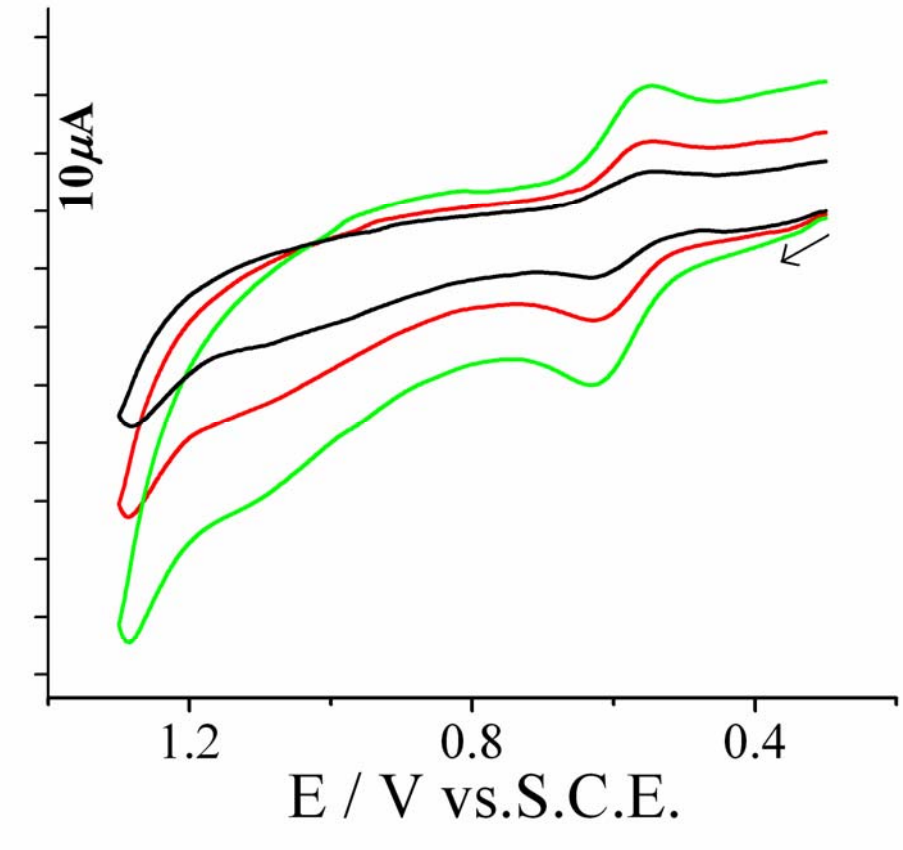

Fig. S18. Cyclic voltammograms of [Pt(Fc-bpa)Cl]Cl (**3**) showing ferrocene oxidation in anodic scan in DMF solution containing 0.1 M TBAP with various scan rates (black, red and green for 50, 100 and 200 mV s^{-1} respectively).

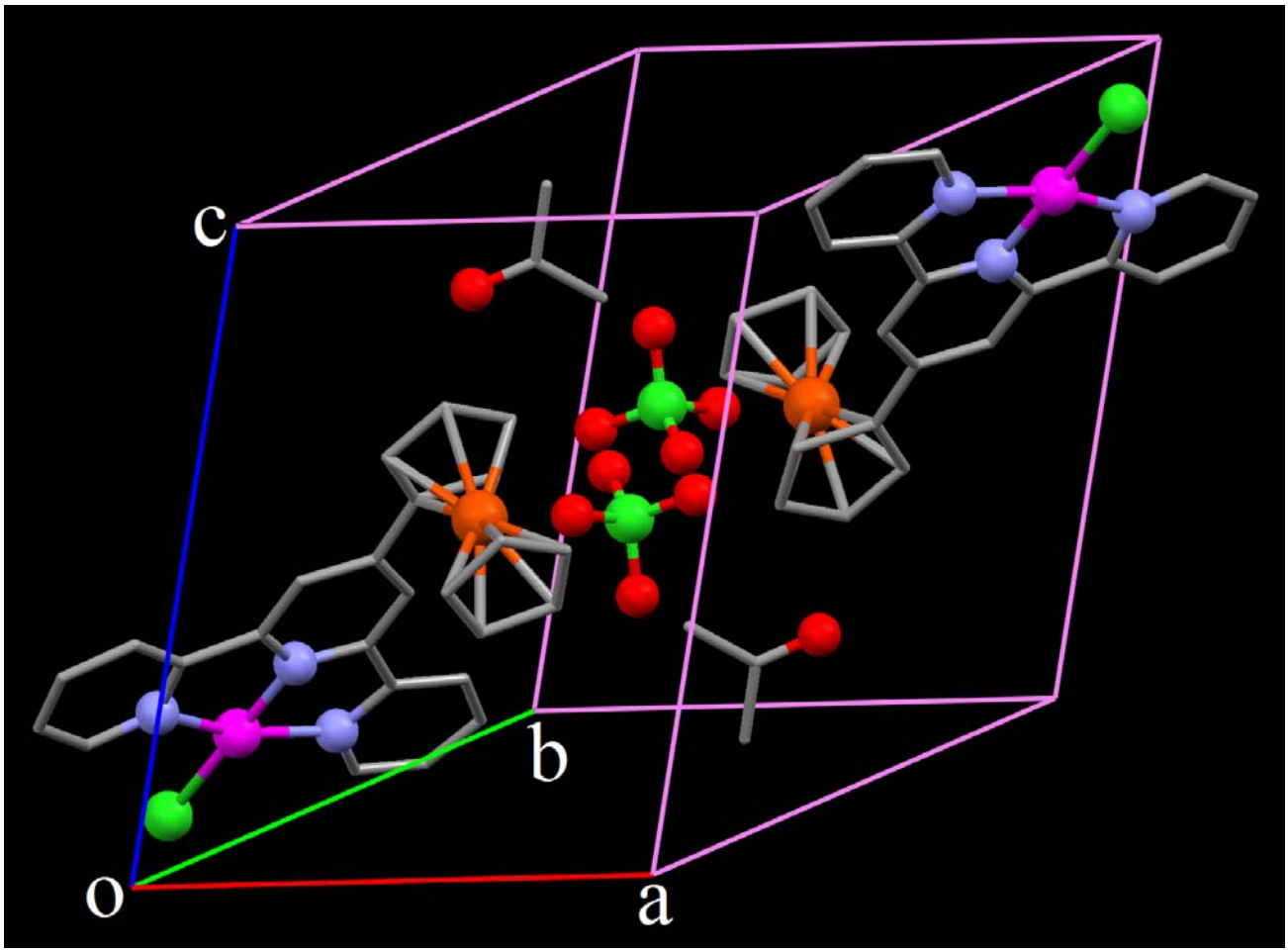

Fig. S19. Unit cell packing diagram for the complex [Pt(Fc-tpy)Cl]ClO_4.CH_3COCH_3 (**1a**.CH_3COCH_3). The complex crystallized in triclinic *P*-1 space group with $Z = 2$. The hydrogen atoms are not shown for clarity.

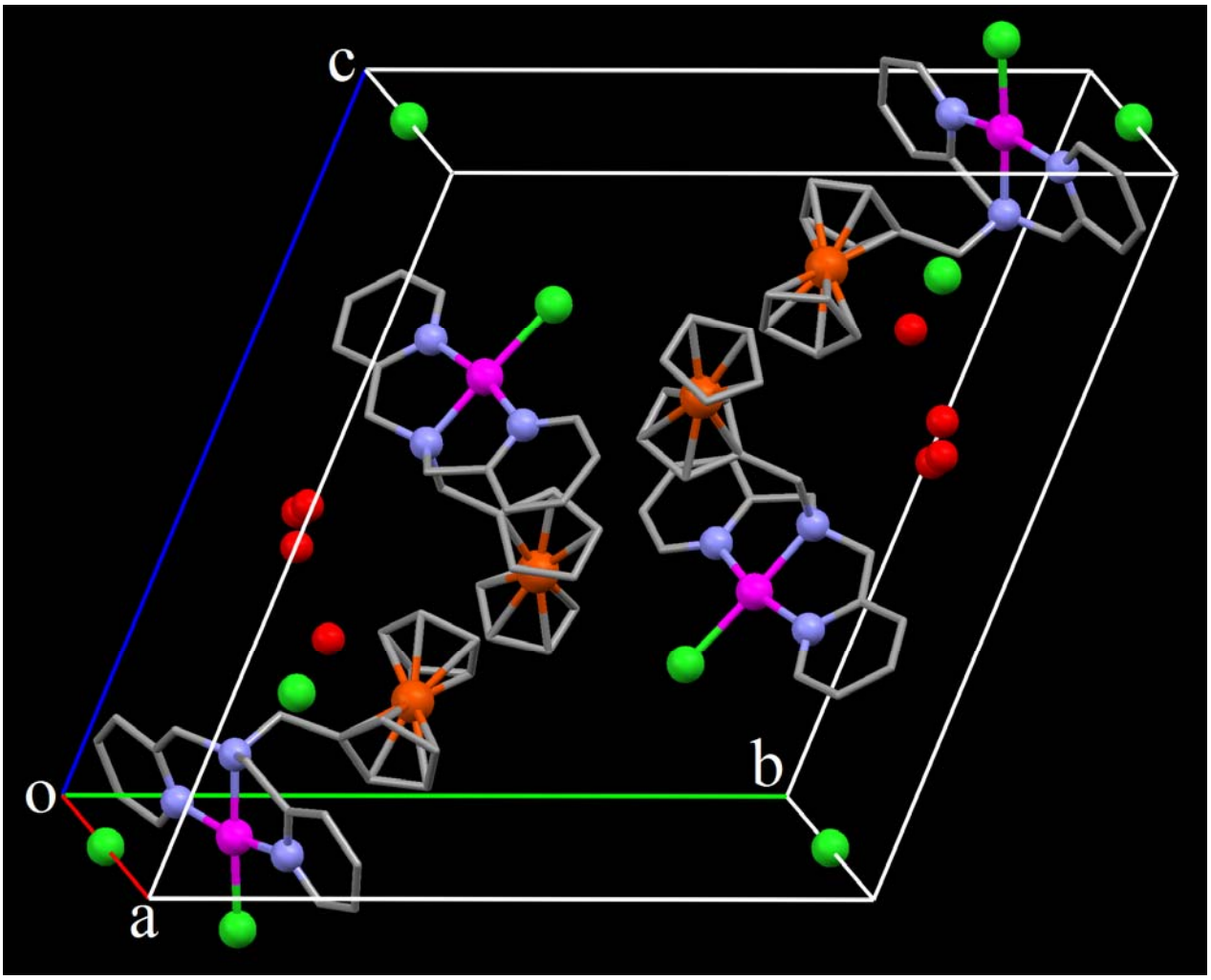

Fig. S20. Unit cell packing diagram for the complex [Pt(Fc-bpa)Cl]Cl.2H_2O (**3**.2H_2O). The complex crystallized in triclinic *P*-1 space group with $Z = 4$. The hydrogen atoms are not shown for clarity.

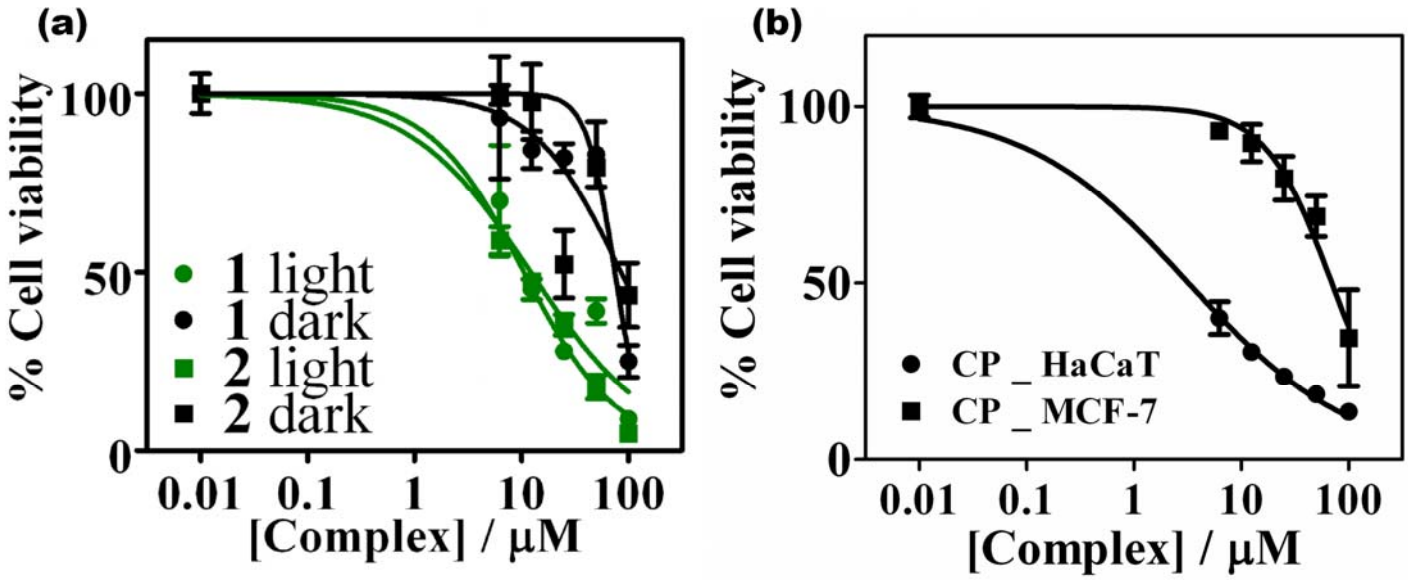

Fig. S21. Photocytotoxicity of (a) complexes **1** and **2** in MCF-7 cells on 24hr incubation in dark, followed by 1 hr exposure to visible light (400-700nm) and (b) cisplatin in HaCaT and MCF-7 cells on 24hr incubation in dark. as determined by the MTT assay. The light-exposed cells and the dark-treated cells are shown by green and black symbols respectively.

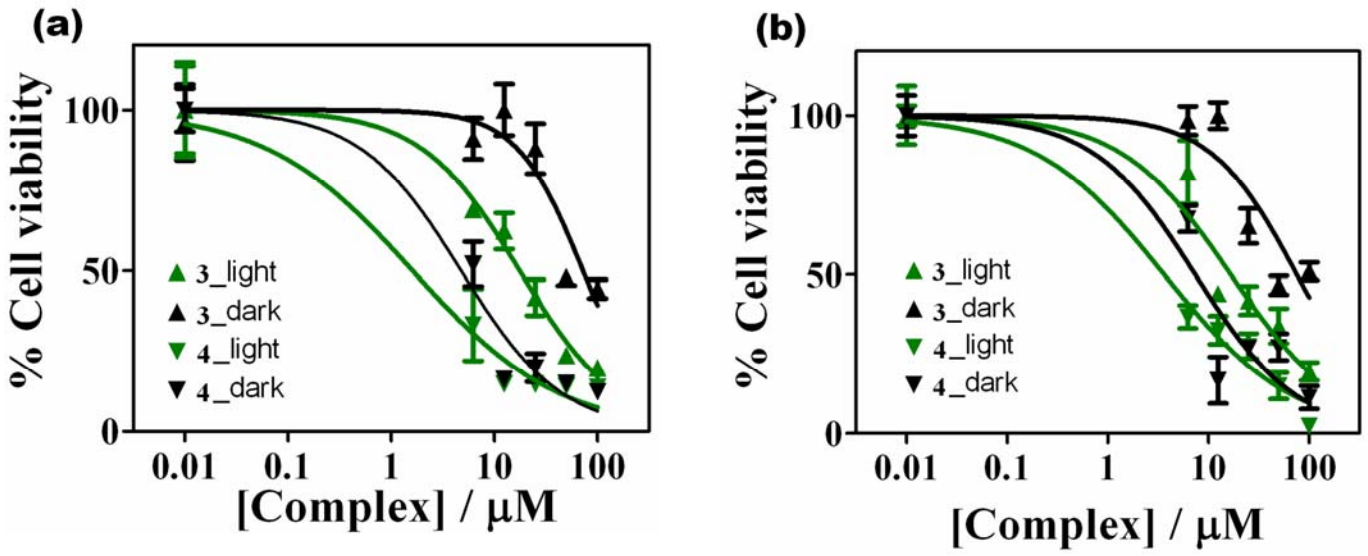

Fig. S22. Photocytotoxicity of complexes **3** and **4** in (a) HaCaT and (b) MCF-7 cells on 24hr incubation in dark, followed by 1 hr exposure to visible light (400-700nm) as determined by the MTT assay. The light-exposed cells and the dark-treated cells are shown by green and black symbols respectively.

(a)

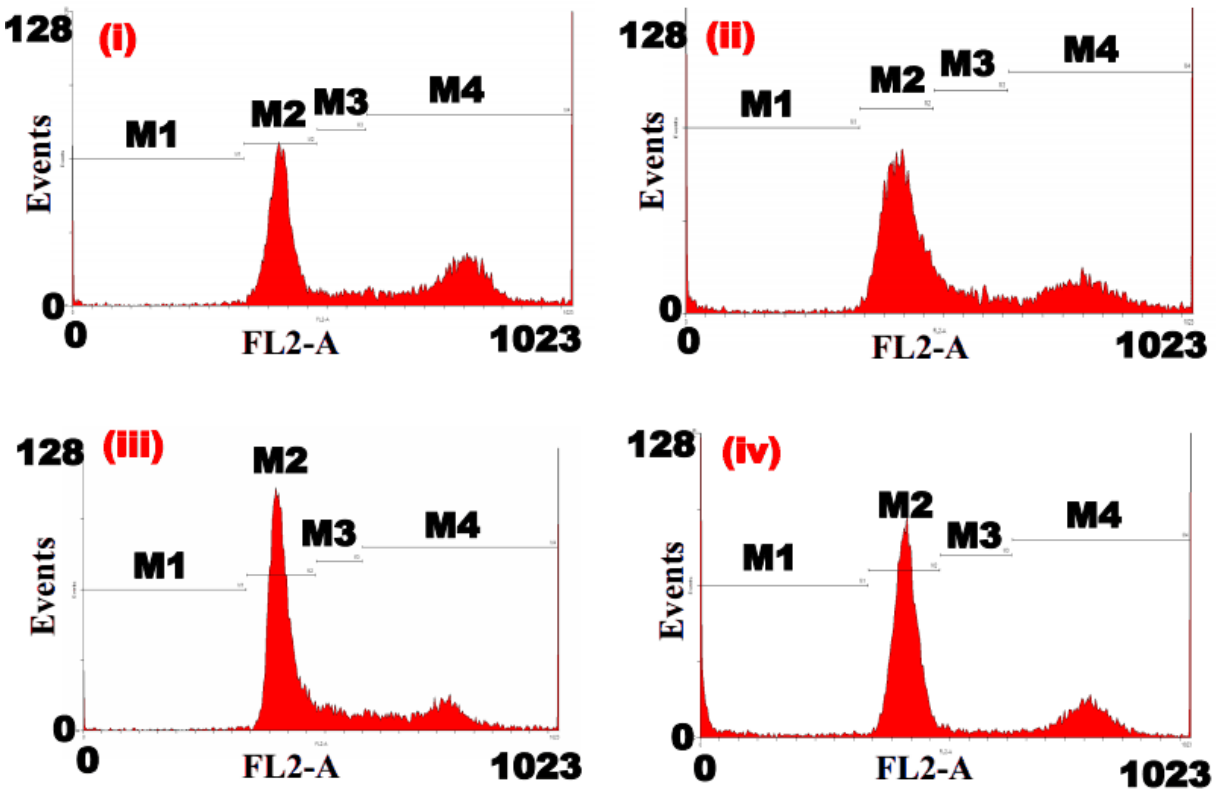

Fig. S23a. Cell cycle analysis done on HaCaT cells using flow cytometry. Figure showing cell populations in different phases of cell cycle as denoted by M1-SubG1, M2-G1, M3-S, M4-G2/M. (i) cells treated with **1** in dark, (ii) cells treated with **1** in light, (iii) cells treated with **2** in dark, (iv) cells treated with **2** in light. Complex concentration : 15 μM, light exposure = 1h.

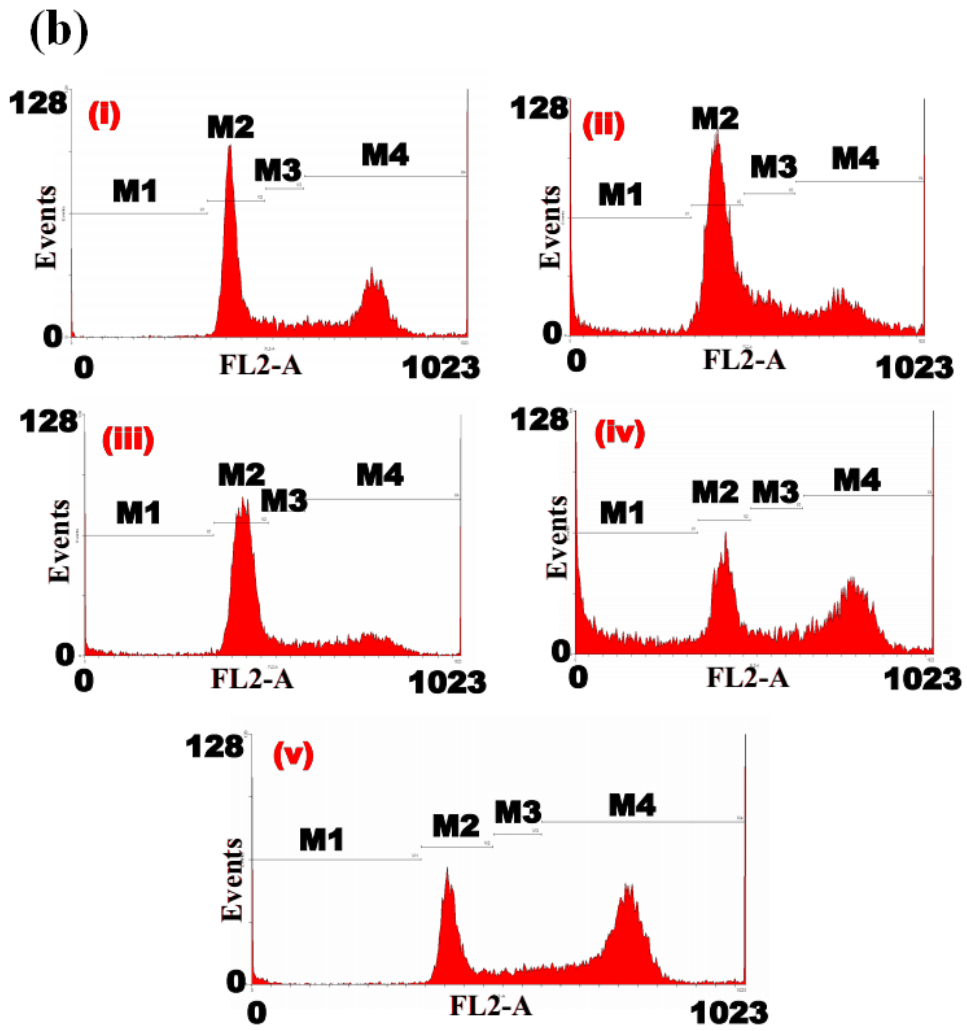

Fig. S23b. Cell cycle analysis done on HaCaT cells using flow cytometry. Figure showing cell populations in different phases of cell cycle as denoted by M1-SubG1, M2-G1, M3-S, M4-G2/M. (i) cells treated with **3** in dark, (ii) cells treated with **3** in light, (iii) cells treated with **4** in dark, (iv) cells treated with **4** in light, (v) cells treated with cisplatin in dark. Complex concentration : **3** (20 μM), **4** (10 μM), cisplatin (10 μM), light exposure = 1h.

(a) Cells alone

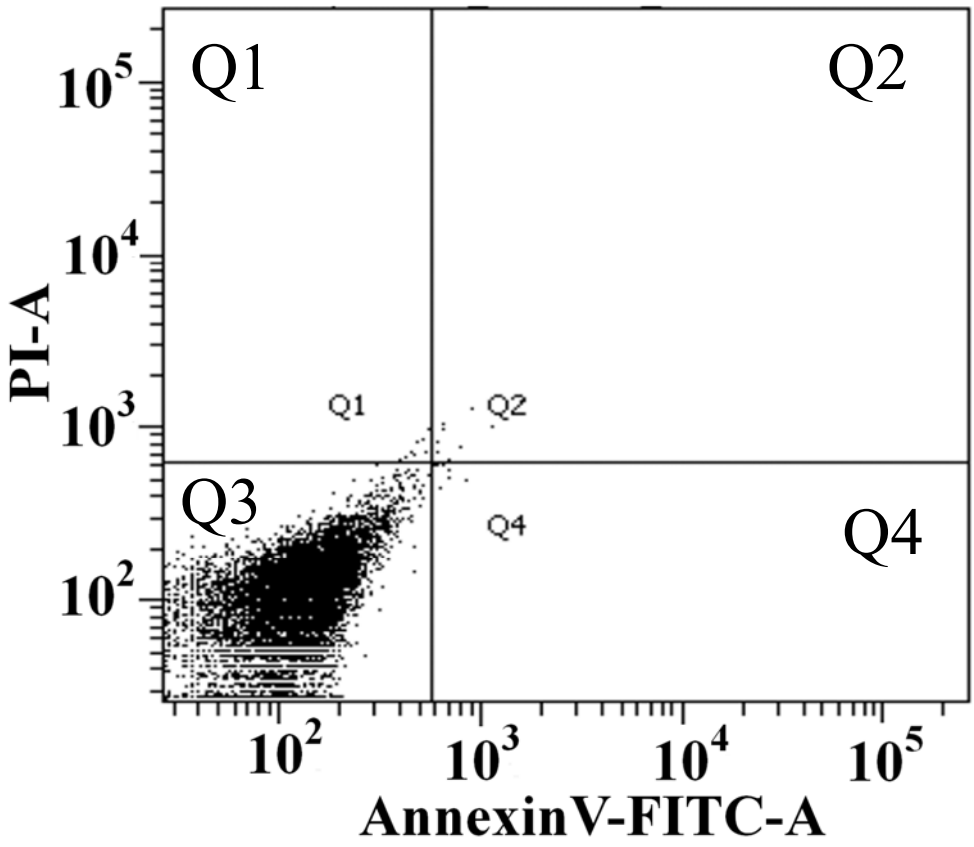

Quadrants	% Population
Q1 (Upper left)	0.1
Q2 (Upper right)	0.1
Q3 (Lower left)	99.7
Q4 (Lower right)	0.1

(b) Cells + PI

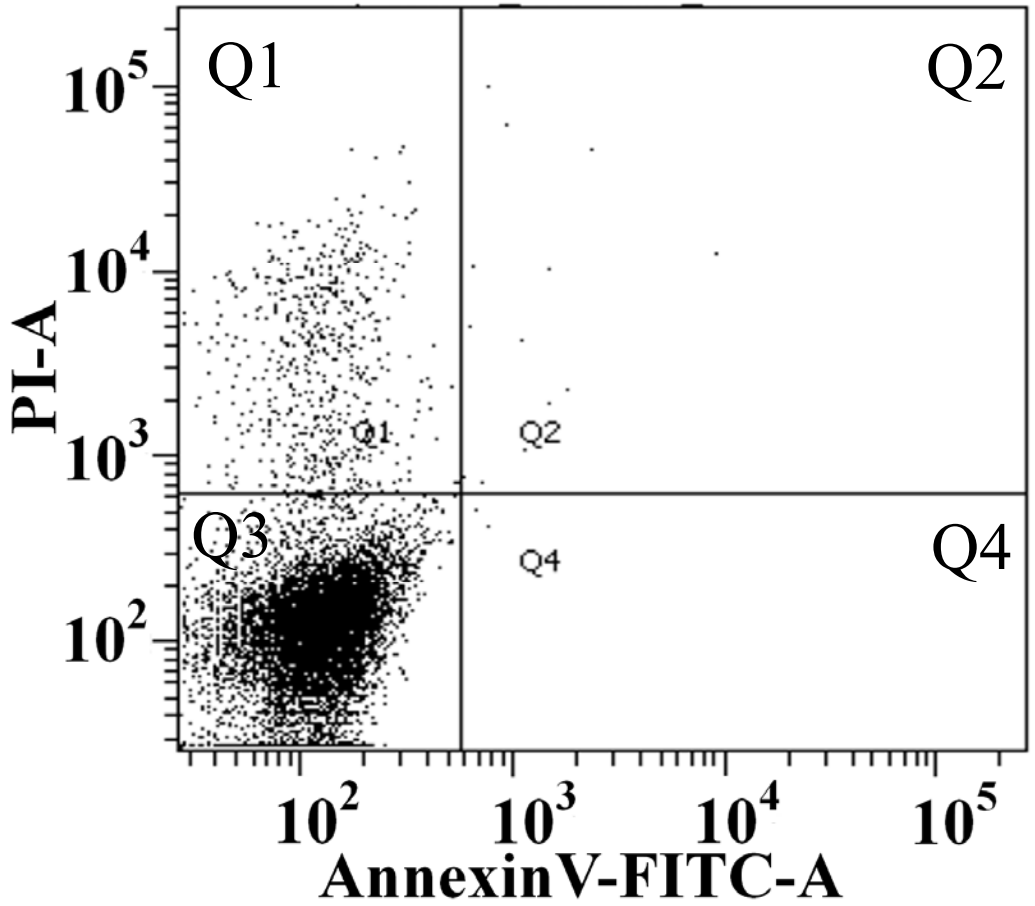

Quadrants	% Population
Q1 (Upper left)	6.0
Q2 (Upper right)	0.1
Q3 (Lower left)	93.7
Q4 (Lower right)	0.0

(c) Cells + Annexin V-FITC

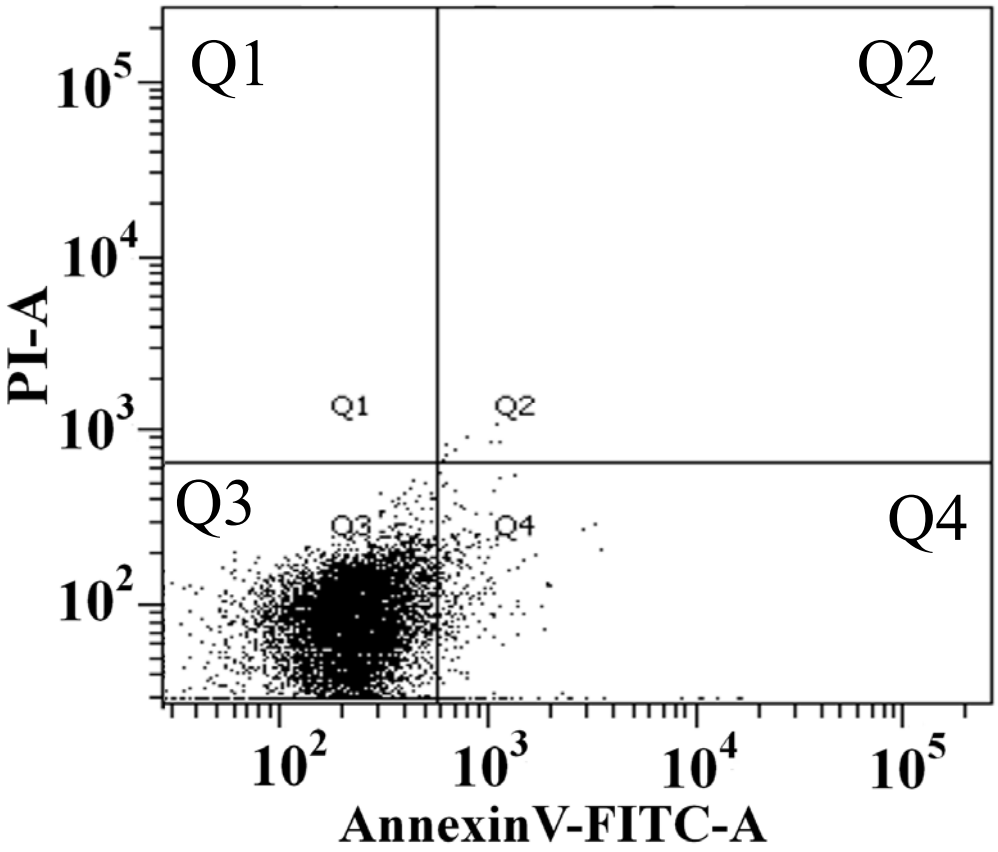

Quadrants	% Population
Q1 (Upper left)	0.0
Q2 (Upper right)	0.1
Q3 (Lower left)	96.9
Q4 (Lower right)	3.0

(d) Cells + PI + Annexin V-FITC

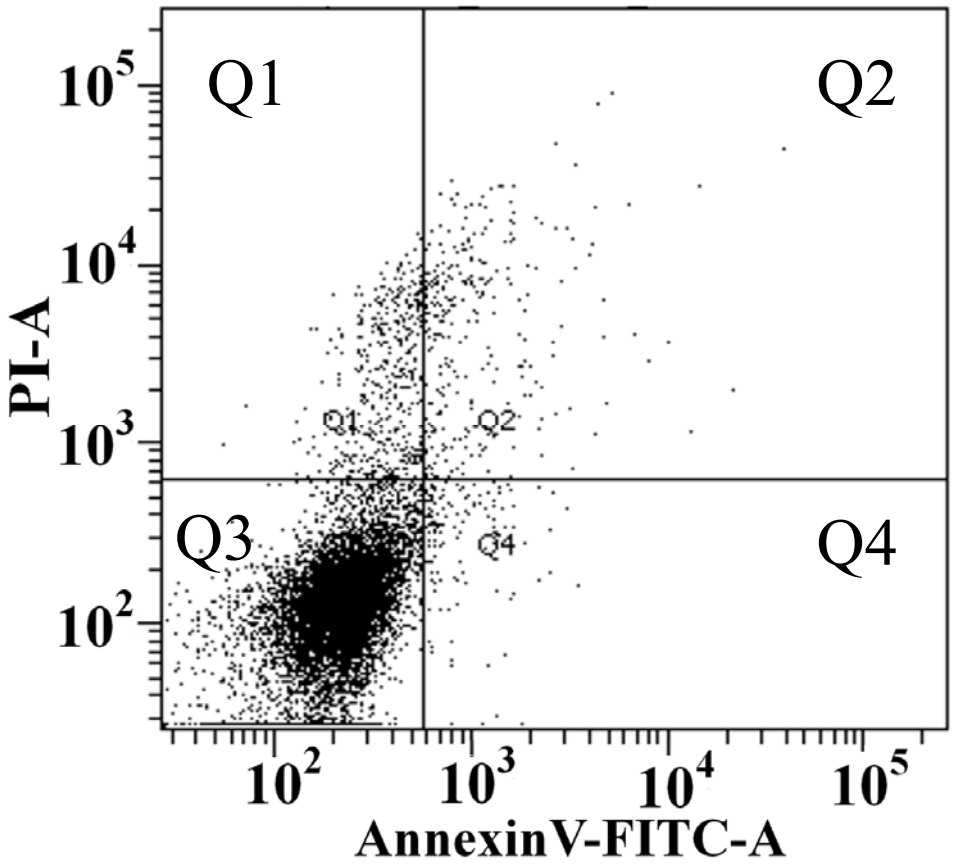

Quadrants	% Population
Q1 (Upper left)	4.1
Q2 (Upper right)	3.2
Q3 (Down left)	90.9
Q4 (Down right)	1.8

Fig. S24. AnnexinV/FITC-PI assay using flow cytometry in HaCaT cell lines for (a) cells alone, (b) cells treated with PI, (c) cells treated with AnnexinV-FITC. The values in the table show the percentage population of cells in each quandrant: dead (Q1), late apoptotic (Q2), viable cells (Q3) and early apoptotic (Q4).

(a) Cells + PI + Annexin V-FITC + **3** (Dark)

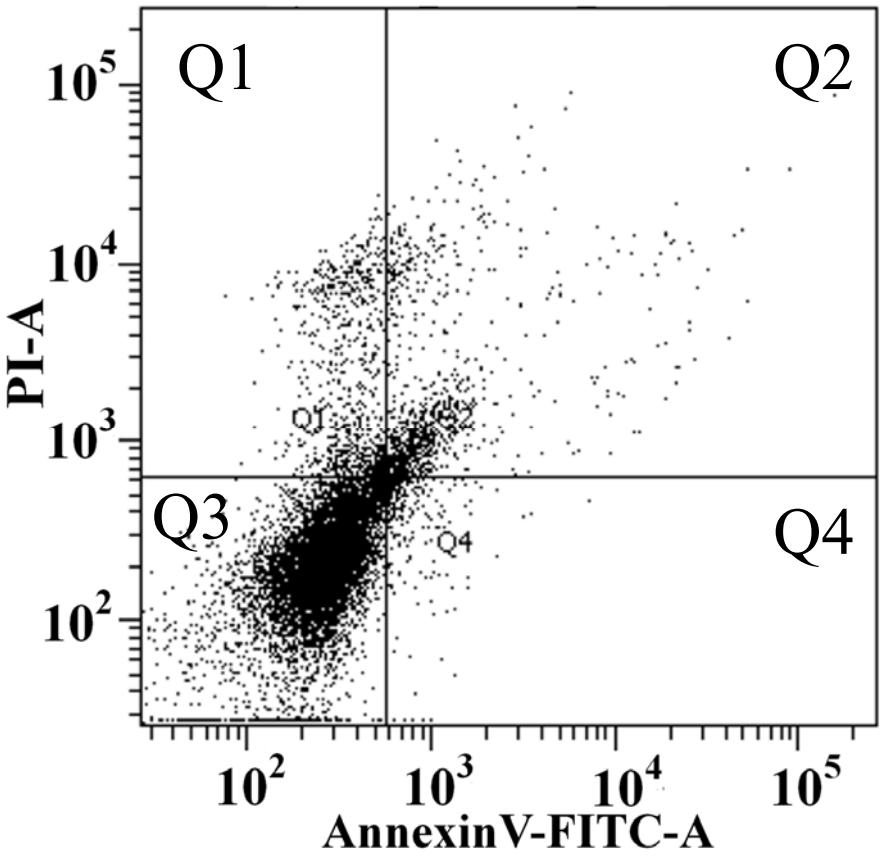

Quadrants	% Population
Q1 (Upper left)	7.4
Q2 (Upper right)	9.6
Q3 (Down left)	79.2
Q4 (Down right)	3.8

(b) Cells + PI + Annexin V-FITC + **3** (Light)

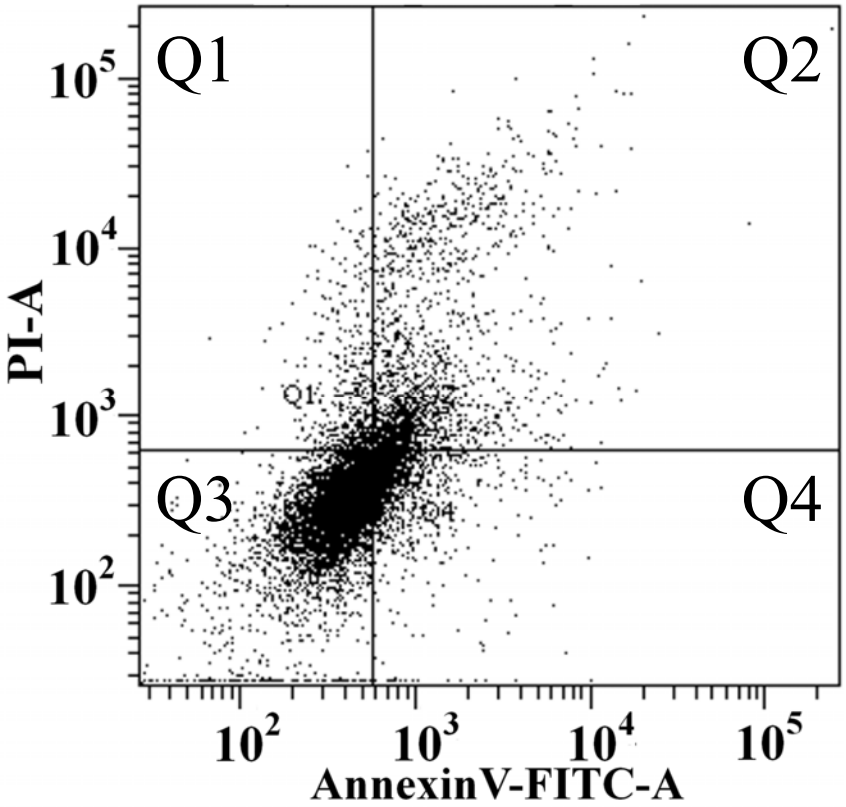

Quadrants	% Population
Q1 (Upper left)	4.0
Q2 (Upper right)	16.9
Q3 (Down left)	57.6
Q4 (Down right)	21.4

Fig. S25. AnnexinV/FITC-PI assay using flow cytometry in HaCaT cell lines treated with complex **3** (10 μM)) for 4 hr (a) in dark (b) in light. The values in the table show the percentage population of cells in each quandrant: dead (Q1), late apoptotic (Q2), viable cells (Q3) and early apoptotic (Q4).

(a) Cells + PI + Annexin V-FITC + **4** (Dark)

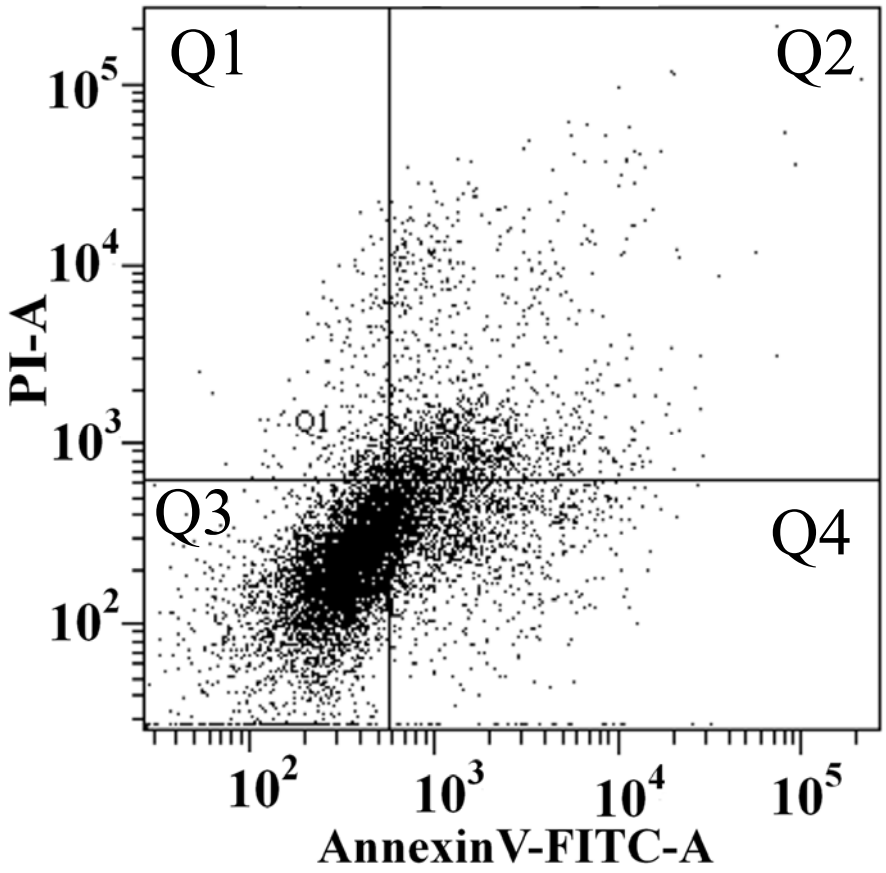

Quadrants	% Population
Q1 (Upper left)	2.9
Q2 (Upper right)	14.1
Q3 (Down left)	60.8
Q4 (Down right)	22.2

(b) Cells + PI + Annexin V-FITC + **4** (Light)

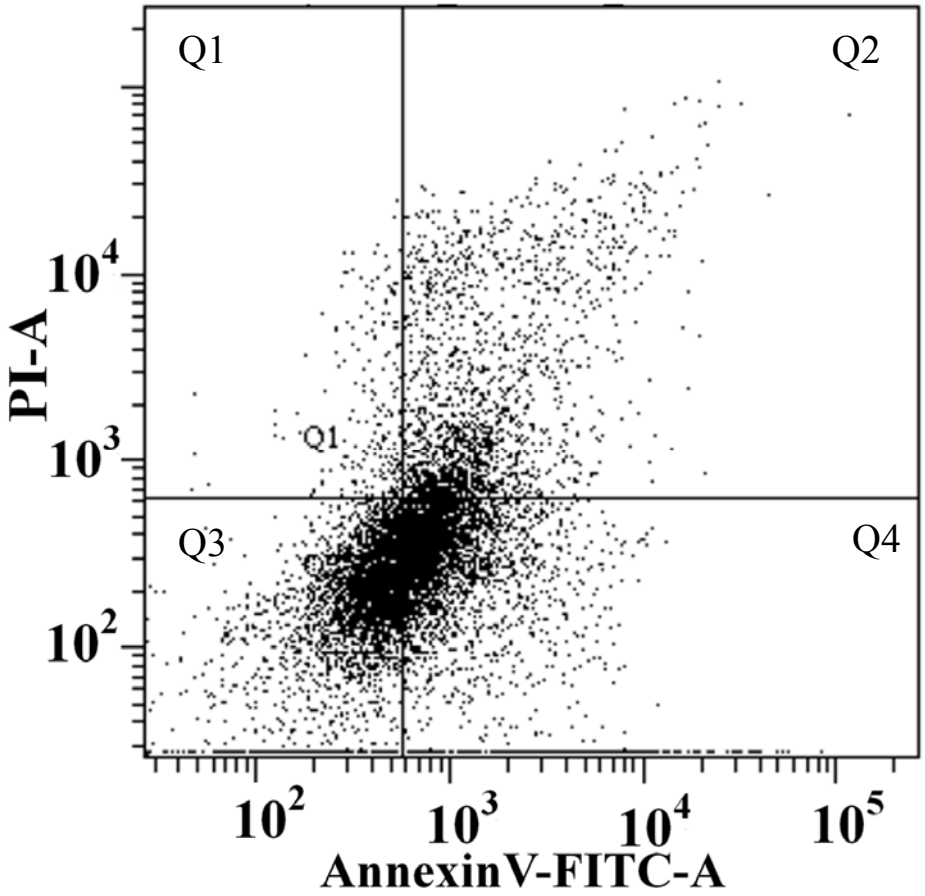

Quadrants	% Population
Q1 (Upper left)	2.0
Q2 (Upper right)	17.5
Q3 (Down left)	37.7
Q4 (Down right)	42.9

Fig. S26. AnnexinV/FITC-PI assay using flow cytometry in HaCaT cell lines treated with complex **4** (10 μM)) for 4 hr (a) in dark (b) in light. The values in the table show the percentage population of cells in each quandrant: dead (Q1), late apoptotic (Q2), viable cells (Q3) and early apoptotic (Q4).

(a) Cells + PI + Annexin V-FITC + cisplatin (dark)

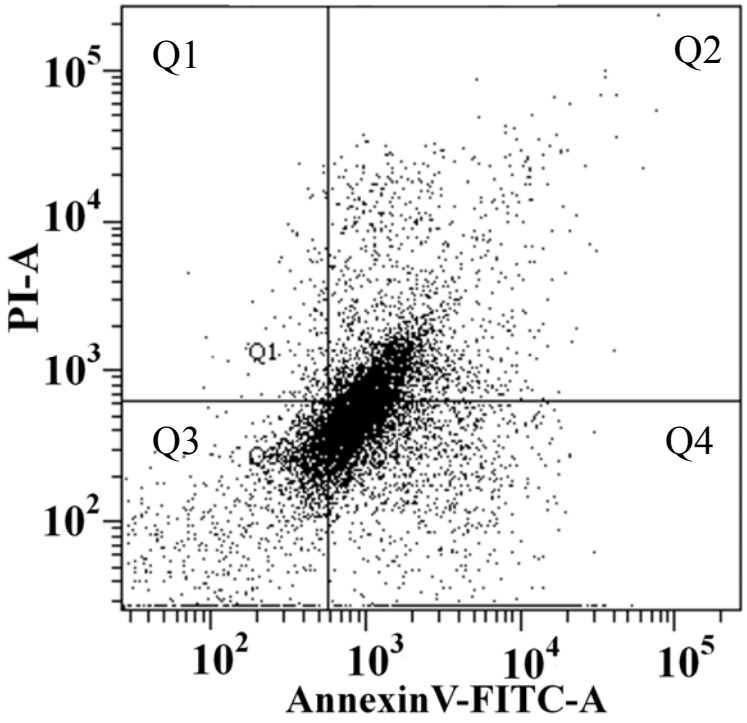

Quadrants	% Population
Q1 (Upper left)	1.3
Q2 (Upper right)	28.5
Q3 (Down left)	17.7
Q4 (Down right)	52.5

Fig. S27. AnnexinV/FITC-PI assay using flow cytometry in HaCaT cell lines treated with cisplatin (10 μM) for 4 hr in dark. The values in the table show the percentage population of cells in each quandrant: dead (Q1), late apoptotic (Q2), viable cells (Q3) and early apoptotic (Q4).

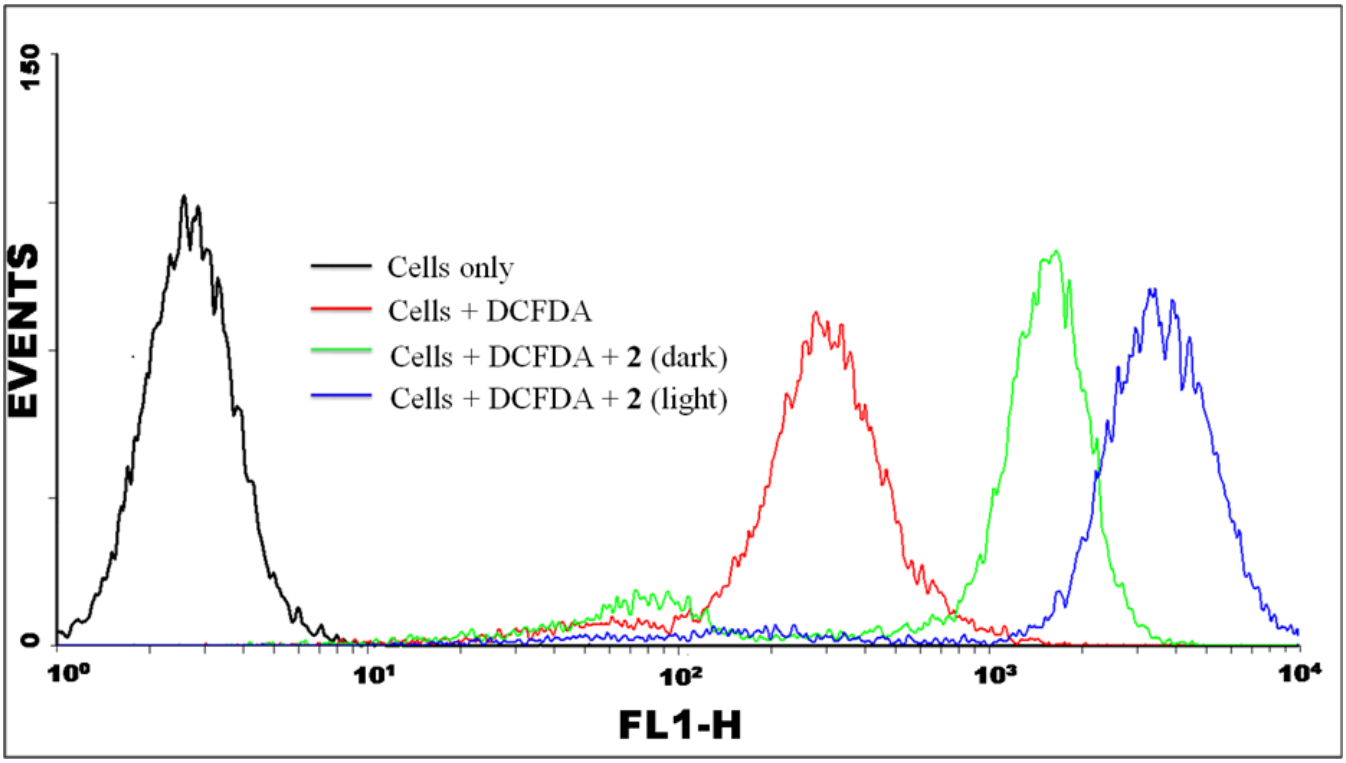

Fig. S28. DCFDA assay in HaCaT cells: A flow cytometric analysis was performed and distribution of differentially stained cells was determined using DCFDA dye. The shift in band positions for complex **2** compared to cells alone highlights higher ROS generation in light compared to dark. Different conditions are shown by different color codes.

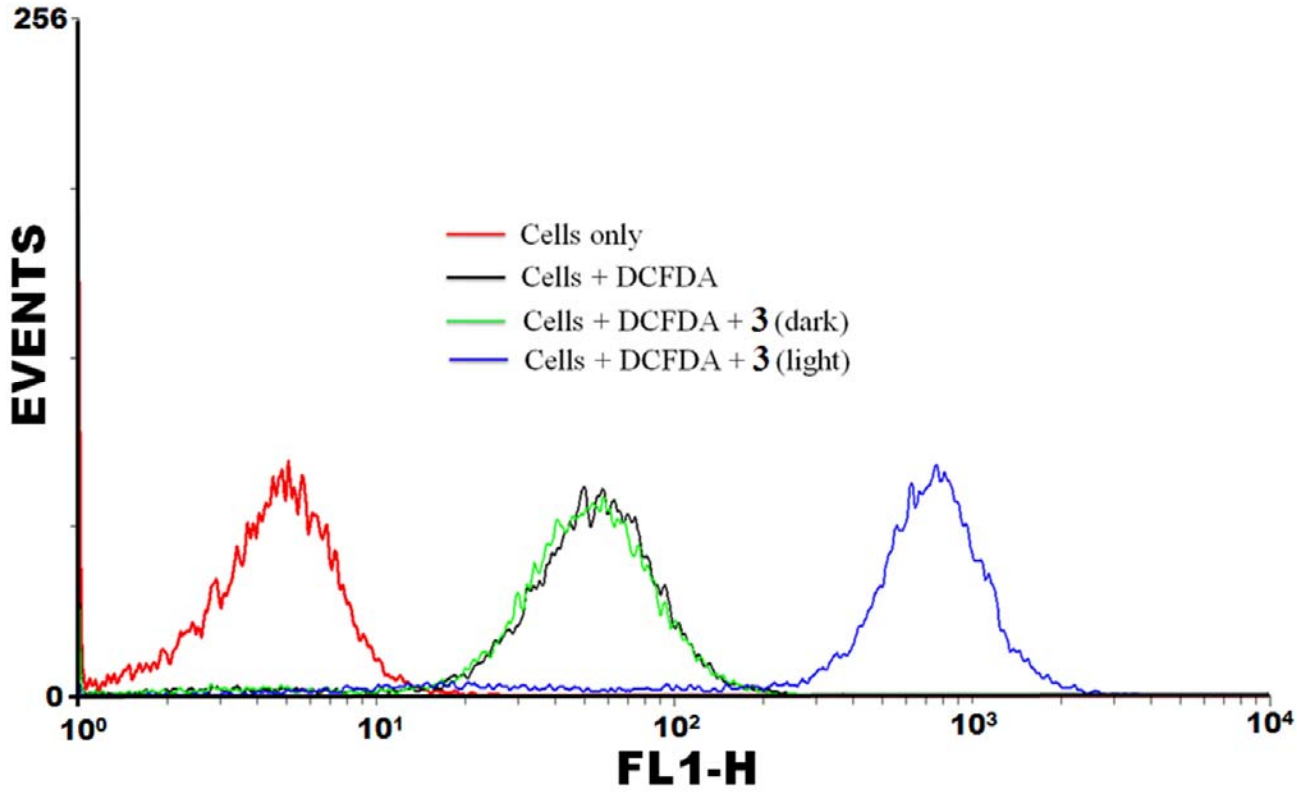

Fig. S29. DCFDA assay in HaCaT cells: A flowcytometric analysis was performed and distribution of differentially stained cells was determined using DCFDA dye. The shift in band positions for complex **3** compared to cells alone highlights higher ROS generation in light compared to dark. Different conditions are shown by different color codes.

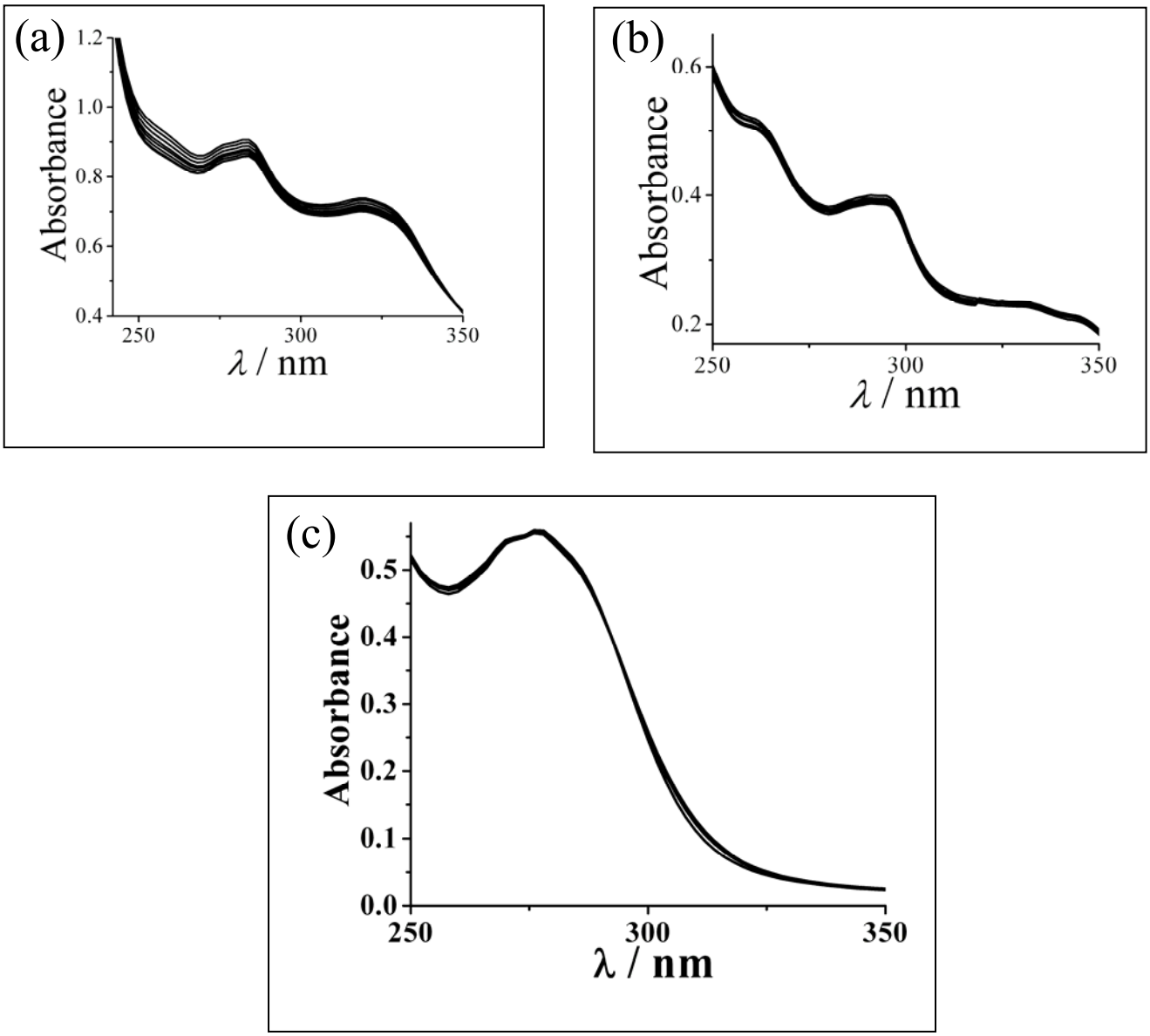

Fig. S30. Spectral traces showing the effect of gradual addition of ct-DNA to the solution of (a) [Pt(Fc-tpy)Cl]Cl (**1**), (b) [Pt(Fc-tpy)NPC]Cl (**2**) and (c) [Pt(Fc-bpa)Cl]Cl, (**3**) in DMF-Tris-HCl buffer medium (pH=7.2).

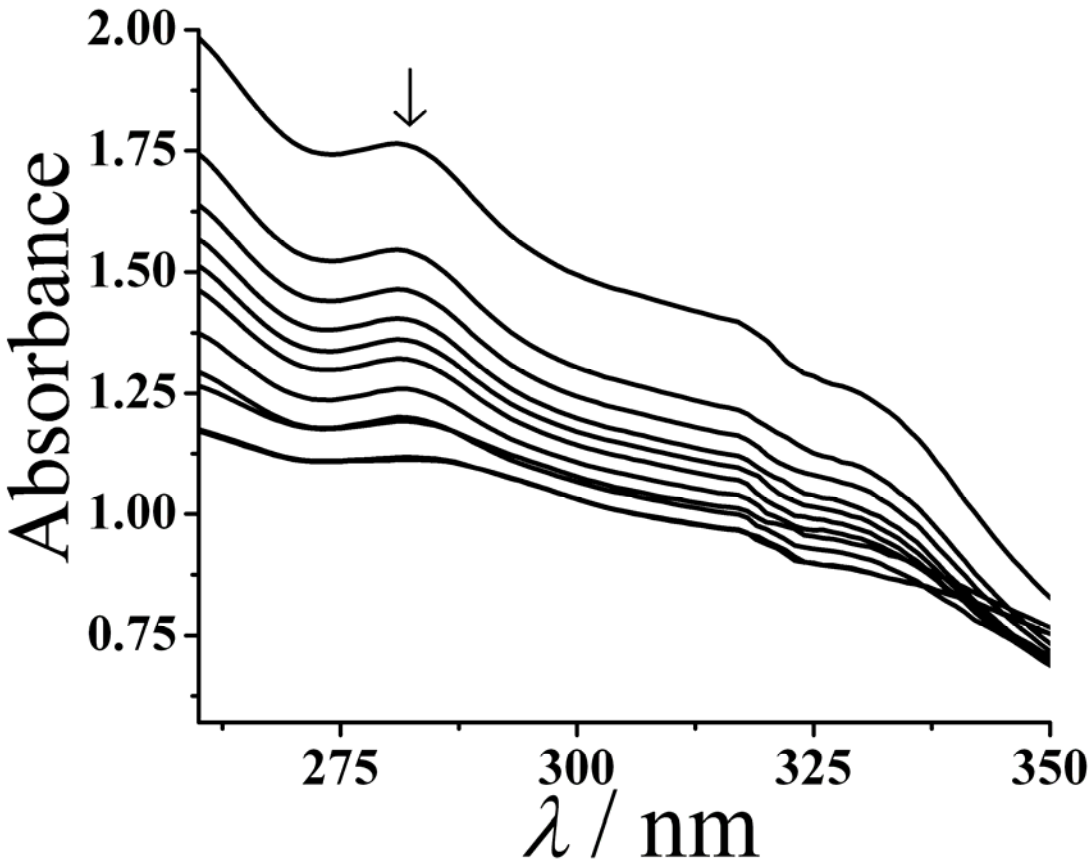

Fig. S31. Spectral traces showing the effect of gradual addition of ct-DNA to the solution of [Pt(Ph-tpy)Cl]Cl (**4**) in DMF-Tris-HCl buffer medium (pH=7.2).

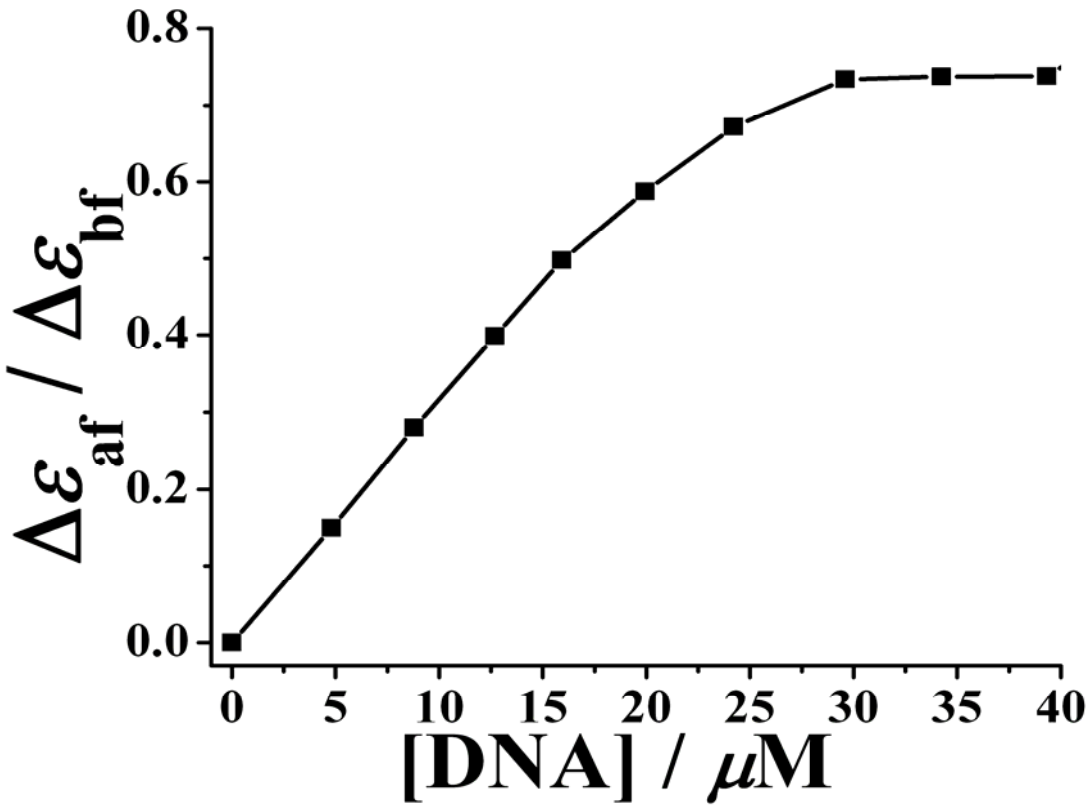

Fig. S32. The nonlinear fit of the absorption data (280 nm) by the McGhee-vonHippel method to the plot of $\Delta\varepsilon_{af}/\Delta\varepsilon_{bf}$ vs. [DNA] for complex **4**.

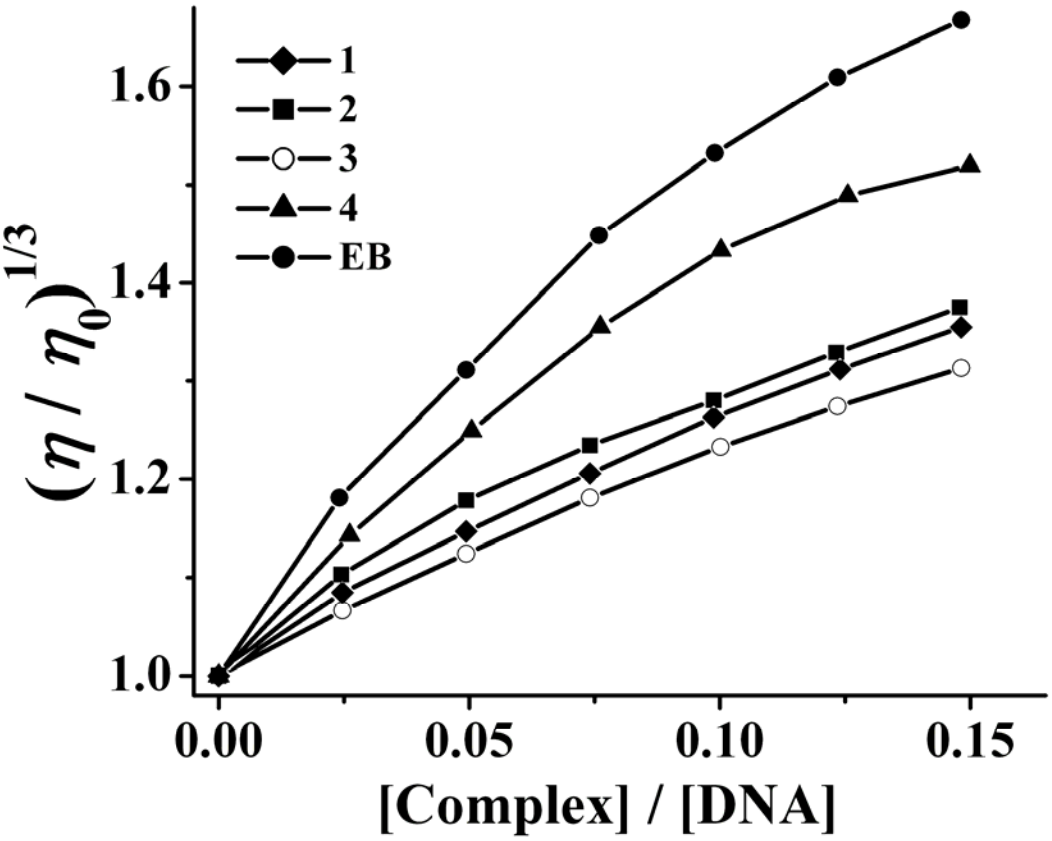

Fig. S33. Effect of addition of increasing amounts of the complexes **1** - **4** along with the DNA intercalator EB and DNA minor groove binder Hoechst 33258 on the relative viscosity of ct-DNA at 37.0 (±0.1)^{o}C in 5 mM Tris-HCl buffer medium (pH = 7.2).

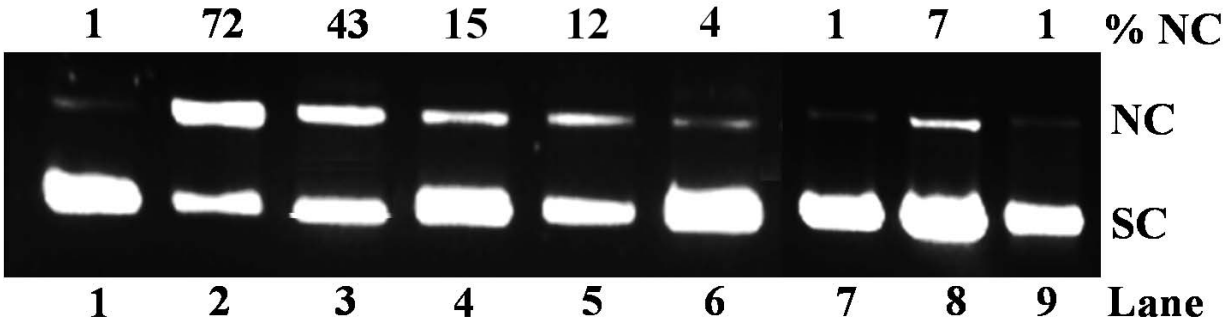

Fig. S34. Gel electrophoresis diagram showing the visible light induced DNA cleavage activity of the complexes **1** - **4** (15 μM) using SC pUC19 DNA (0.2 μg, 30 μM b.p.) in 50mM Tris-HCl (pH=7.2) containing 10% DMF on photo-irradiation with light of 568 nm wavelength (1hr exposure): lane 1, DNA control (in light); lane 2, DNA + **1** (in light); lane 3, DNA + **2** (in light); lane 4, DNA + **3** (in light); lane 5, DNA + **4** (in light); lane 6, DNA + **1** (in dark); lane 7, DNA + **2** (in dark); lane 8, DNA + **3** (in dark); lane 9, DNA + **4** (in dark).

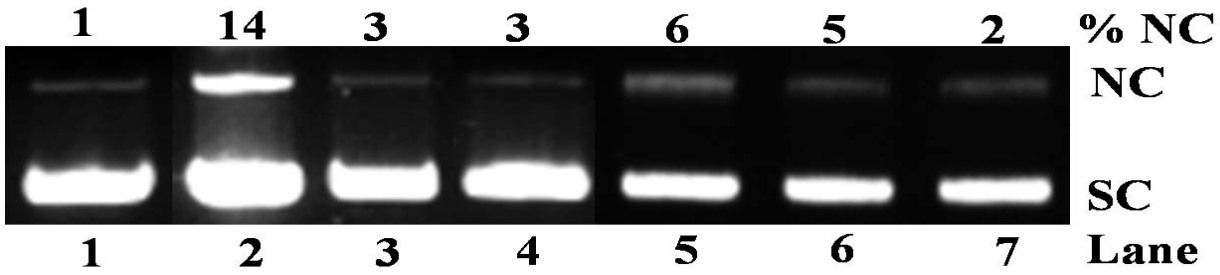

Fig. S35. Gel electrophoresis diagram showing the visible light induced DNA cleavage activity of the ligand controls (15 μM) using SC pUC19 DNA (0.2 μg, 30 μM b.p.) in 50mM Tris-HCl (pH=7.2) containing 10% DMF on photo-irradiation with light of 568 nm wavelength (1hr exposure): lane 1, DNA control (in light); lane 2, DNA + Fc-tpy (in light); lane 3, DNA + Fc-bpa (in light); lane 4, DNA + NPC (in light); lane 5, DNA + Fc-tpy (in dark); lane 6, DNA + Fc-bpa (in dark); lane 7, DNA + NPC (in dark).

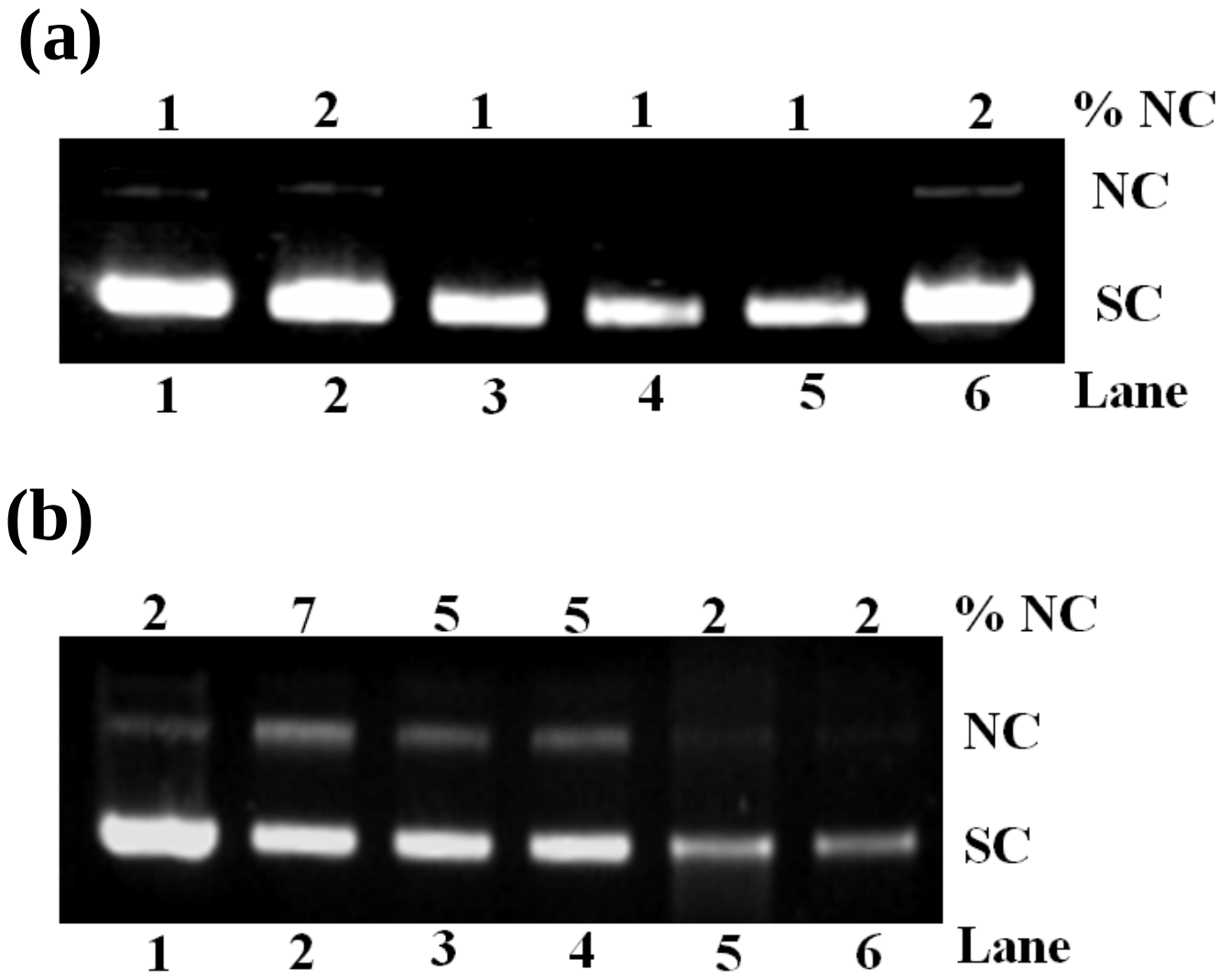

Fig. S36. Chemical nuclease of complexes **1-4** (20 μM) after incubation with H_2O_2 in dark for 1 hr: lane 1, DNA control; lane 2, DNA + H_2O_2 (0.5mM); lane 3, DNA + **1** + H_2O_2; lane 4, DNA + **2** + H_2O_2 (0.5mM); lane 5, DNA + **3** + H_2O_2 (0.5mM) ; lane 6, DNA + **4** + H_2O_2 (0.5mM). **(b)** Chemical nuclease of complexes **1-4** (20 μM) after incubation with GSH in dark for 1 hr: lane 1, DNA control; lane 2, DNA + GSH (0.5mM); lane 3, DNA + **1** + GSH; lane 4, DNA + **2** + GSH (0.5mM); lane 5, DNA + **3** + GSH (0.5mM) ; lane 6, DNA + **4** + GSH

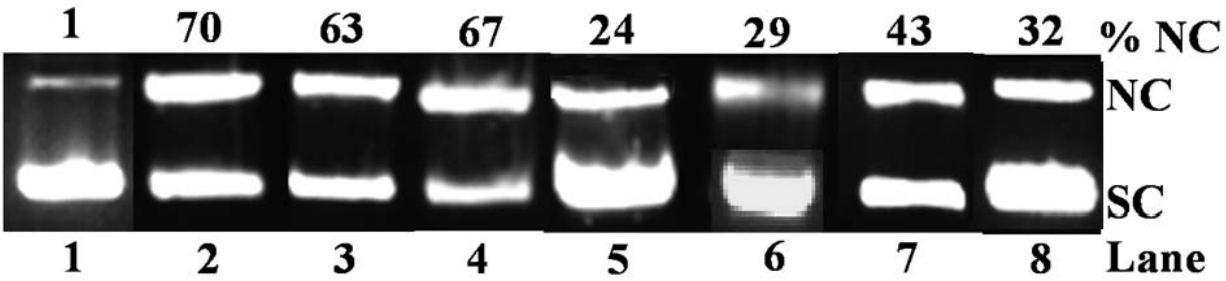

Fig. S37. Mechanistic study for the complex **1** (15 μM) in 568nm (1 hr exposure): lane 1, DNA control; lane 2, DNA + **1**; lane 3, DNA + **1** +NaN_3 (4mM); lane 4, DNA +**1** + TEMP (4mM), lane 5, DNA + **1** + KI (4mM); lane 6, DNA + **1** + DMSO (8μL); lane 7, DNA + **1** + SOD (4 units); lane 8, DNA + **1** + catalase (4 units).

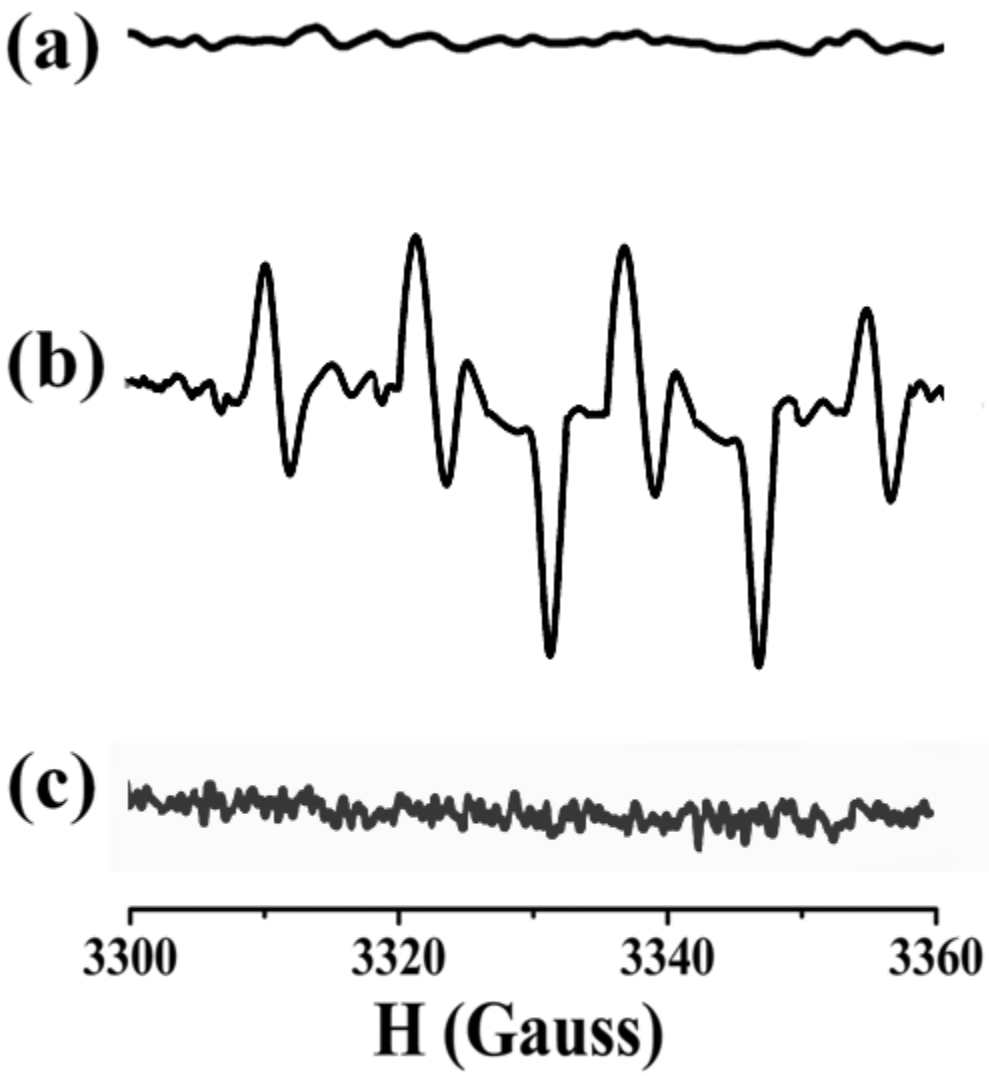

Fig. S38. EPR spectra of complexes **1** and **2** with DMPO (50 mM) in DMF- phosphate buffer (3:1 v/v). The experimental conditions and operating frequency are T = 298 K , ν = 9.3775 GHz, modulation frequency = 100.00 KHz, modulation amplitude = 2.00 G, time constant = 20.48 msec and receiver gain = 1 x 10^4. (a) samples (200 μM) kept in dark for 1 hr. (b) after irradiating the samples (200 μM) for 1 hr with visible light. (c) after irradiating the samples (200 μM) for 1 hr with visible light in argon atmosphere.

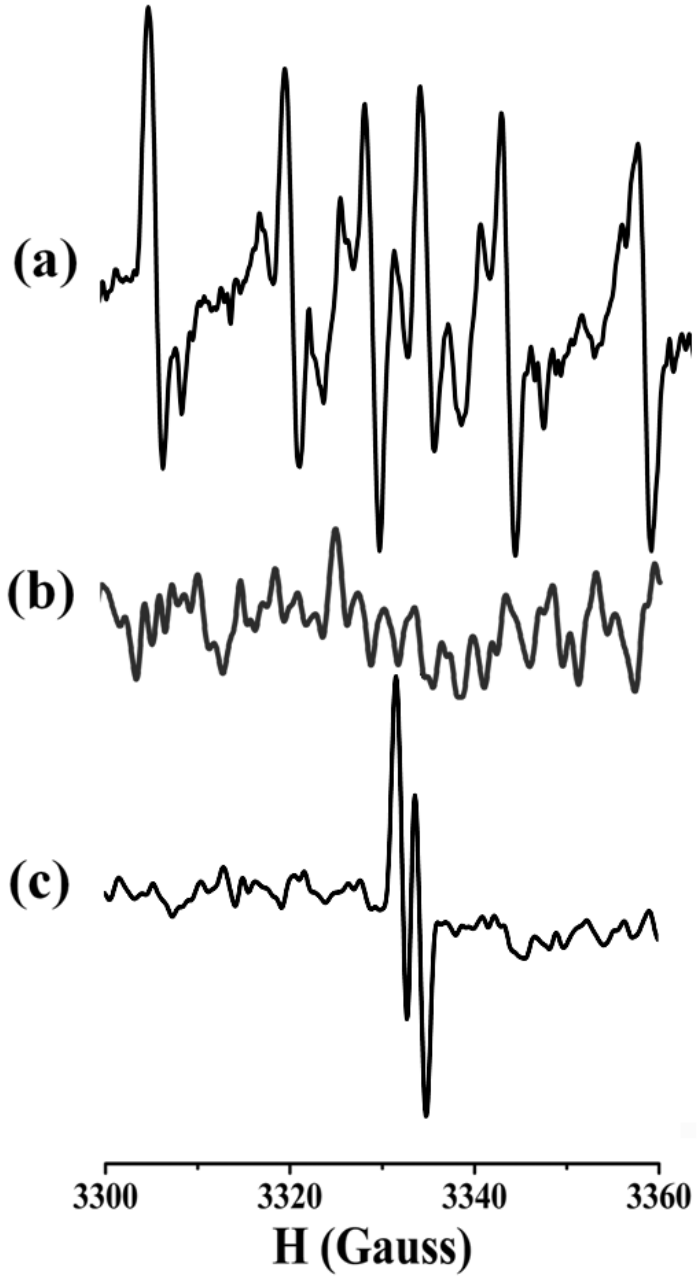

Fig. S39. EPR spectra of complexes **1** and **2** with DMPO (50 mM) in DMF- phosphate buffer (3:1 v/v). The experimental conditions and operating frequency are T = 298 K , ν = 9.3775 GHz, modulation frequency = 100.00 KHz, modulation amplitude = 2.00 G, time constant = 20.48 msec and receiver gain = 1 x 10^4. (a) after irradiating the samples (5 mM) for 15 min in visible light. (b) in presence of SOD (500 units) and catalase (500 units) to the samples(200 μM) and irradiating for 1 hr in visible light. (c) in presence of sodium ascorbate to the samples (200 μM) and irradiating for 1 hr in visible light.

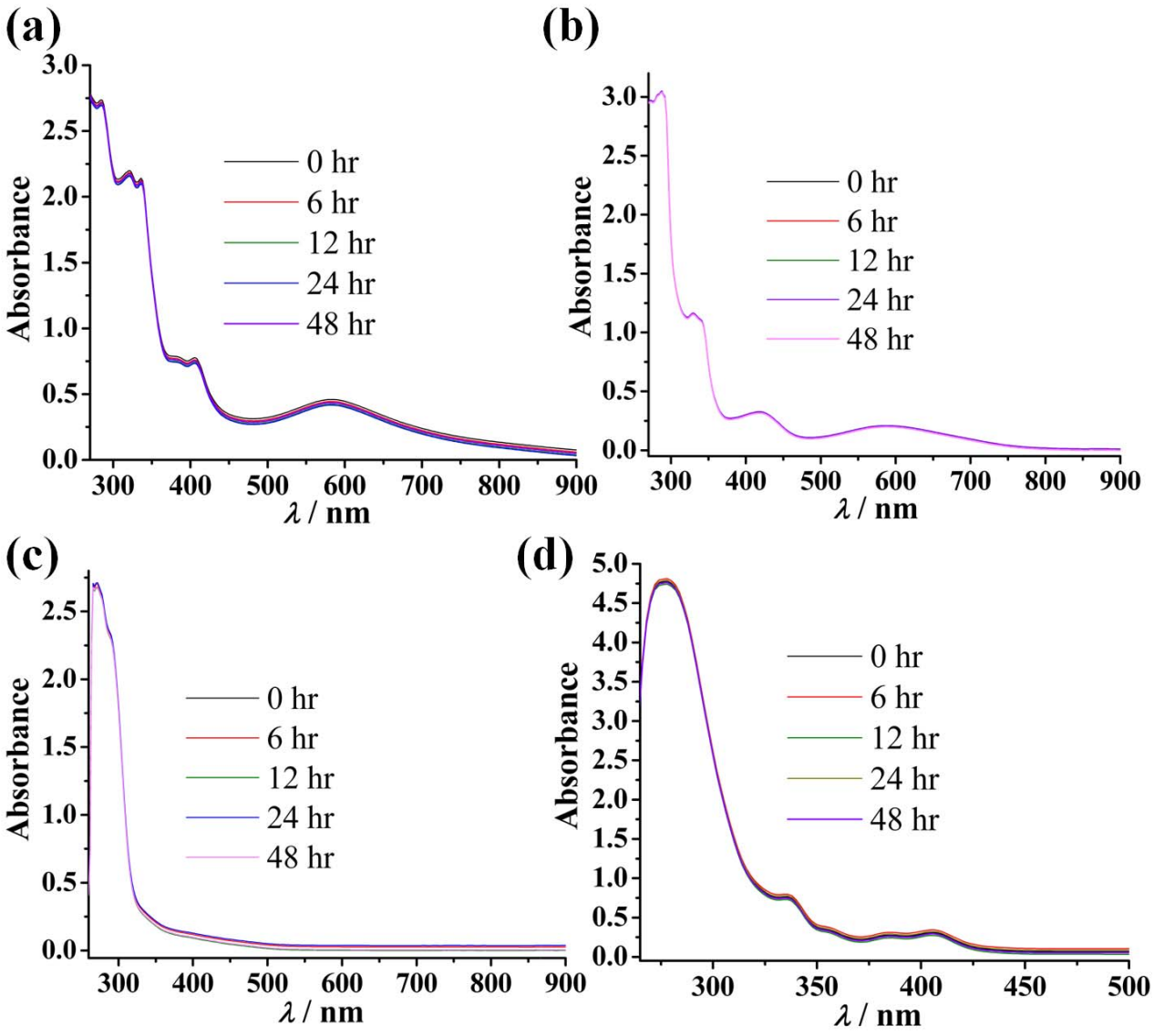

Fig. S40. Absorption spectra recorded at different time points (samples kept in dark) as indicated in the plots of 125 μM of DMF solutions of (a) complex **1**, (b) complex **2**, (c) complex **3** and (d) complex **4**. The complexes were found to be stable till 48 hrs in dark.

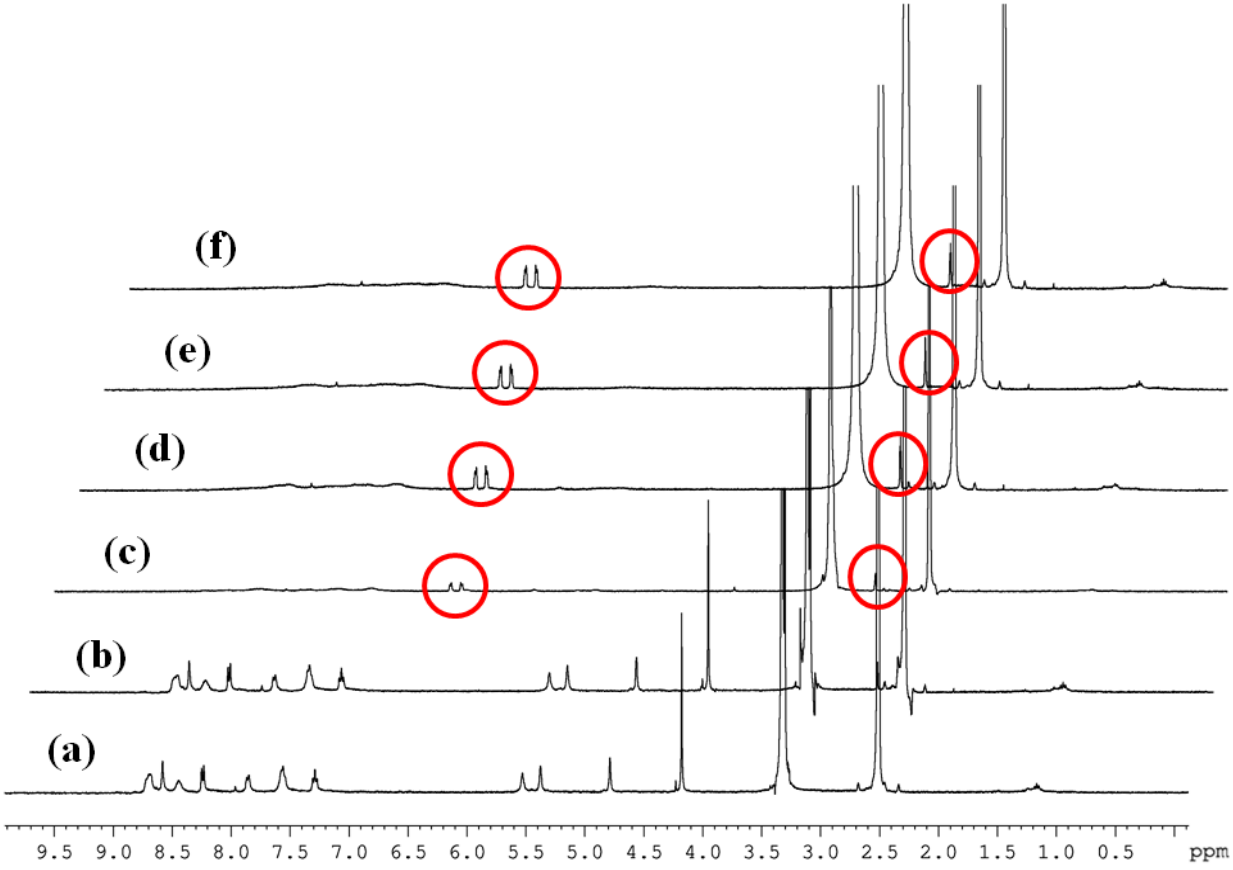

Fig. S41. ^{1}H NMR spectra of complex **2** after different time intervals of irradiation with visible light (400-700) nm (a) 0 hr (b) 48 hrs in dark (c) after 5 mins of irradiation (d) after 15 min of irradiation (e) after 30 mins of irradiation (f) after 1 hr of irradiation in d6-DMSO solutions.

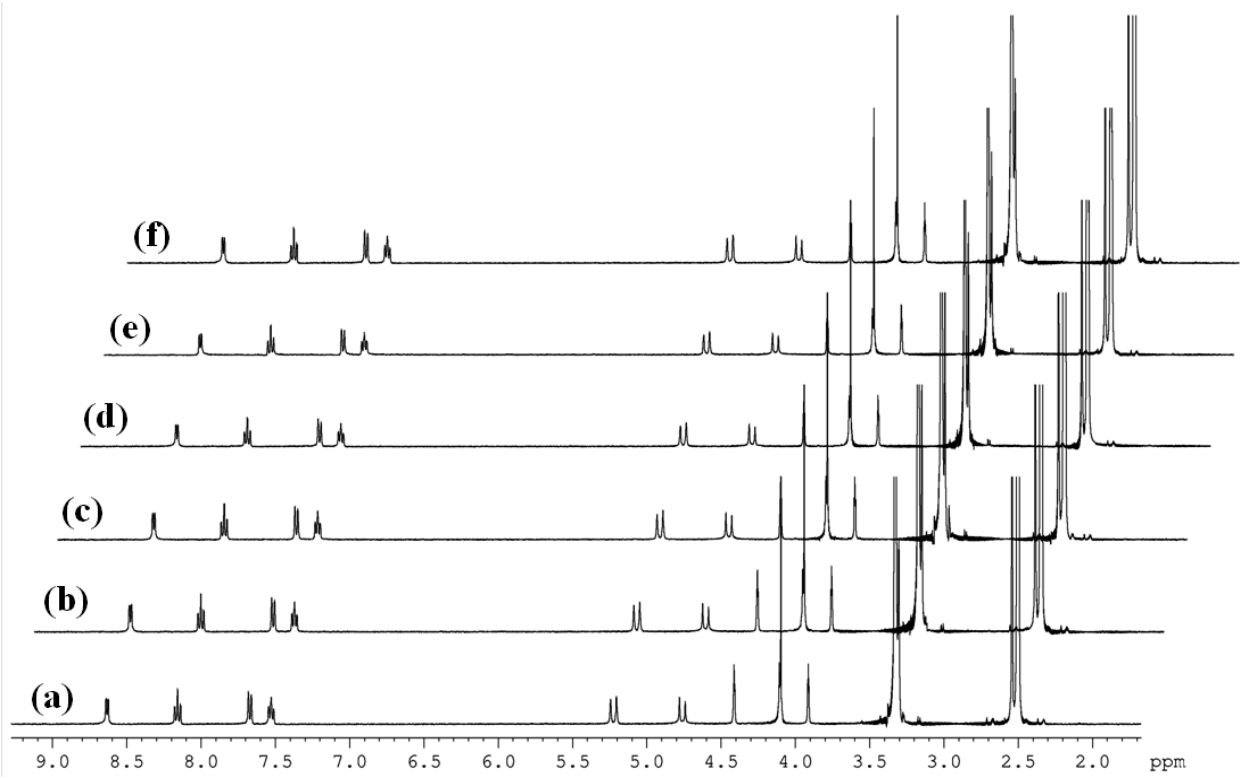

Fig. S42. ^{1}H NMR spectra of complex **3** after different time intervals of irradiation with visible light (400-700) nm (a) 0 hr (b) 48 hrs in dark (c) after 5 mins of irradiation (d) after 15 min of irradiation (e) after 30 mins of irradiation (f) after 1 hr of irradiation in d6-DMSO solutions.

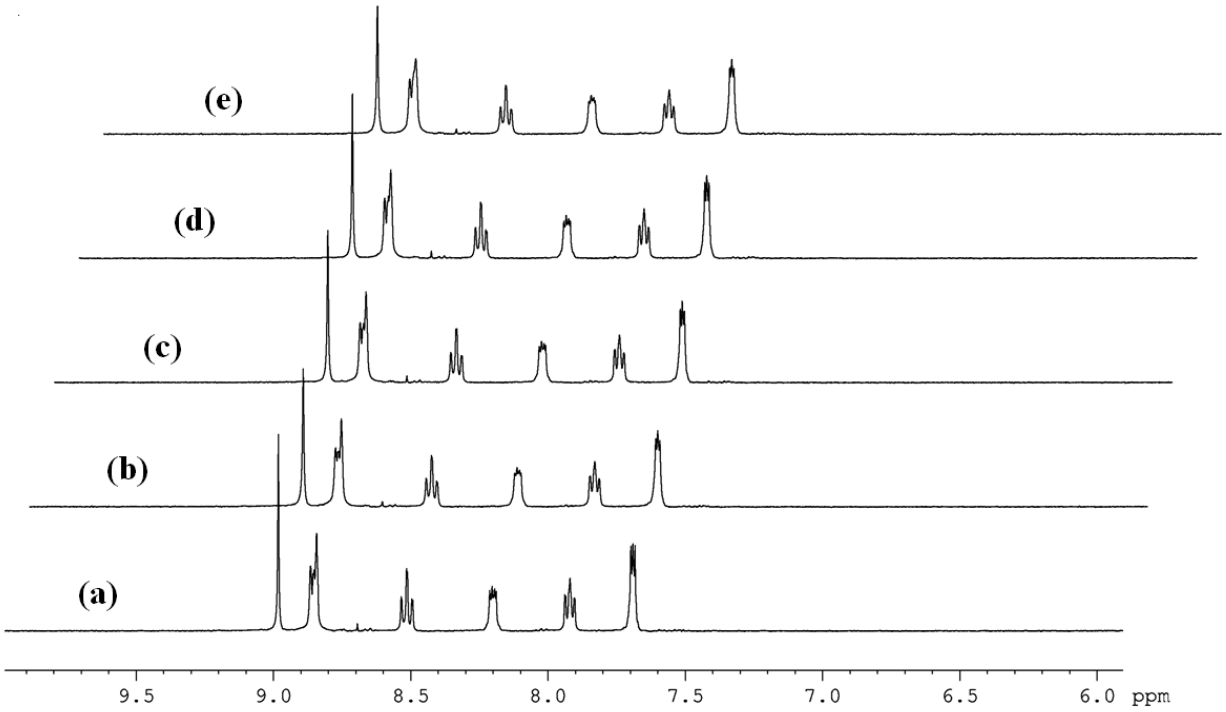

Fig. S43. ^{1}H NMR spectra of complex **4** after different time intervals of irradiation with visible light (400-700) nm (a) 0 hr (b) 48 hrs in dark (c) after 15 min of irradiation (d) after 30 mins of irradiation (e) after 1 hr of irradiation in d6-DMSO solutions.

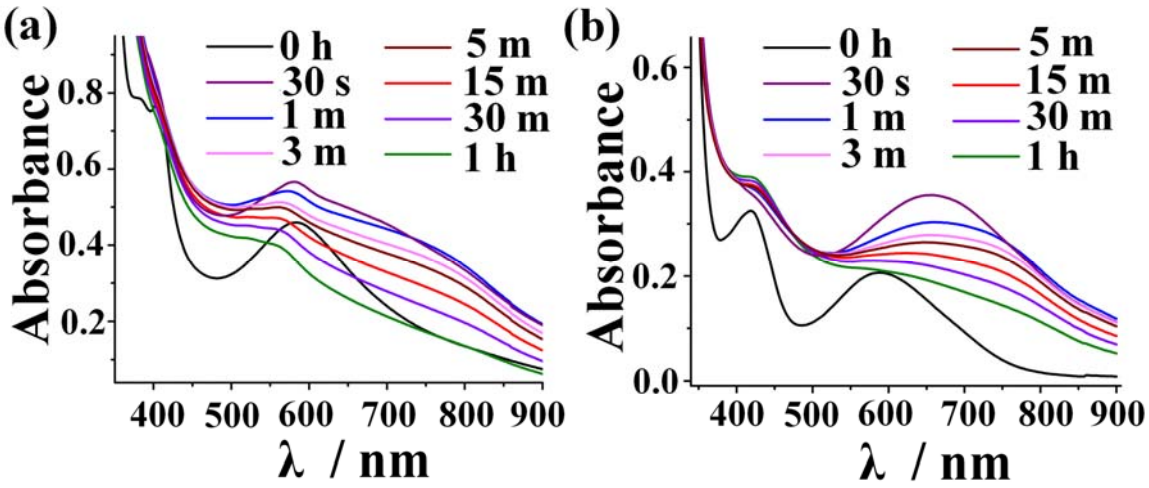

Fig. S44. UV-visible spectra recorded on irradiation of samples with visible light (400-700) nm at different time intervals as depicted in the graph. (a) complex **1** (500 μM). (b) complex **2** (500 μM).

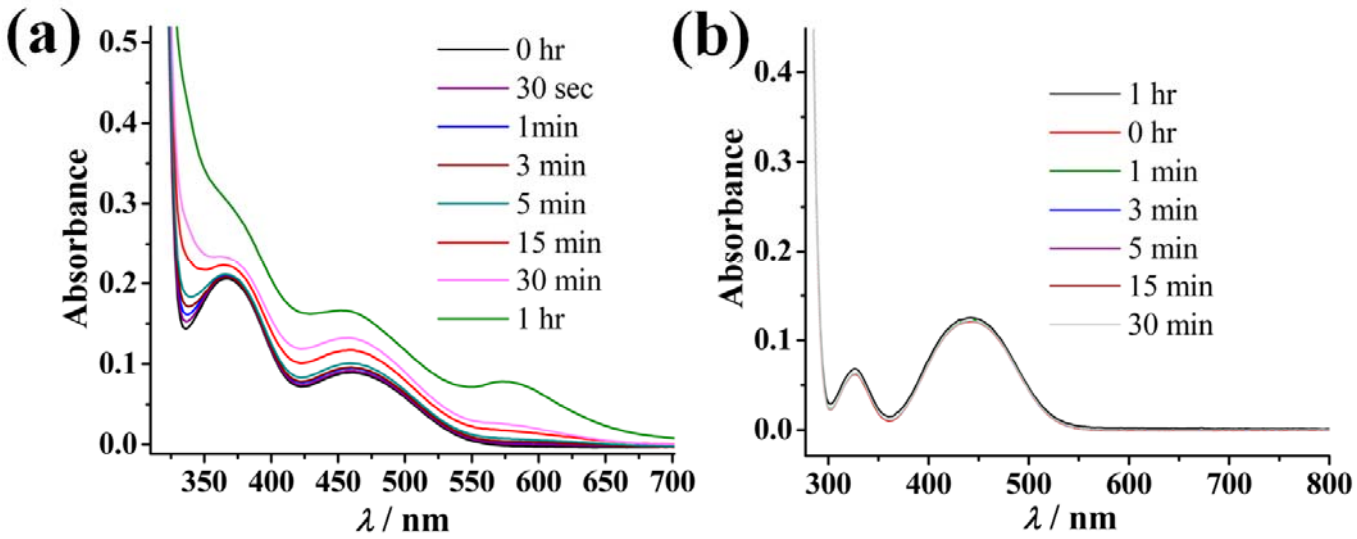

Fig. S45. Absorption spectra recorded at different time points of irradiation with visible light as indicated in the plots of DMF solutions of (a) ligand Fc-tpy (500 μM) and (b) ferrocene (1 mM).

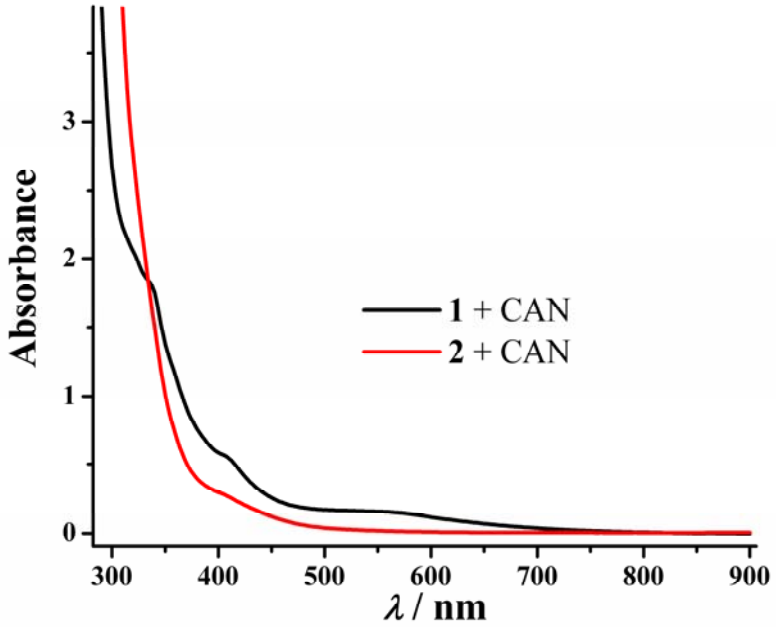

Fig. S46. UV-visible absorption spectra of the complexes **1** and **2** (500 μM) in DMF solutions in presence of excess of an oxidizing agent cerric ammonium nitrate (CAN) in the molar ratio (1 : 5).

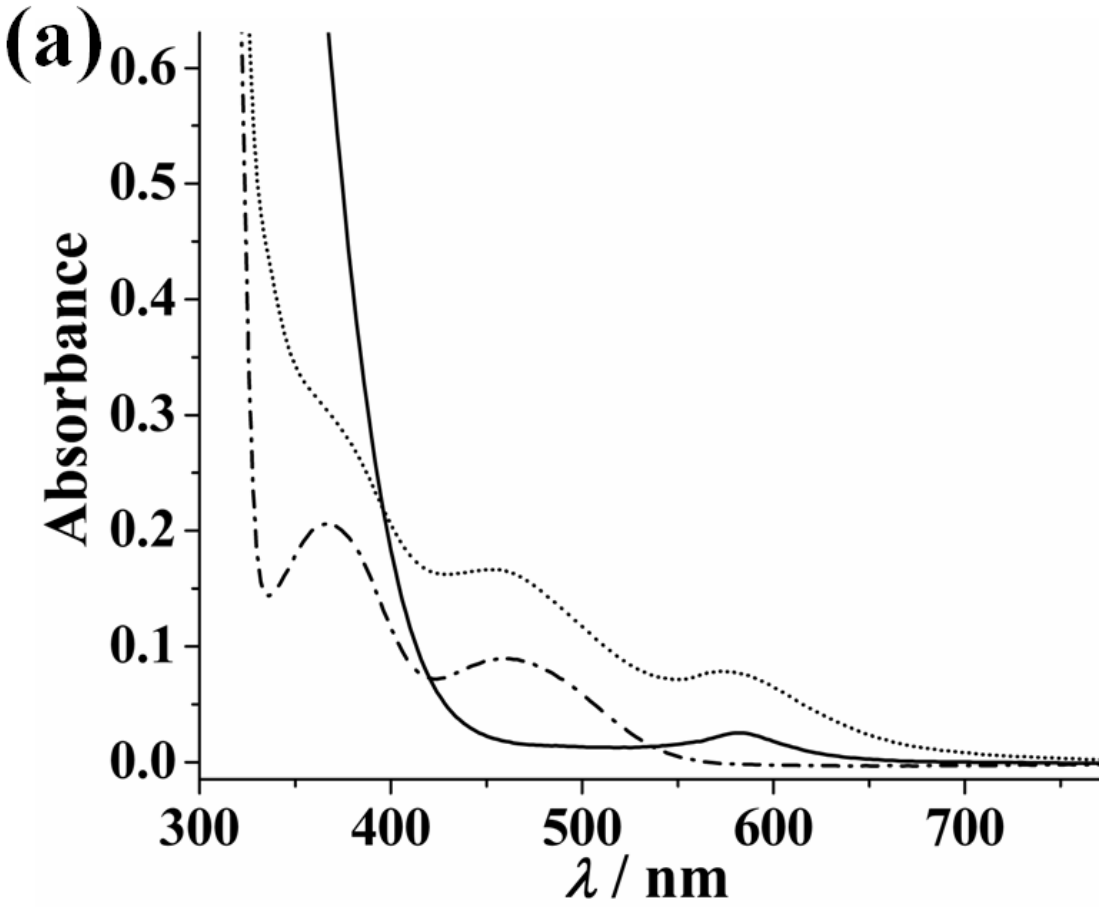

Fig. S47. (a) Absorption spectra of Fc-tpy (500 μM) alone (dash-dot line), after 1 hr irradiation with visible light (dotted line) and in presence of CAN (1 : 5 molar ratio) (bold line).

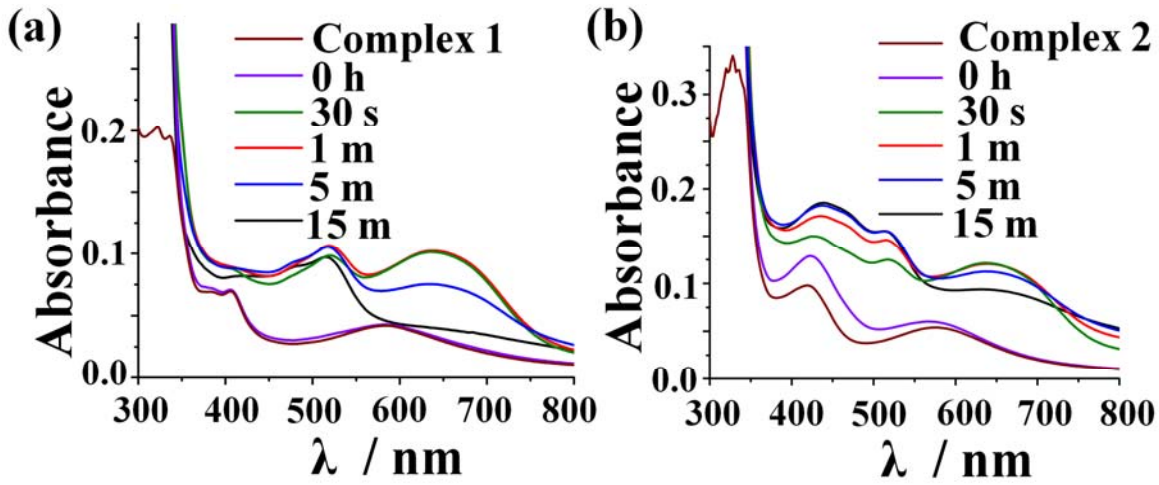

Fig. S48. UV-visible spectra recorded on irradiation of samples with visible light (400-700) nm at different time intervals as depicted in the graph. (a) complex **1** alone and then irradiating in presence of phen (1:5 molar ratio). (b) complex **2** alone and then irradiating after in presence of phen (1:5 molar ratio).

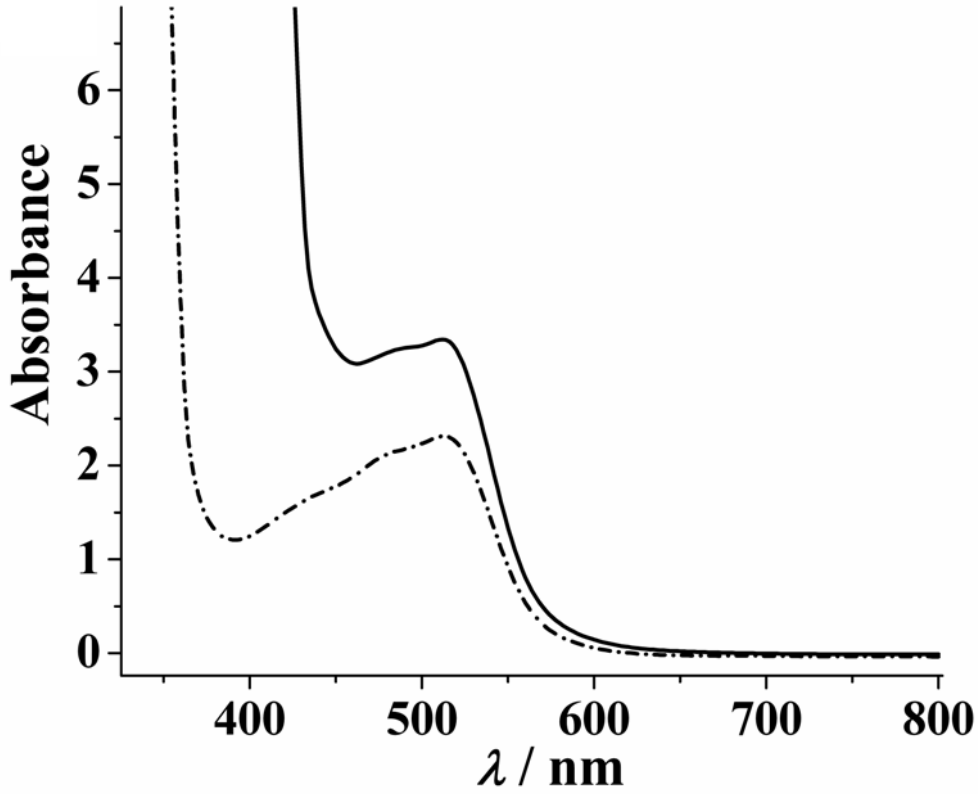

Fig. S49. Absorption spectra recorded after addition of CAN to a solution containing 1,10-phenanthroline and complexes **1-3** (bold line) and the dot-dash line denotes the spectra recorded after mixing 1,10-phenanthroline and ferric chloride. Only one representative spectrum is shown. All the complexes gave similar spectra with different intensities.

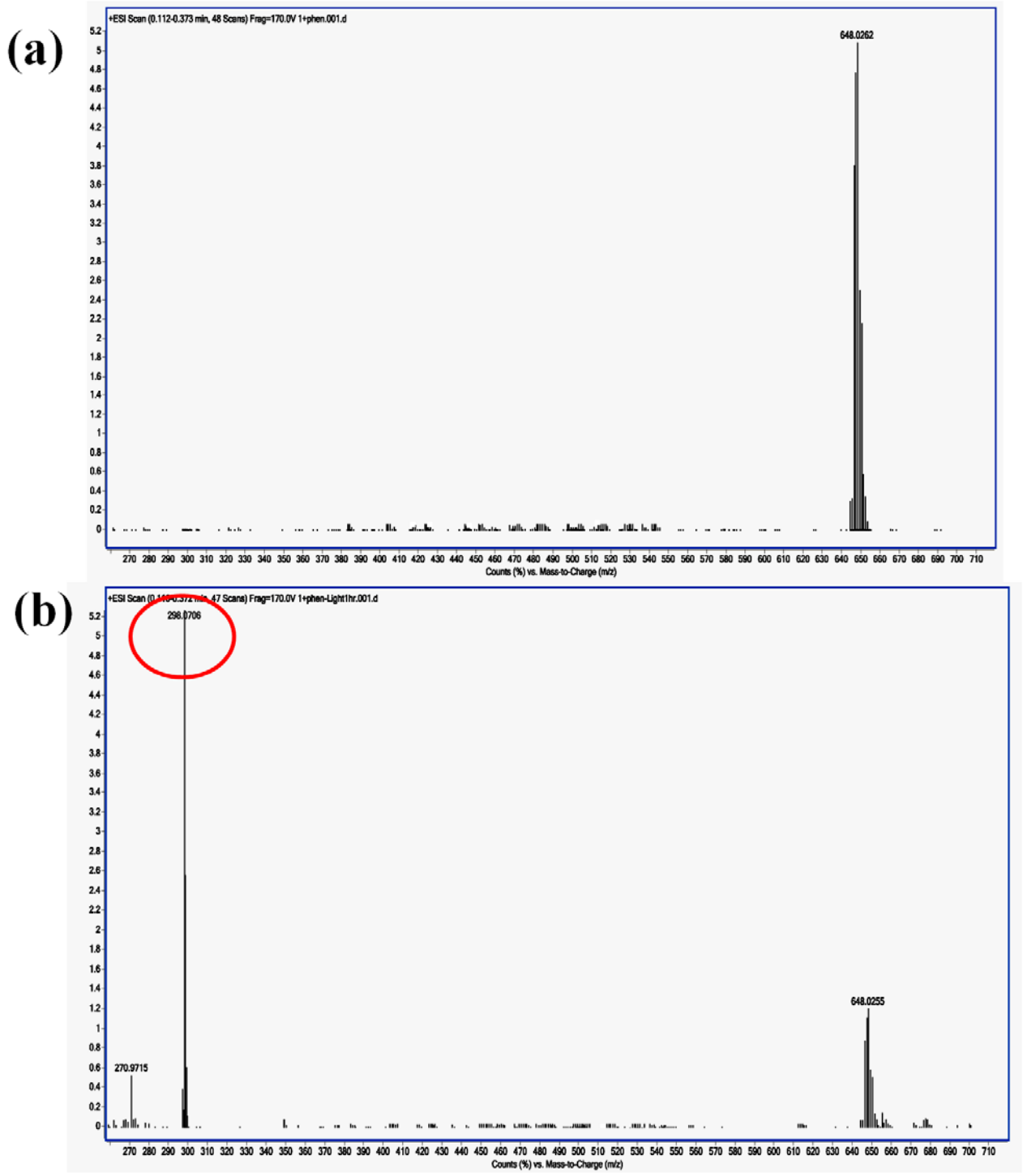

Fig. S50. Mass spectra of complex **1** in presence of 1,10 phenanthroline (1:5 molar ratio) (a) before irradiation and (b) after irradiating with visible light for 1 hr. The peak at 648 in Fig. a corresponds to complex peak. The peak at 298 in Fig b is for the tris phen iron (II) complex.

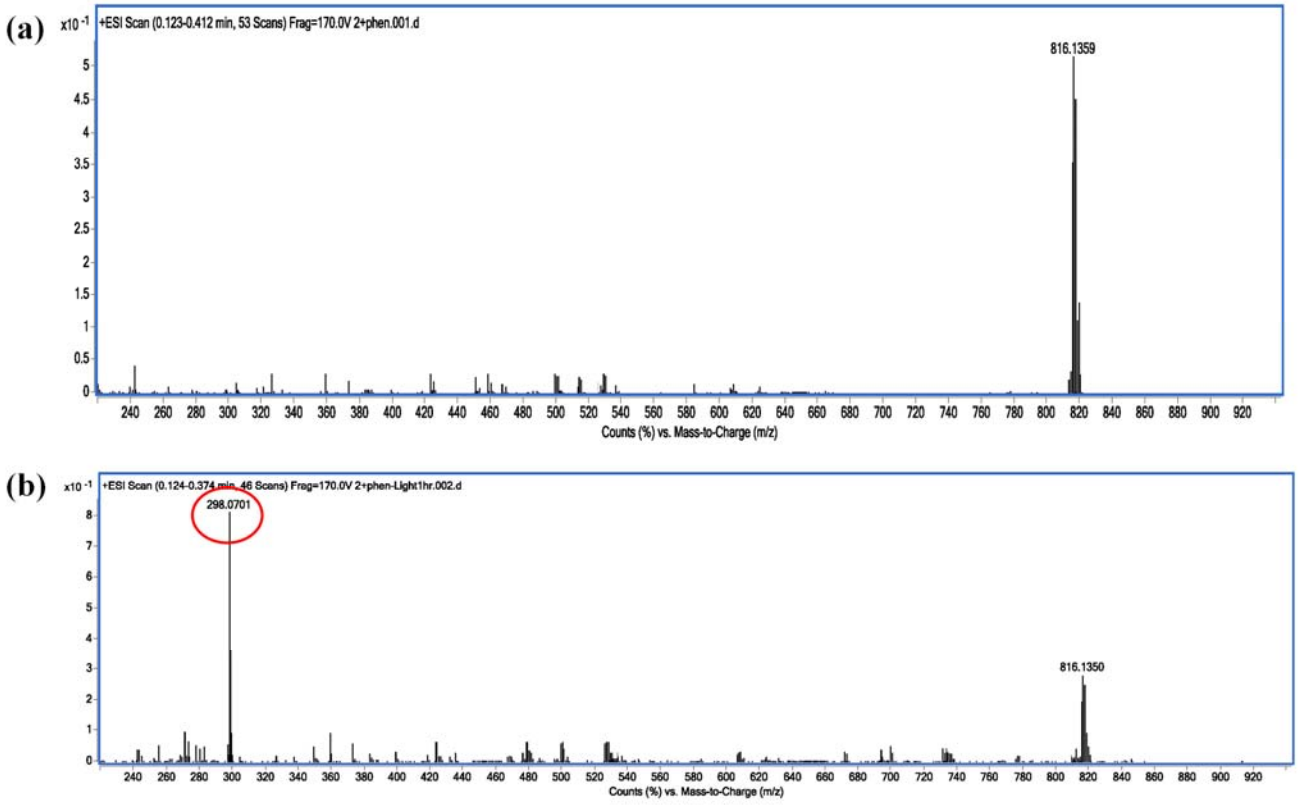

Fig. S51. Mass spectra of complex **2** in presence of 1,10 phenanthroline (1:5 molar ratio) (a) before irradiation and (b) after irradiating with visible light for 1 hr. The peak at 816 in Fig. a corresponds to complex peak. The peak at 298 in Fig b is for the tris phen iron (II) complex.

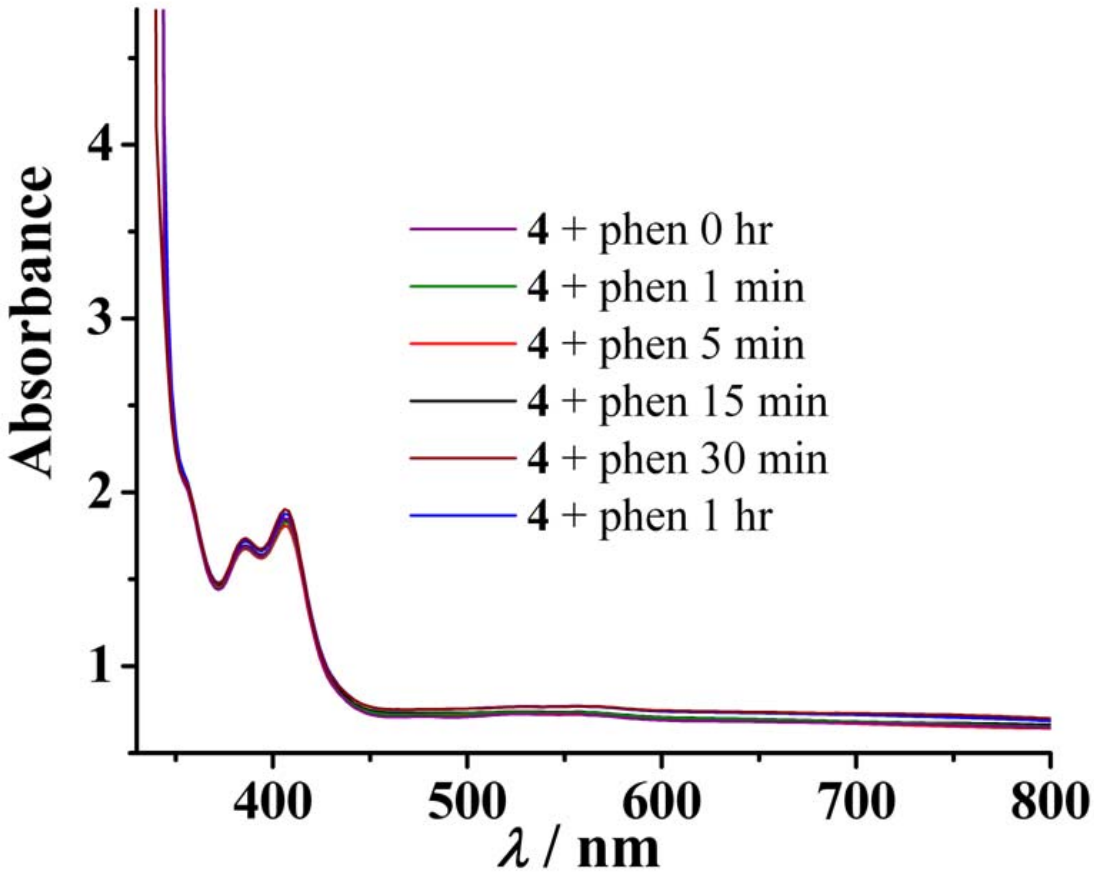

Fig. S52. UV-Visible spectral changes on irradiation in presence of phen (1:5 molar ratio) recorded after different time intervals as depicted in the plot of complex **4** in DMF solution.

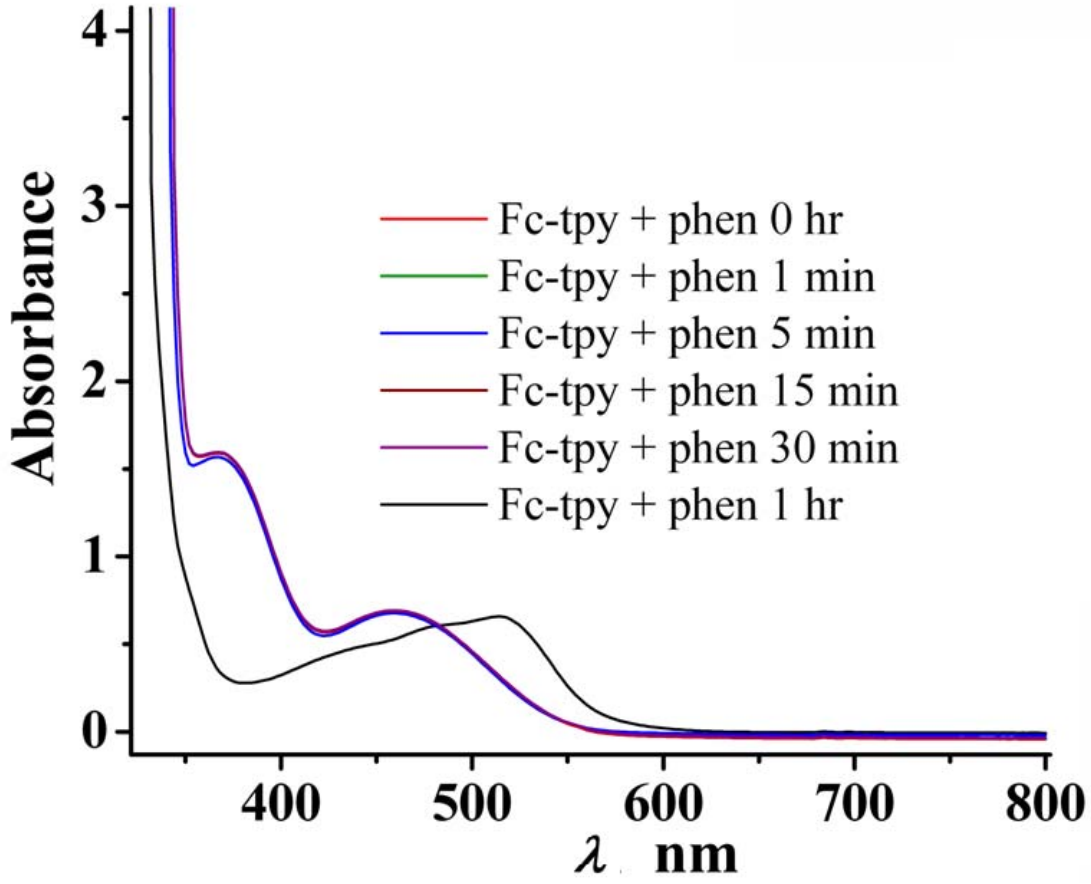

Fig. S53. UV-Visible spectral changes on irradiation in presence of phen (1:5 molar ratio) recorded after different time intervals as depicted in the plot of ligand Fc-tpy in DMF solution.

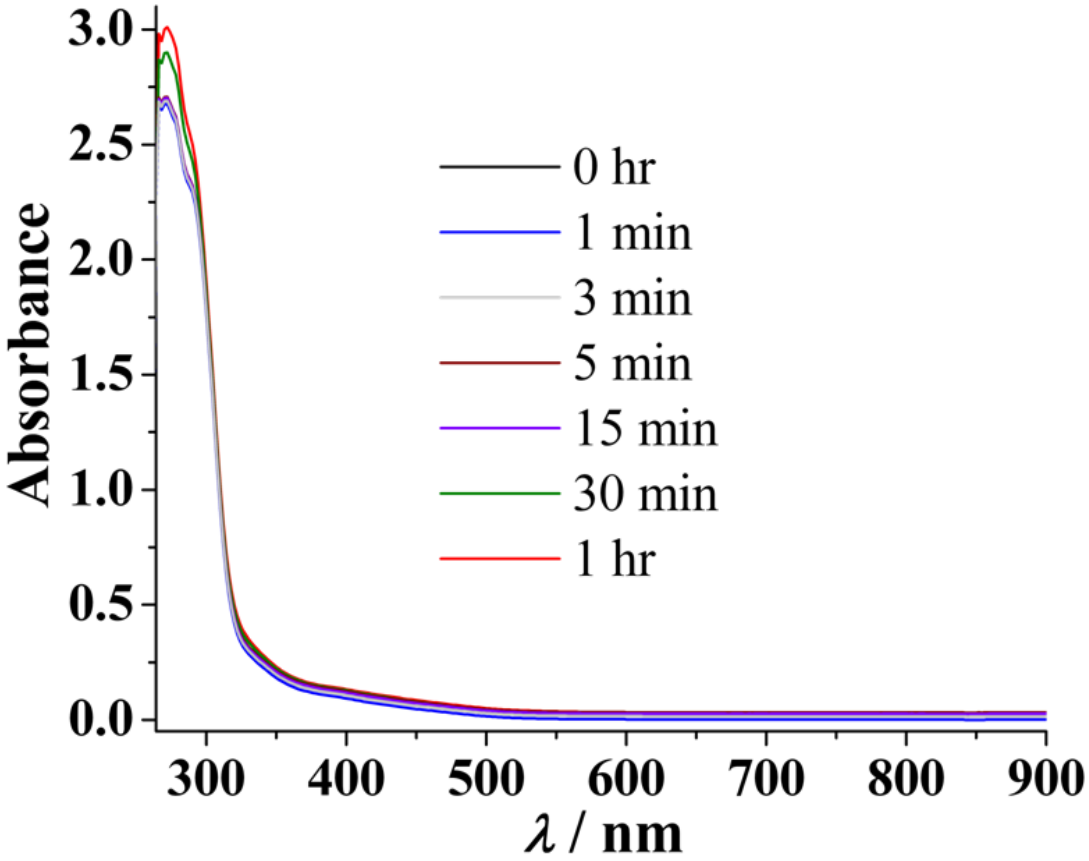

Fig. S54. Absorption spectra recorded at different time points of irradiation with visible light as indicated in the plots of 500 μM of DMF solutions of complex **3.**

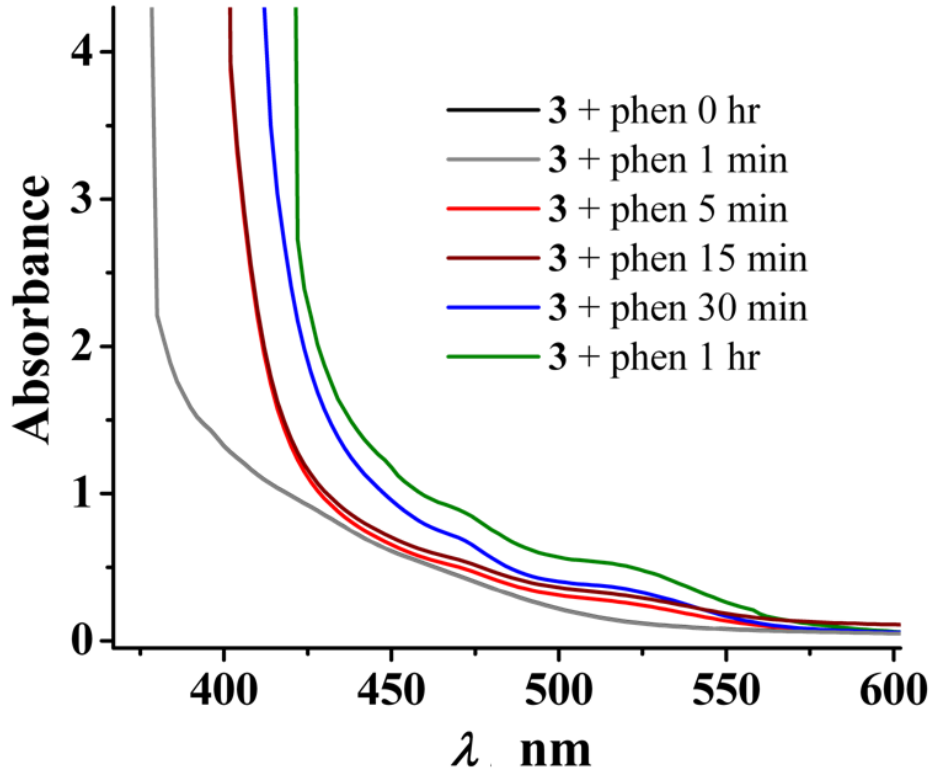

Fig. S55. UV-Visible spectral changes of complex **3** on irradiation with visible light in presence of phen (1:5 molar ratio) recorded after different time intervals as mentioned in graph.

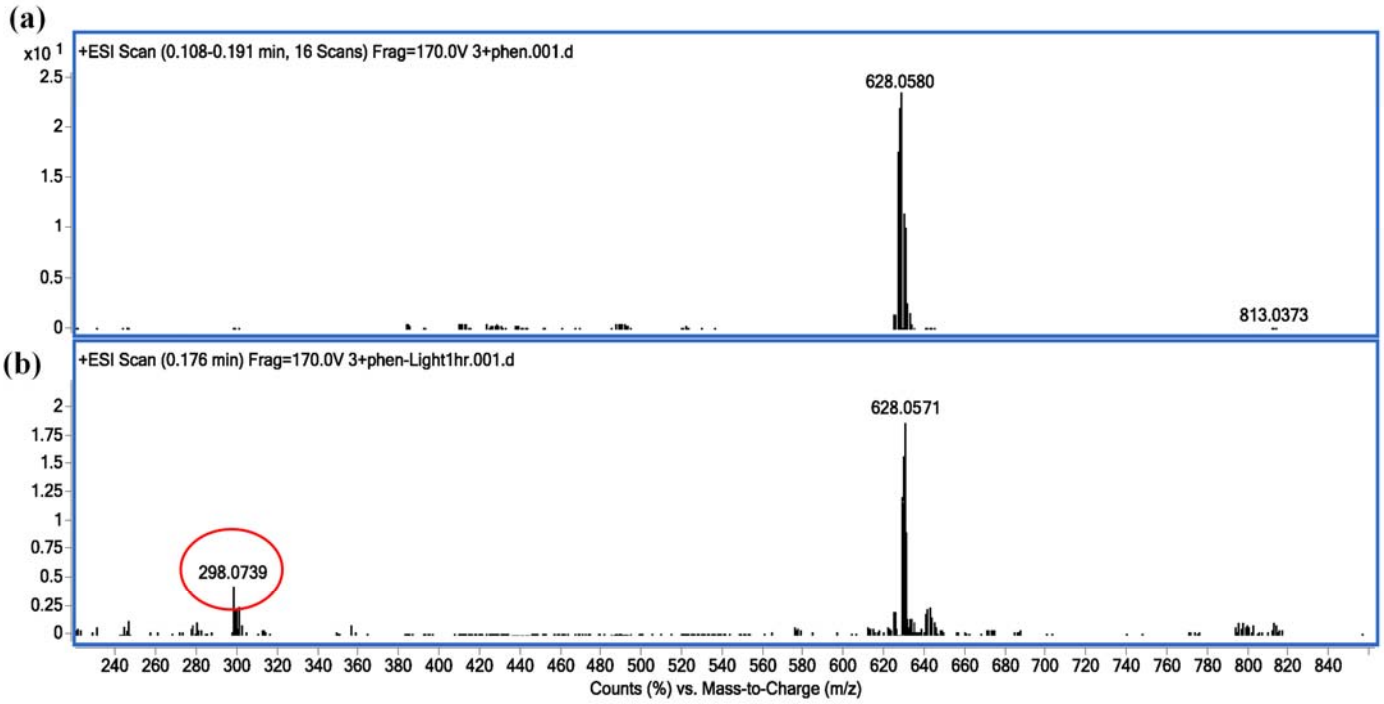

Fig. S56. Mass spectra of complex **3** in presence of 1,10 phenathroline (1:5 molar ratio) (a) before irradiation and (b) after irradiation with visible light for 1 hr. The peak at 628 in Fig. a corresponds to complex peak. The peak at 298 in Fig b is for the tris phen iron (II) complex.

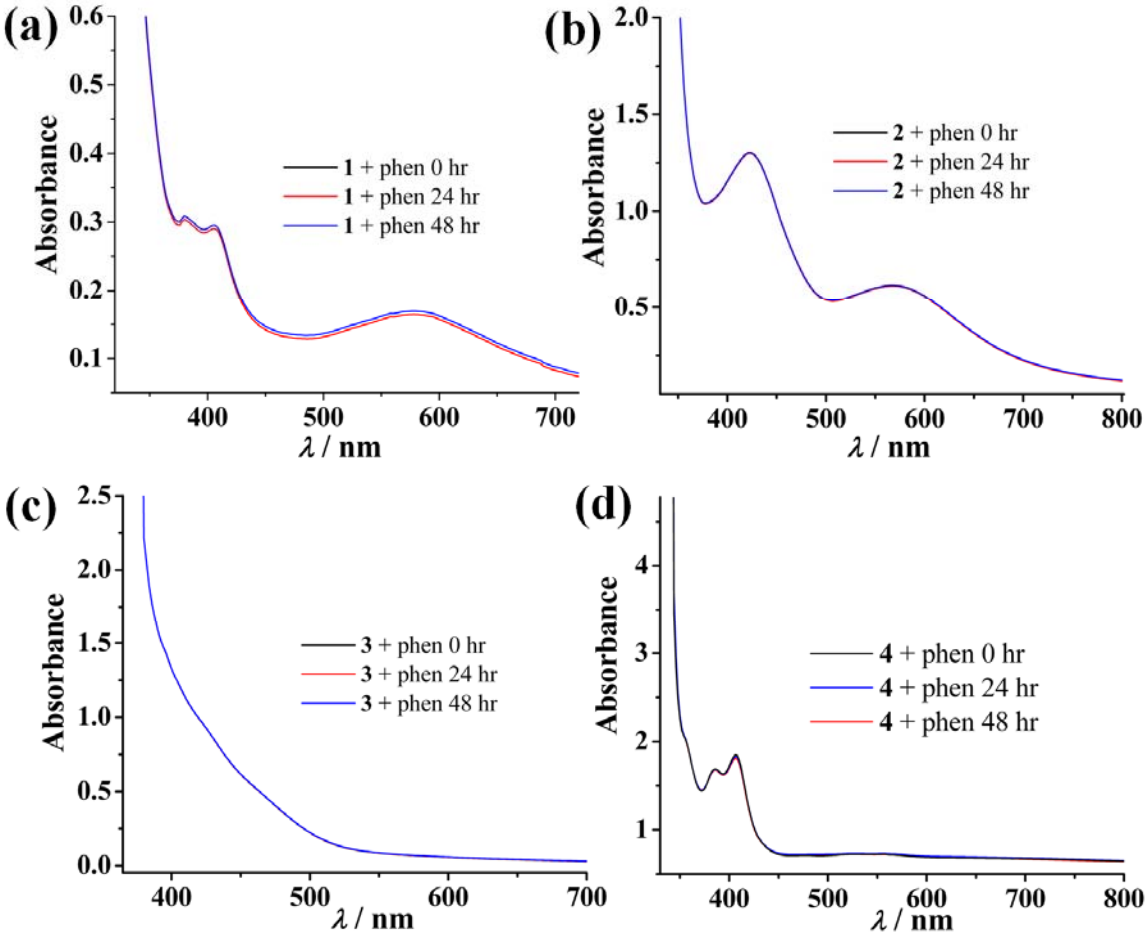

Fig. S57 . UV-Visible spectral changes recorded at various time points in presence of excess phen (1:5 molar ratio) in dark of (a) complex **1**, (b) complex **2**, (c) complex **3** and (d) complex **4**. There is no change in the spectra indicating the stability of the complexes up to 48hrs.

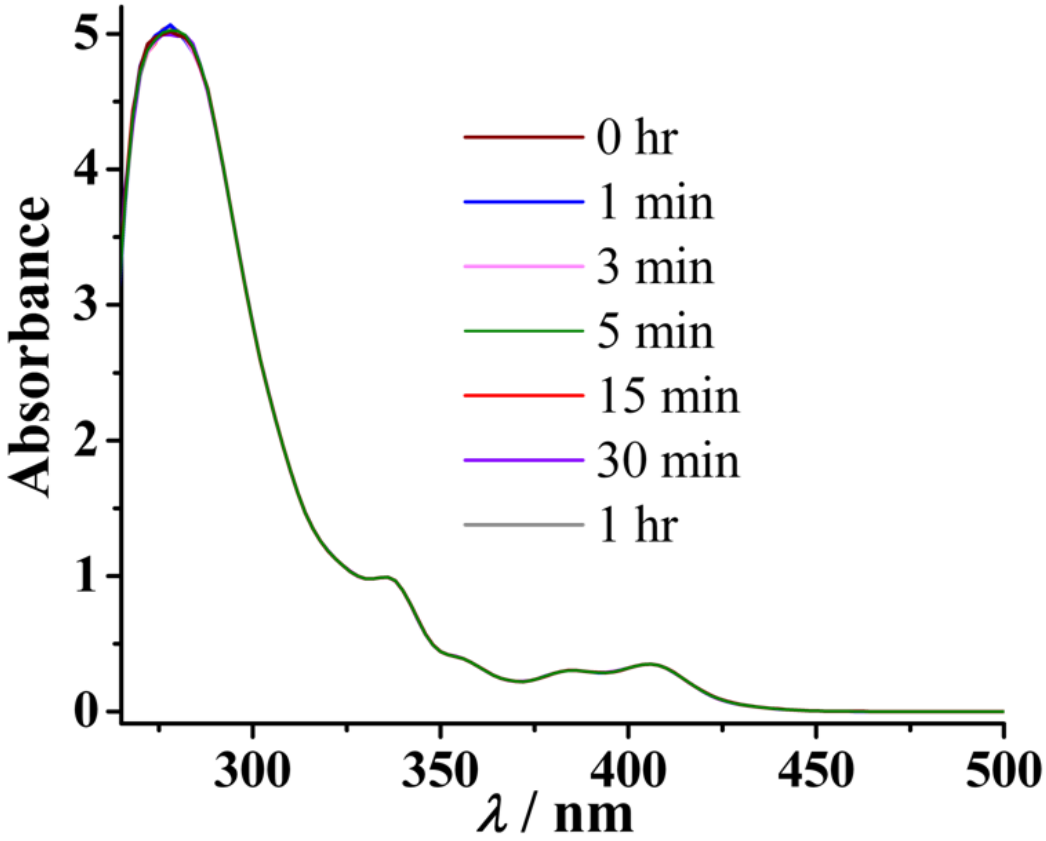

Fig. S58. Absorption spectra recorded at different time points of irradiation with visible light as indicated in the plots of 125 μM of DMF solutions of complex **4.**

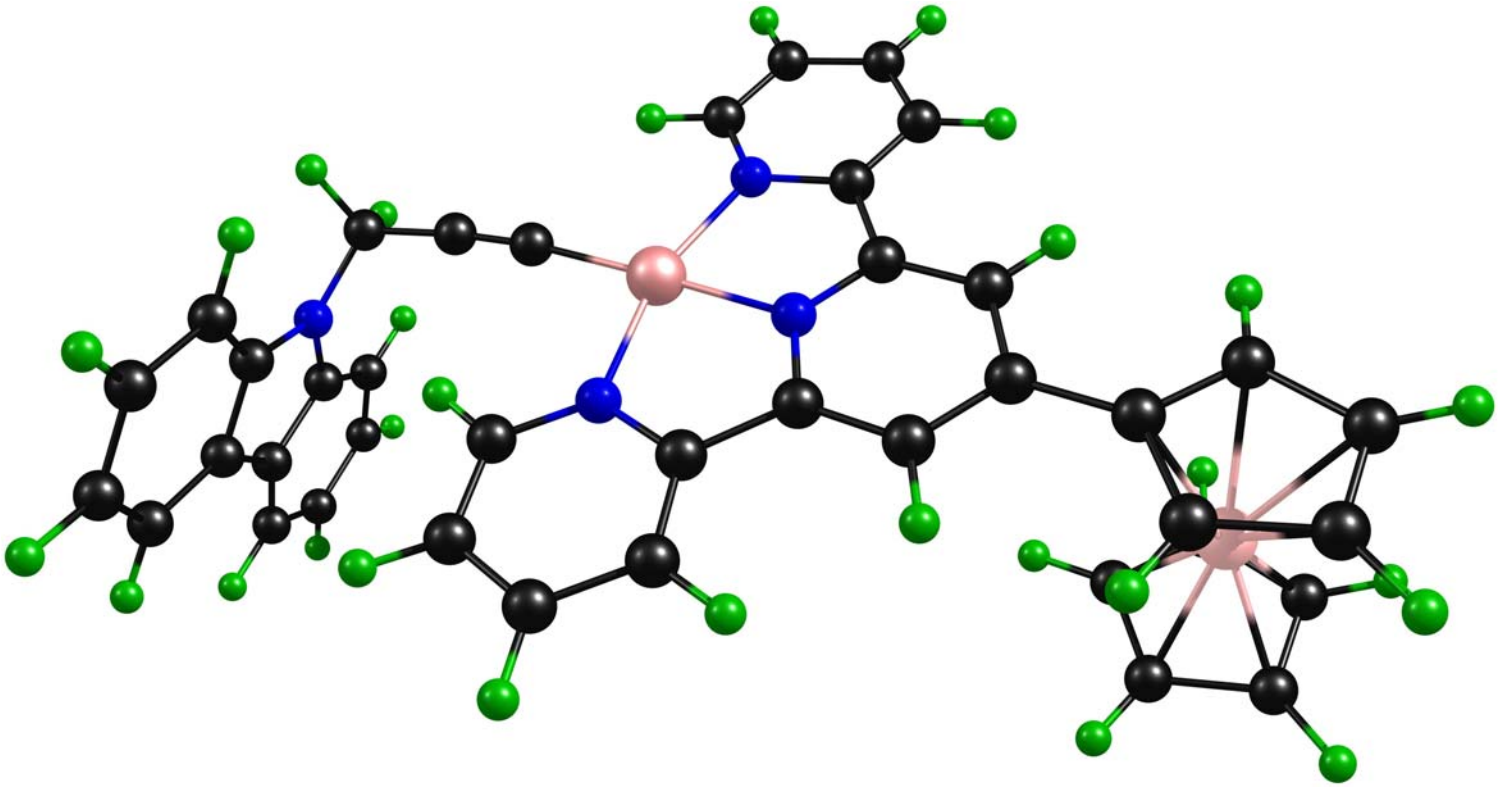

Fig S59. Geometrically optimized structure of complex **2**.

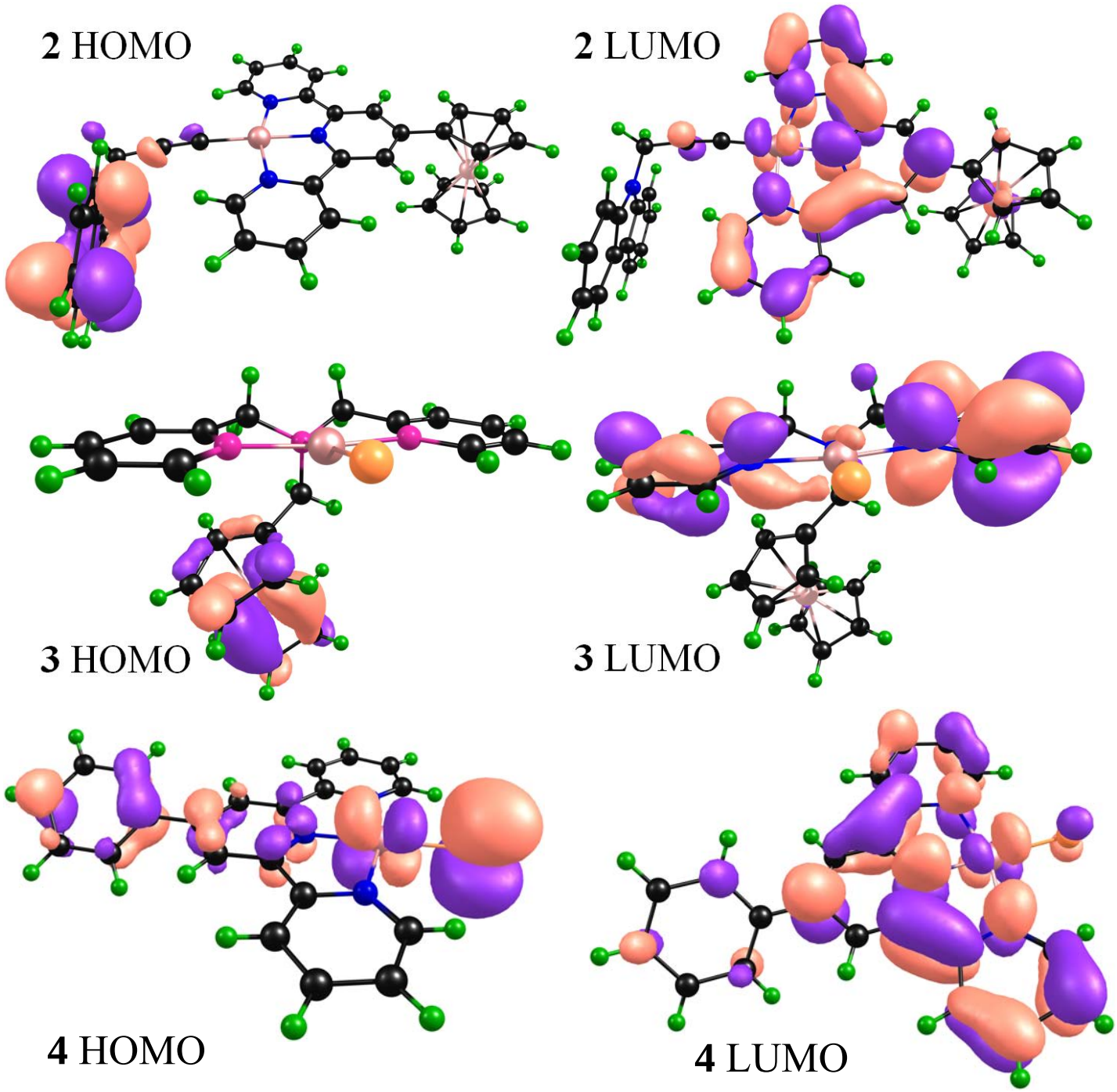

Fig. S60. Frontier orbital diagrams (HOMO and LUMO) of complexes **2**, **3** and **4** [contour value = 0.03]

Table S1. B3LYP/LanL2DZ optimized geometry of **2**

Pt	0.77988	1.1127	-0.53534
Fe	-6.44411	-1.11858	0.69164
N	-0.06752	2.954	-0.24042
N	-1.14807	0.62358	-0.66363
N	0.95528	-0.89935	-0.88438
C	-6.47253	-0.3379	2.6667
H	-6.43804	0.70804	2.93757
C	-7.66688	-1.11025	2.42404
H	-8.68216	-0.74157	2.46581
C	-7.26963	-2.4601	2.11066
H	-7.9352	-3.27887	1.87589
C	-5.82895	-2.52444	2.15818
H	-5.22778	-3.40486	1.9798
C	-5.33757	-1.213	2.50431
H	-4.29925	-0.93452	2.62347
C	-6.38513	0.46402	-0.70557
H	-6.34929	1.51594	-0.46147
C	-7.58781	-0.29029	-0.9083
H	-8.59493	0.09347	-0.83235
C	-7.22064	-1.6485	-1.22384
H	-7.90442	-2.45979	-1.42767
C	-5.78964	-1.74016	-1.21539
H	-5.2261	-2.63552	-1.43478
C	-5.24885	-0.42312	-0.90965
C	-3.83406	-0.06365	-0.81552
C	-2.815	-1.04709	-0.97473
H	-3.08851	-2.07904	-1.15674
C	-1.46872	-0.6797	-0.89261
C	-0.26891	-1.54631	-1.02351
C	-0.30819	-2.92397	-1.27145
H	-1.2622	-3.42822	-1.38068
C	0.89334	-3.65048	-1.38159

H	0.86824	-4.71834	-1.57534
C	2.11825	-2.97859	-1.24053
H	3.07013	-3.49182	-1.32252
C	2.11374	-1.59677	-0.98924
H	3.03012	-1.03221	-0.87363
C	0.5976	4.11774	-0.03093
H	1.67872	4.049	-0.01533
C	-0.08548	5.32976	0.15216
H	0.47954	6.24064	0.31611
C	-1.49038	5.33519	0.11749
H	-2.04216	6.25986	0.25486
C	-2.17794	4.12688	-0.09857
H	-3.26185	4.11421	-0.12938
C	-1.45814	2.93793	-0.27663
C	-2.07621	1.6073	-0.51097
C	-3.43434	1.28497	-0.58559
H	-4.18624	2.05661	-0.47492
C	2.69928	1.54502	-0.39427
C	3.92276	1.68701	-0.30175
C	5.40066	1.71215	-0.19797
C	6.71346	-1.35142	1.47814
C	7.18011	-1.96325	2.65794
C	6.36906	0.03651	1.48867
C	7.29066	-1.19281	3.82692
H	7.4556	-3.01504	2.66671
C	6.47125	0.81175	2.65671
N	5.9599	0.41177	0.19327
C	6.93658	0.17981	3.82296
H	7.65205	-1.64823	4.74497
H	6.2024	1.8642	2.67492
H	7.02846	0.75658	4.74007
C	6.47492	-1.83612	0.12479
C	6.002	-0.71954	-0.63608
C	6.61665	-3.09052	-0.49926
H	6.98801	-3.94743	0.05758

C	6.28356	-3.2199	-1.86022
6	5.6631	-0.84076	-1.9963
H	6.40729	-4.17781	-2.35917
H	5.30875	0.00801	-2.57442
C	5.81297	-2.10423	-2.59855
H	5.57754	-2.2223	-3.65384
H	5.72569	2.46091	0.53238
H	5.83513	2.01125	-1.16174

Table S2. Selected TDDFT transition energies (in eV), corresponding wavelengths of transitions (in nm), oscillator strength (f), the major contributions and the weight percentage and the nature of the transitions in the visible region (400-700) nm are shown for all the complexes **1-4** using B3LYP/LanL2DZ level of theory.

Complex	Energy (eV)	λ (nm)	Oscillator strength (f)	Major contributions (weight percentage)	From → to (Nature of transition)
1	2.0495	604.95	0.0422	HOMO→LUMO (70%)	MLCT
	2.5023	495.49	0.0026	HOMO→LUMO+1 (82%)	MLCT
	2.5341	489.27	0.0261	HOMO-1→LUMO+1 (31%)	MLCT
				HOMO-1→LUMO+6 (35%)	d-d transition (Fc)
	2.5975	477.32	0.0045	HOMO-1→LUMO (24%)	MLCT
				HOMO→LUMO+1 (18%)	MLCT
				HOMO→LUMO+6 (18%)	d-d transition (Fc)
	2.6128	474.53	0.0037	HOMO-1→LUMO (43%)	MLCT
	2.6908	460.77	0.0745	HOMO-2→LUMO	MLCT

				(84%)	
	2.9135	425.54	0.0026	HOMO-4→LUMO+6 (37%)	d-d transitions (Fc)
	2.9513	420.10	0.0151	HOMO-2→LUMO+1 (92%)	MLCT
2	2.1013	590.03	0.0429	HOMO-3→LUMO+6 (47%)	d-d transitions (Fc)
				HOMO-2 → LUMO (43%)	MLCT
	2.2607	548.44	0.0847	HOMO-4→LUMO (68%)	LMCT
				HOMO-2→LUMO (11%)	MLCT
	2.3144	535.70	0.0097	HOMO-2→LUMO+1 (84%)	MLCT
	2.4173	512.90	0.0246	HOMO-6→LUMO (55%)	MLCT
	2.4353	509.11	0.0048	HOMO→LUMO+3 (84%)	LMCT
	2.5566	484.97	0.0100	HOMO-4→LUMO+1 (92%)	LMCT
	2.9450	412.00	0.0057	HOMO→LUMO+4 (60%)	LMCT

3	2.8293 2.9269	438.21 423.60	0.0025 0.0011	HOMO→LUMO (64%) HOMO→LUMO (29%)	MLCT MLCT
4	2.6641 2.8568	465.39 434.00	0.1097 0.0206	HOMO→LUMO (100%) HOMO→LUMO+1 (100%)	LMCT LMCT